Quantum Effects in Atom-Surface Scattering

May 13, 2015

Thesis For the degree of PhD presented to the Scientific Council of the Weizmann Institute of Science

Submitted by: Shauli Daon

Advisor: Professor Eli Pollak

Contents

I List of Abbreviations **7**

II Abstract - English **8**

III Abstract - Hebrew **9**

IV Introduction **10**

1 Scientific Background **10**

2 Review of Current State of Knowledge **11**

3 Open Questions **13**

4 Noticeable Gaps in Theories **13**

5 Our Theory and Hypothesis **13**

6 Our Goals **15**

7 Scientific Importance **17**

V Methods **18**

8 Theoretical Background **18**

9 The Debye-Waller Factor **19**

10 Initial Assumptions and Approximations **19**

10.1 The In-plane Scattering Approximation for Atom-Surface Scattering 20

10.2 The Corrugation Potential 21

11 The Model Hamiltonian **22**

12 The Corrugation Function **23**

13 The Spectral Density **23**

14 Bragg's Law For Atom-Surface Scattering **23**

15 The Final Momentum Distribution **24**

16 The Final Angular Distribution **24**

17 The Diffraction Probability **24**

18 Thermal Averaging **25**

19 The Thermally Averaged Final Angular Distribution **25**

20 Semiclassical Perturbation Theory **26**

20.1 Preliminaries 26

20.2 The Hamiltonian using the New Coordinates 27

20.3 Equations of Motion for the System Variables 27

20.3.1 The Exact Equations of Motion for the System 27

20.3.2 Perturbation Expansion 28

20.3.3 0th Order Equations of Motion 29

20.3.4 Solution of 0th Order Equations of Motion 30

20.3.5 1st Order Equations of Motion 30

20.3.6 Solution of 1st Order Equations of Motion 30

20.3.7 Solution after the Collision is Over 31

20.4 Equations of Motion for the Bath Variables 31

20.4.1 The Exact Equations of Motion for the Bath 31

20.4.2 Perturbation Expansion 32

20.4.3 0th Order Equations of Motion 32

20.4.4 Solution to 0th Order Equations of Motion 32

20.4.5 1st Order Equation of Motion 33

20.4.6 Solution to 1st Order Equation of Motion 33

20.4.7 Solution after the collision is over . . . 33
20.5 Separation of the S-Matrix Element to Bath and System . . . 34
20.6 The System Term of the S-Matix Element . . . 36
20.6.1 The Phase Function for the System . . . 36
20.6.2 The Final Term for the System . . . 37
20.7 The Bath Term of the S-Matrix Element . . . 39
20.7.1 The Phase Function for the Bath . . . 40
20.7.2 The Final Term for the Bath . . . 42
20.8 The Final S-Matrix Element . . . 43

21 The Discretized Theory for the Bath **43**
21.1 Thermal Averaging for the SCP . . . 43
21.2 The Thermally Averaged Angular Distribution . . . 44
21.3 Factorization of the Transition Probability . . . 47
21.4 Perturbation Expansion . . . 47
21.4.1 Zero Phonon Transitions . . . 49
21.4.2 One Phonon Transitions . . . 51
21.5 The Debye-Waller Factor . . . 54
21.6 Modeling of the Spectral Density . . . 55
21.7 Bath Discretization . . . 55
21.8 Evaluating the Fourier Transform of the Form Factor . . . 55

22 The Morse Potential Model **56**

23 The Continuum Theory for the Bath **56**
23.1 Derivation of the Continuum Theory . . . 56
23.1.1 Derivation of the Angular Distribution . . . 56
23.1.2 The Zero-Phonon Contribution . . . 59
23.1.3 The Single Phonon Contribution . . . 61
23.1.4 Two Phonon Contributions . . . 66
23.2 The Total Angular Distribution for 0,1 and 2-phonon Contributions . . . 72

24 Beam collimation **72**
24.1 The Model System . . . 72

24.2 Averaging over Initial Velocities 73
24.3 The Angular Distribution 74
24.4 The Classical Angular Distribution 75

VI Results **77**
24.5 Experimental Setup 77

25 Parametrization **79**

26 Results for the Continuum Theory (only 0,1 and 2-phonon Transitions) **79**
26.1 The Debye-Waller Factor 79
26.2 The Angular Distribution 80

27 Results for Discretized Multiphonon Theory - for All Phonon Transitions **82**
27.1 The Debye-Waller Factor and Its Comparison for Both Theories 82
27.2 The Angular Distribution 82
27.3 Assessment of Convergence of the Discretized Theory 86

28 Demonstration of Beam Collimation Effects for the Ar-LiF(100) System **86**

VII Discussion **95**

29 Summary of Results as a Whole, and Main Conclusions **97**

30 Implications of Our Work **98**

31 Possible Future Developments **98**

VIII Literature **99**

32 List of Papers Published As Part of This Thesis **103**

IX Declaration **104**

X Acknowledgements **105**

XI Appendices **106**

33 Appendix 1: Full Text of Published Paper: "Semiclassical perturbation theory for diffraction in heavy-atom surface scattering" **106**

34 Appendix 2: Full Text of Published Paper: "Communication: Semiclassical perturbation theory for the quantum diffractive scattering of atoms on thermal surfaces" **114**

35 Appendix 3: Full Text of Published Paper: "Semiclassical multi-phonon theory for atom-surface scattering: Application to the Cu(111) system" **119**

Part I

List of Abbreviations

- AFM - Atomic Force Microscopy
- Ar - Argon
- Cu - Copper
- DWBA - Distorted Wave Born Approximation
- HREELS - High Resolution Election Energy Loss Spectroscopy
- Kr - Krypton
- LEED - Low Energy Electron Diffraction
- LiF - Lithium Fluoride
- Ne - Neon
- SCP - SemiClassical Perturbation
- SCPT - SemiClassical Perturbation Theory
- STM - Scanning Tunneling Microscopy
- UHV - UltraHigh Vacuum

Part II

Abstract - English

Abstract

This thesis consists mainly the analysis of results of atom-surface scattering experiments. We use and derive new theoretical methods for the study of such experiments. We consider quantum mechanical effects as well as classical effects. These include diffraction, beam collimation effects, and more. We provide illuminating explanations to the experiments, with qualitative as well as quantitative expalantions. Our theory is the first to fully explain the quantum-diffractive scattering of measured angular distributions of Ne, Ar and Kr scattered from a Cu(111) surface. We also explain the form of the Debye-Waller factor as measured in experiments.

Our main tool as we go through this endeavor is the semiclassical perturbation theory of Hubbard and Miller (J. Chem. Phys. **80**, 5827 (1984)). Forty years ago, Miller and co-workers derived this theory to account for the quantum superposition effects inherent in many scattering experiments. They found a simple way to account for these effects by using purely classical particle trajectories, but with quantum probabilities.

In this work we further improve and extend their theory by including special effects that are of interest to us and others that conduct and/or analyze such experiments. We investigate beam collimation, i.e. what happens when one changes the width of the incident atomic beam (see our paper - J. Chem. Phys. **136**, 204707 (2012)).We also explore the effects of a phonon bath that affects the particle trajectories, as all realistic experiments are affected by a temperature, which may cause surface movement - vibrations/rotations/translations (see our paper - J. Chem. Phys. 137 (20), 201103-4 (2012)). We account for the contributions of zero, one and two phonon transitions and also plot them separately, analyzing carefully the effect of each contribution. We do this by a numerical discretization applied to each phonon mode - at our last paper (see our last paper at the Appendix, submitted to the Journal of Chemical Physics). Lastly, we improve upon and validate our simple model to account for all bath modes using a numerical calculation (also at our last submitted paper).

The theory developed by us provides a complete description of the quantum dominated low energy and low surface temperature measurement of the scattering of Ne, Ar and Kr on a Cu(111) surface. It can be used to further analyze other atom-surface scattering experiments. It can also be further generalized for molecule-surface scattering, can be extended to 3-dimensional atom-surface scattering, and can be also used to explore other experimental observables, such as energy-loss distributions, sticking probabilities, and more.

Part III

Abstract - Hebrew

Part IV

Introduction

Atom-surface scattering has a long history, dating back to the 19th century. It was initially conceived as a surface-analysis tool. It was believed that by observing the properties of atoms reflected from crystalline surfaces, one may be able to better characterize the surface at the atomic level. The earliest gas-surface scattering experiments can be traced back to 1875, when Kundt and Warburg [1] attempted to test Maxwell's predictions on the properties of gas viscosity, and to the beginning of the 20th century, when Knudsen [3] and Smoluchowski [4] carried out first measurements (1898 and 1934). However in the modern sense of definition of a laboratory tool, atomic and molecular beam scattering has been used as an experimental technique in the studies of structural and dynamic properties of surfaces only since the advent of quantum mechanics. Stern and collaborators [5] and Johnson [7] carried out first gas-surface diffraction experiments with the goal of demonstrating the wave nature of atomic particles. In these studies the beams of He, H and H_2 from effusive sources were scattered from (001) surfaces of LiF, NaF and NaCl. The scattered beams have been found to exhibit diffraction, thereby verifying the basic quantum principles contained in the de Broglie relations.

The investigations of inelastic gas particle interactions with well-defined and monocrystal surfaces were at that time to a large extent hampered by the absense of ultra-high-vacuum (UHV) technology and adequate analytical surface science techniques needed to maintain and control the microscopic structure and cleanliness of surfaces. The development of modern UHV technology gave a strong push to the studies of gas-surface dynamics and scattering.

About 40 years ago, with the development of surface science, the atomic and molecular beam scattering technique has emerged as one of the most sensitive and universal experimental methods for investigations of the structural and dynamical properties of surfaces. It became complementary to the electron-based spectroscopies like low-energy electron diffraction (LEED), high-resolution electron energy loss spectroscopy (HREELS) and scanning tunneling mlicroscopy (STM). The surface scattering experiments complement with information regarding the various aspects and modes of utilization of thermal energy.

1 Scientific Background

In this study we deal mostly with the quantum-diffractive effects observed in atom-surface scattering, and some background as to the experimental results in the field is in order. The first observations of quantum diffraction

of He scattered from a LiF surface were reported 80 years ago [5]. Since then, many authors repeated such experiments with increasing sophistication [8]. It is well understood that diffraction peaks found in surface scattering of atoms as heavy as Kr are due to the periodic corrugation of the surface.

The interpretation of the results of atom and molecular beam scattering experiments, and in particular of the beam diffraction and phonon excitation intensities, has strongly motivated and simulated the development of quantum-mechanical descriptions of elastic and inelastic projectile-surface scattering. The quantum theory of atom-surface scattering has followed two main directions: one is the description of elastic scattering phenomena like diffraction, selective adsorption and diffuse scattering. The other is the description of inelastic phenomena like single- and multiphonon atom-surface scattering. Of course, in a scattering experiment all these scattering channels may be open simultaneously and theoretical approaches accounting for the effects of multichannel scattering have also been developed. We will next review with some detail the current state with respect to the scientific theories that were derived to explain the quantum-diffractive scattering of atoms from surfaces. Many suggested explanations have been offered, and it is our task to review and judge the importance and contribution of each, and see what is still missing.

2 Review of Current State of Knowledge

We will split our description of the current state of the literature to two. First we will describe the efforts and achievements with respect to a quantum theory of atom-surface scattering. This is also the main goal of this work. Next we will also review the available classical theories of atom-surface scattering. Classical theories, while being classical and thus limited, have their own advantages as well. They can more clearly describe simpler effects which may result from classical mechanics, and may have an appealing, more intuitive explanation of the observed effects.

The quantum theory of scattering from surfaces has been developed extensively. Manson and coworkers used a Distorted Wave Born Approximation (DWBA) approach [9, 10, 11]. A semiclassical theory of atom-surface scattering was proposed by Billing [12, 13]. The surface was treated as a set of coupled quantum oscillators perturbed by the time-dependent force imposed by the colliding atom/molecule. Mirét-Artés and others used a quantum trajectory-based formalism to describe quantum mechanical phenomena such as selective adsorption [14, 15] and quantum close-coupling calcuations to describe the He surface interaction potential on scattering from Sb(111) and ZnO surfaces. [16, 17, 18] Jackson used a time-dependent mean-field approach [19] and wavepacket propagation methods [20] in a restricted two-dimensional model to simulate the underlying quantum dynamics. Gumhalter and co-workers developed an evolution operator theory and applied it

to atom-surface scattering [22, 23, 21]. Gross used reduced-dimensional quantum mechanics simulations [24] along with a potential obtained using density functional theory to study the scattering of hydrogen molecules from a Pd(100) surface [25]. Similarly, they studied dissociative chemisorption of particles on metal surfaces [26].

The classical theory of atom surface scattering has also been developed [27]. The double lobe structure found in many measurements of the angular distribution of the scattered particle was attributed to classical rainbows. These structures are usually termed “surface rainbows”. They are usually recognized by the intensity maxima observed in the scattering probability as a function of the incident angle.

The study of model corrugated potentials has shown that for weak corrugation, one should expect that at the inflection points of the corrugation, the derivative of the angular deflection function vanishes, leading to a divergence of the classical scattering probability. Smearing of this divergence due to thermal fluctuations then leads to the double lobe structure. The earliest models considered a hard wall corrugated potential for which one can solve the scattering analytically [28, 29, 30, 31, 32, 33, 34]. Adding a potential well in front of the hard wall accounted for the energy dependence of the angular distance between the rainbow peaks. As the energy is increased, the refraction caused by the potential well decreases, and the rainbow angles come closer to each other. This class of models was then improved to include thermal effects, by treating the surface as a particle with an effective mass and thermally distributed velocity and is known as the washboard model [30].

In recent years the classical theory has been further developed to include more realistic "soft" potentials and a harmonic continuum description of surface phonons [35, 36, 37, 38, 39]. Noting that both the corrugation height and the friction felt by the incoming particle are typically small, one can solve for the classical dynamics using a classical perturbation theory. This accounts well for many of the qualitative features of the angular distributions, including the dependence on incident energy, incident angle, surface temperature, and more. If one models the interaction potential in terms of a Morse potential and sinusoidal corrugations along the horizontal surface directions one can derive an analytic theory for the scattering. This approach was then used to invert the measured angular distributions in terms of interaction potentials. Very recently, the perturbation theory has been expanded to include the second order corrections due to the surface corrugation [40].

A critical property which determines the quantum nature of the scattering event is the extent of collimation of the incident beam. A well collimated beam will have a large coherence wavelength in the direction perpendicular to the motion, so that diffraction may still be observed. This is why diffraction was observed for very fast atoms impinging on a surface at grazing conditions[6]. It was also found in the scattering of very heavy molecules through gratings. Moix and Pollak[54] have recently used model wavepacket propagation methods to demonstrate how the collimation of a beam of incident Ar atoms may affect the measured angular distribution. When the collimation was strong, such that the perpendicular coherence wavelength was longer

than the lattice length, one found that the angular distribution was dominated by diffraction peaks. When the angular resolution of the beam was poor, the angular distribution reverted to its classical limit.

3 Open Questions

Despite the many theoretical descriptions offered, several experimental effects can be observed which have not yet been well-understood. These are the main topic of this work. In the following sections we will review our theory and the relevant problems that we address. These include a theoretical study on the effects of beam collimation and the development of a theory for surface-temperature effects in atom-surface scattering.

While the precise location of the diffraction peaks can be deduced using Bragg's law, there are other features in the experimental results which may require further attention. The experimental results of Andersson and co-workers [50, 49] are presented in Figure 1, and will be further discussed in the next section, reviewing the open questions they pose.

4 Noticeable Gaps in Theories

So far we've reviewed several experimental features and effects that were observed, and briefly reviewed the relevant theories that were suggested to explain these. These theories represent great improvement in our understanding of many effects in atom-surface scattering. These developments notwithstanding, there still remain many experimental features, associated with the quantum scattering of heavy atoms on surfaces which have yet to receive a satisfactory explanation. Andersson and co-workers [50, 49] studied in some detail the scattering of Ne, Ar and Kr on a Cu(111) surface. Using very cold surfaces and low energy beams, they were able to observe diffraction peaks in the angular distribution even for an atom as heavy as Kr. They also observed a relatively smooth "background" angular scattering. A theory which correctly accounts for both the diffraction peaks and the smooth background as well as their temperature dependence has not been yet derived. It is the central objective of this work.

5 Our Theory and Hypothesis

We hypothesize that using a semiclassical method, which will be extensively presented in the following chapters, we may be able to provide an explanation to the experimental results of Andersson and co-workers, as presented above. We therefore follow a semiclassical route, pioneered by Miller and coworkers. Using Semi-

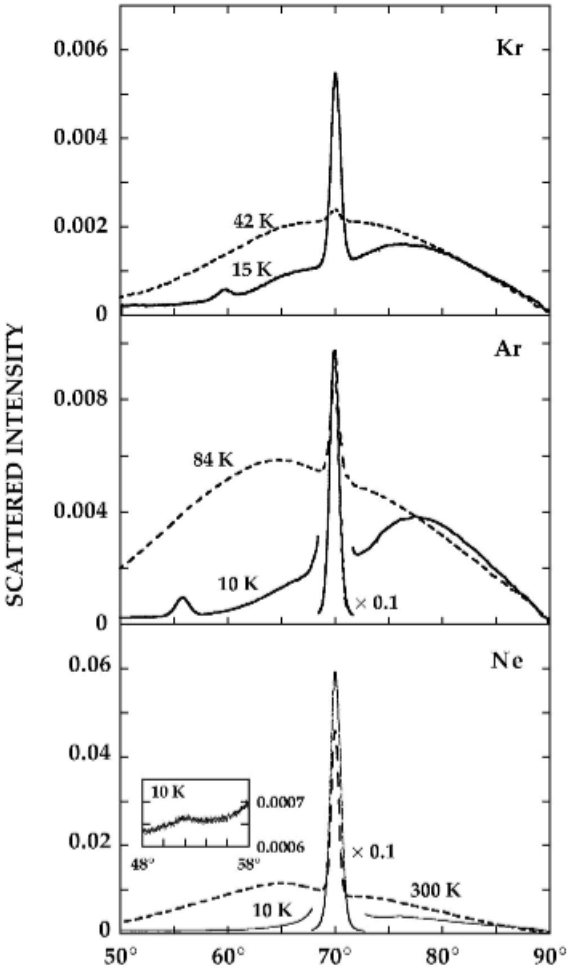

Figure 1: Experimental results of Andersson and co-workers [50, 49]. They measured the angular distribution of Ne, Ar and Kr atoms on a Cu(111) surface for very low surface temperatures. As can be observed, certain discrete peaks can be spotted as well as a broad "background". A full understanding of the broad background has not been provided prior to this work. Full details will be provided in the Results section.

Classical Perturbation Theory (SCPT) [41] Hubbard and Miller derived [47] simple expressions, in terms of Bessel functions for the elastic scattering of an atom from a frozen surface. They then also considered thermal effects [47] albeit in a limited manner, considering an Einstein phonon spectrum.

Our main hypothesis, which we will stress throughout this work, is that we believe that by following this semiclassical route, it will be possible to explain quantum effects observed in experiments. The original theory by Miller suggested using purely classical trajectories, but to average their contributions. That is, although the particle behaves classically, we may still observe diffraction, resulting from quantum superpostion. We will follow this suggestion, which greatly simplifies our treatment of the underlying quatum effects, yet preseves their representation in our theory.

We thus start from the SemiClassical Perturbation Theory (SCPT) of Hubbard and Miller [47]. Our starting point is a Hamiltonian description of the scattering in which the particle is coupled linearly to a bath of harmonic oscillators, whose properties are described by a continuum spectral density. Systematic application of SCPT enables us to derive an analytic theory which includes realistic force fields as well as thermal effects of the surface.

The SCPT approach is based on the observation that often, especially when scattering from metal surfaces, the corrugation of the surface is weak so that the corrugation height may be considered as a small parameter justifying a perturbative solution of the equations of motion. Similarly, the coupling to the phonons is weak so that this coupling too may be considered within perturbation theory. A few more initial assumptions will be outlined later on.

6 Our Goals

This research intends to shed some light over the experimental results which have been reported in the literature. Some open issues still remain, among them: effects of collimation on the diffraction pattern, characterizing the spectral density of the surface from the diffraction pattern, and understanding temperature effects on the diffraction pattern. We would also like to be able to fully explain the experimental measurements of Andersson, as presented in figure 1. This includes the shape and magnitude of the broad "background" shown below the diffraction peaks, as well as its asymmetry.

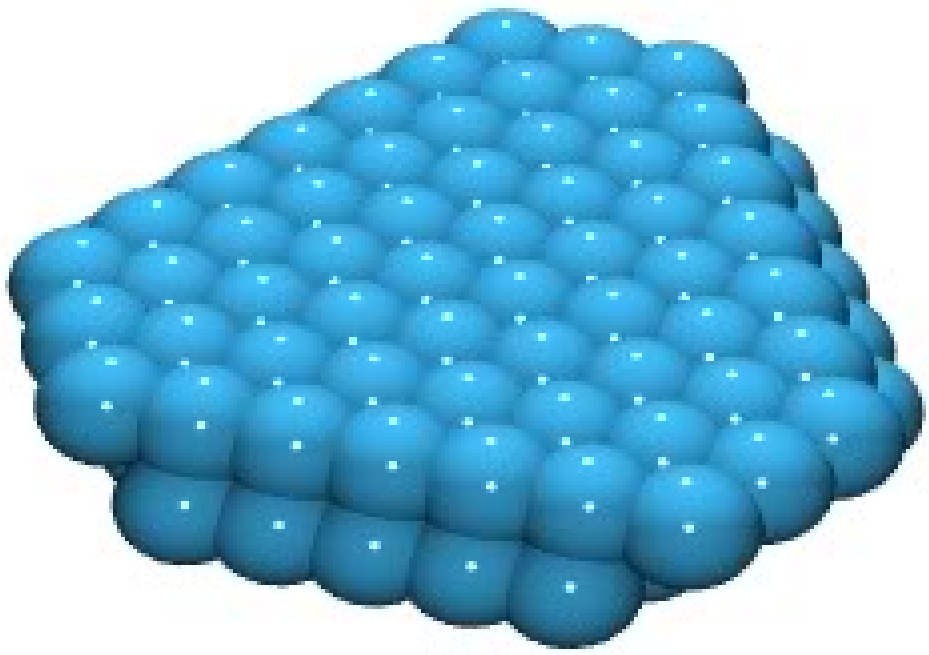

Figure 2: Structure of the Cu(111) surface. This metallic surface will be used for most surface scattering experiments that we analyze in this work. The projectiles used are Ne, Ar and Kr atoms.

7 Scientific Importance

The theory developed in this work is of importance to experimentalists and theoreticians working in the field of atom-surface scattering. It provides for the first time a complete description of the quantum-dominated diffraction effects observed in atom-surface scattering experiments. In has the potential to explain many future experimental findings. The way we later suggest to obtain the spectral density is also novel. Today, many surface characterization methods exist, such as AFM (Atomic-Force Microscopy) and STM (Scanning Tunneling Microscopy). However, none of these are able to obtain the dynamic surface properties, such as the spectral density. Only by using indirect experimental measurements it was found to be possible to obtain the spectral density. For dynamic surface properties in particular, our novel method may find practical use in the future.

Part V

Methods

In this section we will extensively review the theoretical, numerical and analytical tools that were used in our analysis of atom-surface scattering experiments. We will start with a theoretical background regarding the theoretical tools on which we base our work, namely the Semiclassical Perturbation Theory.

8 Theoretical Background

To model the surface scattering phenomena and observe the quantum effects we choose to use semiclassical theory. Semiclassical theory allows us to capture the many quantum effects while retaining the simplicity of classical mechanics. We follow the SemiClassical Perturbation (SCP) theory of Hubbard and Miller [47]. Their theory provides us with the S-matrix element which provides the (quantum) transition amplitude between diffraction modes. Apart from this our treatment of the problem is classical and thus simple. The trajectories are classical trajectories, which are approximated using first-order perturbation theory, and the bath is a harmonic bath. This enables us to provide an analytic theory which includes realistic force fields.

One may ask, why not conduct a purely classical study? Although particle diffraction is of quantum nature, a classical study can be illuminating for several reasons. Classical singularities such as the rainbow effect can induce changes in diffraction intensities. Another reason is the appealing intuitive picture that classical dynamics can offer in the visualization of scattering processes. Over the years, many purely-classical studies have been performed and provided many such insights. [40, 28, 29, 30, 31, 32, 34, 33, 35, 36, 37, 38, 39] This picture has to be taken with some caution, though. For example, it has been often conjectured that the classical counterpart of a selective adsorption resonance in atom–surface scattering is the temporal trapping of the incident atoms on the surface. A purely classical approach can offer at most a qualitative analysis of these effects, since interference is not taken into account. Therefore semiclassical approximations or a quantum trajectory analysis should be used to provide an alternative approach to some diffraction phenomena while complementing the classical picture.

9 The Debye-Waller Factor

In this work we will analyze the experimental findings for the Debye-Waller factor and show how it may be derived from the SCPT.

The Debye-Waller Factor, named after Peter Debye and Ivan Waller, is a term for the elastic fraction of a scattering experiment. It is used not only in atom-surface scattering, but also in x-ray scattering, neutron scattering, and other similar particle-surface scattering experiments. It has been also termed the "Temperature Factor" as it is temperature-dependent.

In an atom-surface scattering experiment, the atom will interact with the surface. The atom may exchange energy with the surface, and we will call this "inelastic scattering". In some cases, the atom may be reflected with the exact same energy, not exchanging any energy with the surface, and we will call this "elastic scattering". The energy that is exchanged with the surface is governed by the rules of quantum mechanics, and is thus quantized according to Bragg's law, which we will meet later on.

If the particle-surface interaction is purely elastic (as may happen with very low temperatures and very low energy atomic beams), the Debye-Waller Factor will be very close to 1. If the particle-surface interaction is highly inelastic, the Debye-Waller factor value will be close to zero. To obtain the inelastic fraction of the scattering, we may compute the value $(1-DWF)$.

In diffraction studies, we wish to learn about the discrete diffraction peaks. For this, only the elastic scattering part is useful. Inelastic scattering events are undesirable as they cause a diffuse background and make it more difficult to observe the sharp elastic peaks.

The Debye Waller Factor is usually written in terms of the Debye-Waller Exponent W:

$$DWF = exp(-2W) \tag{1}$$

10 Initial Assumptions and Approximations

The problem which we are dealing with, namely atom-surface scattering, is very complex in nature.

Its complexity arises from the following:

1. The particle trajectory is three-dimensional.
2. The particle may interact with the surface at many impact points, that form a two-dimensional surface.
3. The surface interaction potential is complicated and arises from the quantum nature of the surface.

4. The surface has a temperature and is thus at constant vibration, with particles vibrating, rotating and translating.

5. The particle may oftentimes stick to the surface, or sometimes cause other surface particles to detach from the surface.

6. The particle trajectory is governed by quantum mechanics and is thus probabilistic and has the form of a wavefunction.

7. The particle may undergo many kinds of chemical interactions with the surface atoms.

From these complexities we may understand that a full, exact, quantitative treatment of the atom-surface interaction is a very difficult endeavor. Even if it was possible to formulate a theory to take into account all of the above considerations, the theory would be very complicated and likely mask the underlying basic "effects" that are observed in experiment, which we wish to understand. To understand experimental effects better qualitatively, and perhaps also quantitatively, it is desirable to have a relatively "simple" theory with simple analytical expressions, which will allow us to tell a "story" and better understand what is happening when the particle interacts with the surface. Also, it may be found that some of the complexities mentioned above are more dominant than the others, and it is our job as theorists to discern the importance of certain characteristics and also neglect the nonessential complexities.

Therefore, in the following sections we will describe the underlying assumptions and approximations of our theory as will be formulated. We will justify each assumption and understand how it affects our theoretical results.

10.1 The In-plane Scattering Approximation for Atom-Surface Scattering

As mentioned, the surface is two-dimensional and the particle trajectory is three dimensional. However, the typical experimental measurements are carried out in the plane of the incident and outgoing beam. Therefore it is reasonable to restrict the particle potential to this plane. We will restrict ourselves here and model the dynamics in terms of two degrees of freedom. One is the vertical distance z (with conjugate momentum p_z) describing the distance of the atom (whose mass is M) from the surface, the other is the horizontal coordinate x (with conjugate momentum p_x) parallel to the surface. Such an approximation is further justified if there is no coupling between the motion along the two horizontal directions. We will call this treatment "in-plane scattering".

We define variables for the initial and final conditions of the particle that is scattered from the surface. The particle is initiated at the time $-t_0$ with initial (negative) momentum p_{z_i} and (positive) horizontal momentum p_{x_i}. To zeroth order in the corrugation, as we shall see, at $t = 0$ the particle impacts the surface. We are then interested in the final momenta of the particle at the time $+t_0$, which is taken to be sufficiently large to assure that the scattering event is over. The final momenta variables are then termed p_{z_f} and p_{x_f} for the z and x degrees of freedom, respectively, such that:

$$p_x(t = -t_0) = p_{x_i} \tag{2}$$

$$p_z(t = -t_0) = p_{z_i} \tag{3}$$

$$p_x(t = +t_0) = p_{x_f} \tag{4}$$

$$p_z(t = +t_0) = p_{z_f} \tag{5}$$

10.2 The Corrugation Potential

As mentioned above, we limit ourselves to in-plane scattering. Therefore, we first have to model the particle-surface in-plane interaction potential. The surface is considered to be "corrugated", i.e. periodic as in an eggs' carton. The corrugation represents the potential inflicted by the surface atoms, which are also arranged in a periodic fashion. Since we restricted ourselves to only 2 degrees of freedom, we have only one horizontal coordinate for the surface potential, which we term the "corrugation function" $h(x)$. This function will later be approximated by a simple sine function. The period of the corrugation function $h(x)$ will be chosen to be the lattice length l.

While the realistic particle-surface potential may be more complicated, this simplifying assumption is one of the ingredients which will allow us to greatly simplify our theory, and also provide many analytical results.

We assume that the interaction of the particle with the surface is a function of the instantaneous distance of the particle from the surface, $z + h(x)$, and so the potential function obtained for a particle with vertical coordinate z and horizontal coordinate x is $V(z + h(x))$.

To simplify further treatment of the potential, we expand the potential function as a series with the corrugation function $h(x)$, which is considered to be small:

$$\bar{V}(z + h(x)) = \bar{V}(z) + \bar{V}'(z)h(x) + \frac{1}{2}\bar{V}''(z)h^2(x) + ... \tag{6}$$

$V(z)$ gives the zero-th order term, which will later be taken as a Morse potential. The first order perturbation term is given by the product of the first derivative of the vertical potential and the periodic corrugation function $h(x)$. Within our analytical theory we will assume that the corrugation is "weak" and so consider only terms up to first order. Therefore, only the first two terms will appear in the resulting Hamiltonian. This is a reasonable assumption for many metallic surfaces.

11 The Model Hamiltonian

Since the typical experimental measurements are carried out in the plane of the incident and outgoing beam, we will restrict ourselves here and model the dynamics in terms of two degrees of freedom. One is the vertical distance z (with conjugate momentum p_z) describing the distance of the atom (whose mass is M) from the surface, the other is the horizontal coordinate x (with conjugate momentum p_x) parallel to the surface. Recent classical studies have shown [58] that the two planar degrees of freedom (x and y) are not necessarily separable so that inclusion of the second planar degree of freedom can change the classical scattering dynamics. It should be thus understood that the present treatment is valid provided that the coupling between the two horizontal degrees of freedom may be neglected. Furthermore, we will assume that the coupling to the vertical phonons is much more important than the coupling to the horizontal surface phonons. This assumption has been verified in recent on the fly molecular dynamics computations [58].

The model Hamiltonian we use is based on the assumption that the interaction of the particle with the surface is only dependent on the instantaneous distance of the particle from the fluctuating surface which is $z + h(x) + \frac{1}{\sqrt{M}}\sum_{j=1}^{N} c_j x_j$. The fluctuational part is assumed small so that to leading order in the coupling, the potential of interaction is a sum of three terms $\bar{V}(z + h(x) + \frac{1}{\sqrt{M}}\sum_{j=1}^{N} c_j x_j) \simeq \bar{V}(z) + \bar{V}'(\hat{z})h(\hat{x}) + \bar{V}'(\hat{z})\frac{1}{\sqrt{M}}\sum_{j=1}^{N} c_j x_j$. The resulting "standard" model Hamiltonian [27, 51] describing the scattering dynamics is

$$\hat{H} = \frac{\hat{p}_x^2 + \hat{p}_z^2}{2M} + \bar{V}(\hat{z}) + \bar{V}'(\hat{z})h(\hat{x}) + \sum_{j=1}^{N}\left[\frac{\hat{p}_j^2}{2} + \frac{\omega_j^2}{2}\left(\hat{x}_j - \frac{c_j \bar{V}'(\hat{z})}{\sqrt{M}\omega_j^2}\right)^2\right] \tag{7}$$

where $\bar{V}(\hat{z})$ is the potential of interaction in the vertical direction; $h(\hat{x})$ is the horizontal corrugation function. $\hat{p}_j$ and $\hat{x}_j$ are the respective mass weighted momentum and coordinate operators for the j-th bath oscillator and c_j is the dimensionless coupling constant which couples the j-th bath oscillator to the vertical motion. ω_j is the frequency of the j-th bath oscillator.

In this work we concentrate on the angular distribution of the scattered particle initiated far away from the surface at the time $-t_0$ with initial (negative) momentum p_{z_i} and (positive) horizontal momentum p_{x_i}. We are

then interested in the distribution of the final momenta p_{z_f} and p_{x_f} of the particle at the time $+t_0$, which is taken to be sufficiently large to assure that the scattering event is over. The initial state of the system is also characterized by the initial quantum number n_{j_i} of the j-th bath oscillator and the final quantum state n_{j_f} of the j-th oscillator after the collision is over.

12 The Corrugation Function

In this work the corrugation function will take the simple form

$$h(\hat{x}) = h\sin\left(\frac{2\pi\hat{x}}{l}\right) \tag{8}$$

where h is the corrugation height parameter, considered to be small compared to the lattice length l of the surface in the horizontal direction.

13 The Spectral Density

The continuum limit is introduced through the spectral density defined as

$$J_z(\omega) = \frac{\pi}{2}\sum_{j=1}^{N}\frac{c_j^2}{\omega_j}\delta\left(\omega-\omega_j\right). \tag{9}$$

The associated friction function is

$$\gamma(t) = \sum_{j=1}^{N}\frac{c_j^2}{\omega_j^2}\cos(\omega_j\, t). \tag{10}$$

14 Bragg's Law For Atom-Surface Scattering

The periodicity of the surface in the horizontal direction implies that the final momentum must obey the Bragg condition, that is

$$p_{x_f} = p_{x_i} + \frac{2\pi\hbar n}{l} \tag{11}$$

with n an integer and referred to as the Bragg number. Energy conservation then implies that the vertical momentum of the particle, after the collision is over $p_{z_{t_0}}$ is related to all other observables through the energy

conservation relationship:

$$\frac{p_{z_{t_0}}^2 + \left(p_{x_i} + \frac{2\pi\hbar n}{l}\right)^2}{2M} + \sum_{j=1}^{N}\left(n_{j_f} + \frac{1}{2}\right)\hbar\omega_j = \frac{p_{z_i}^2 + p_{x_i}^2}{2M} + \sum_{j=1}^{N}\left(n_{j_i} + \frac{1}{2}\right)\hbar\omega_j. \tag{12}$$

15 The Final Momentum Distribution

The exact quantum mechanical final particle momentum distribution, summed over all possible final bath states is then by definition

$$P(p_{x_f}, p_{z_f}; \mathbf{n_i}) = \sum_{n,\mathbf{n_f}} \delta(p_{x_f} - p_{x_i} - \frac{2\pi\hbar n}{l})\, \delta(p_{z_f} - p_{z_{t_0}}) P_{n,\mathbf{n_f};0,\mathbf{n_i}} \tag{13}$$

where the vector notation $\mathbf{n} = (n_1, \cdots, n_N)$ is used to describe all the bath mode quantum numbers. $P_{n,n_f;0,n_i}$ is the quantum probability for going from the initial state of the bath (n_i) and the initial momenta of the particle $(p_{x_i}, p_{z_i}$with Bragg number $n_i = 0$ by definition) to the respective final momenta and oscillator quantum states.

16 The Final Angular Distribution

The associated angular distribution is:

$$P(\theta_f; n_i) = \sum_{n,n_f} \int_{-\infty}^{\infty} dp_{x_f} \int_{-\infty}^{\infty} dp_{z_f} \delta(\theta_f - \tan^{-1}\frac{p_{x_f}}{p_{z_f}})\, P(p_{x_f}, p_{z_f}; n_i) \tag{14}$$

For future use, we note that the change in the occupation numbers of the oscillators is defined as:

$$\Delta\mathbf{n} = \mathbf{n}_f - \mathbf{n}_i. \tag{15}$$

17 The Diffraction Probability

The heart of the theory is the diffraction probability

$$P_{n,\mathbf{n_f};0,\mathbf{n_i}} = |S_{n,\mathbf{n_f};0,\mathbf{n_i}}|^2 \tag{16}$$

where $S_{n,\mathbf{n_f};0,\mathbf{n_i}}$ is the corresponding S-matrix element.

18 Thermal Averaging

Typically, the surface is in thermal equilibrium with temperature T, so that the initial condition for the bath is described by the thermal bath density operator

$$\hat{P}_B = \frac{\exp\left(-\beta \hat{H}_B\right)}{Z_B} \tag{17}$$

where $Z_B = Tr_B \exp\left(-\beta \hat{H}_B\right)$ is the bath partition function, the bath Hamiltonian is defined as

$$\hat{H}_B = \sum_{j=1}^{N} \left[\frac{\hat{p}_j^2}{2} + \frac{\omega_j^2}{2} \hat{x}_j^2 \right] \tag{18}$$

and $\beta = 1/(k_B T)$. The thermally averaged final momentum distribution is then

$$\begin{aligned} \left\langle P(p_{x_f}, p_{z_f}) \right\rangle_\beta &= \sum_{n_i=0}^{\infty} \sum_{n,n_\mathbf{f}} \delta(p_{x_f} - p_{x_i} - \frac{2\pi\hbar n}{l}) \, \delta(p_{z_f} - p_{z_{t_0}}) \\ &\quad \cdot P_{n,\mathbf{n_f};0,\mathbf{n_i}} \frac{\exp\left(-\beta\hbar\left(\left(\mathbf{n}_i + \frac{1}{2}\mathbf{I}\right)\cdot\omega\right)\right)}{Z_B}. \end{aligned} \tag{19}$$

19 The Thermally Averaged Final Angular Distribution

The (negative) angle of incidence θ_i and the final scattering angle θ_f relative to the normal to the surface are by definition

$$\theta_j = \tan^{-1}\left(\frac{p_{x_j}}{p_{z_j}}\right), \quad j = i, f. \tag{20}$$

The thermally averaged final angular distribution of the scattered particle is then given in terms of the final momentum distribution as,

$$\left\langle P(\theta_f) \right\rangle_\beta = \int_{-\infty}^{\infty} dp_{x_f} \int_0^{\infty} dp_{z_f} \delta\left(\theta_f - \tan^{-1}\left(\frac{p_{x_f}}{p_{z_f}}\right)\right) \left\langle P(p_{x_f}, p_{z_f}) \right\rangle_\beta \tag{21}$$

$$\tag{22}$$

20 Semiclassical Perturbation Theory

20.1 Preliminaries

Forty five years ago, Miller [42, 43] formulated an initial value representation expression for the S-matrix element. To introduce his expression we first define the classical action angle variables for the system and the bath. The system angle variable q_x is defined in terms of the horizontal coordinate of the particle and the period of the surface as

$$q_x = \frac{2\pi x}{l}. \tag{23}$$

The corresponding horizontal action variable is defined as:

$$I_x = \frac{l p_x}{2\pi}. \tag{24}$$

The bath action (I_j) and angle (q_j) variables are defined by the canonical transformation:

$$x_j = \sqrt{\frac{2I_j}{\omega_j}}\cos(q_j) \tag{25}$$

$$p_j = -\sqrt{2\omega_j I_j}\sin(q_j). \tag{26}$$

The initial conditions for the classical actions are

$$I_{j_i} = \hbar\left(n_{j_i} + \frac{1}{2}\right), \quad j = 1,...,N. \tag{27}$$

To get rid of infinities at long times after the collision, Miller also introduced the pseudo angle variables:

$$\bar{q}_{j_t} = q_{j_t} - \frac{M z_t \omega_j}{p_{z_t}}, \quad j = 1,...,N \tag{28}$$

such that at long times after the classical collision is over, when the particle is moving freely so that for the j-th oscillator $\frac{d\bar{q}_{j_t}}{dt} = 0$. Similarly one introduces a pseudo angle variable for the horizontal motion

$$\bar{q}_{x_t} = q_{x_t} - \frac{M z_t \omega_{x_t}}{p_{z_t}} \tag{29}$$

where the horizontal frequency is defined as

$$\omega_{x_t} = \frac{2\pi p_{x_t}}{Ml}. \tag{30}$$

Miller derived the following initial value representation expression for the classical S-matrix element: [42]

$$\begin{aligned} S_{n_{x_f},n_f;0,n_i} &= \lim_{t_0\to\infty} \int_0^{2\pi} \frac{dq_{x_i}}{2\pi} \int_0^{2\pi} \prod_{j=1}^{N} \frac{dq_{j_i}}{2\pi} |\mathbf{D}|^{1/2} \\ &\quad \cdot \exp\left(\frac{i}{\hbar}\left[\varphi_{t_0} + \bar{q}_{x_{t_0}}(I_{x_{t_0}} - \hbar n_{x_f}) + \sum_{j=1}^{N} \bar{q}_{j_{t_0}}\left(I_{j_{t_0}} - \hbar\left(n_{j_f} + \frac{1}{2}\right)\right)\right]\right) \end{aligned} \tag{31}$$

where $I_{x_{t_0}}$, $\bar{q}_{x_{t_0}}$ and $I_{j_{t_0}}, \bar{q}_{j_{t_0}}, j = 1,...,N$ are the values of the respective action and pseudo angle variables, after the collision is over. The action is

$$\varphi_{t_0} = -\int_{-t_0}^{t_0} dt\ [q_{x_t}\dot{I}_{x_t} + z_t\dot{p}_{z_t} + \sum_{j=1}^{N} q_{j_t}\dot{I}_{j_t}]. \tag{32}$$

The matrix D is the Jacobian of the transformation from the $N+1$ final pseudo action action variables to the $N+1$ initial variables.

20.2 The Hamiltonian using the New Coordinates

We plug the bath action (I_j) and angle (q_j) variables as defined in Eqs. 26 and 25 into the Hamiltonian (Eq. 7) to obtain:

$$\hat{H} = \frac{\hat{p}_x^2 + \hat{p}_z^2}{2M} + \bar{V}(\hat{z}) + \bar{V}'(\hat{z})h(\hat{x}) + \sum_{j=1}^{N}\left[\omega_j I_j - c_j\bar{V}'(\hat{z})\sqrt{\frac{2I_j}{M\omega_j}}\cos(q_j) + \frac{1}{2}\frac{c_j^2\bar{V}'(\hat{z})^2}{M\omega_j^2}\right] \tag{33}$$

20.3 Equations of Motion for the System Variables

20.3.1 The Exact Equations of Motion for the System

The equations of motion are derived by using Hamilton's equations:

$$\frac{dp}{dt} = -\frac{\partial H}{\partial q} \tag{34}$$

$$\frac{dq}{dt} = +\frac{\partial H}{\partial p} \tag{35}$$

We have two sets of conjuate variables, the position and momentum for the x coordinate and for the z coordinate.

For the z coordinate, we have for the momentum:

$$\frac{dp_{z_t}}{dt} = M\ddot{z_t} = -\frac{\partial H}{\partial z_t} = -V'(\hat{z}_t) - \bar{V}''(\hat{z}_t)h(\hat{x}_t) + \bar{V}''(\hat{z}_t)\sum_{j=1}^{N} c_j \left[\sqrt{\frac{2I_j}{M\omega_j}}\cos(q_{j_t}) - \frac{c_j\bar{V}'(\hat{z}_t)}{M\omega_j^2}\right]$$

And finally:

$$M\ddot{z_t} + V'(\hat{z}_t) + \bar{V}''(\hat{z}_t)h(\hat{x}_t) = \bar{V}''(\hat{z}_t)\sum_{j=1}^{N} c_j \left[\sqrt{\frac{2I_j}{M\omega_j}}\cos(q_{j_t}) - \frac{c_j\bar{V}'(\hat{z}_t)}{M\omega_j^2}\right] \tag{36}$$

For the x coordinate, we have for the momentum:

$$\frac{dp_{x_t}}{dt} = M\ddot{x_t} = -\frac{\partial H}{\partial q_{x_t}} = -\bar{V}'(\hat{z}_t)h'(\hat{x}_t) \tag{37}$$

and for the position:

$$\frac{dx_t}{dt} = \frac{\partial H}{\partial p_{x_t}} = \frac{\hat{p}_x}{M} \tag{38}$$

20.3.2 Perturbation Expansion

We would like to solve the equations of motion using perturbation theory. We assume that the corrugation is weak, and solve perturbatively for the different orders of the corrugation height h which is assumed to be small compared to the lattice length l of the surface in the horizontal direction. We also solve perturbatively for the bath coefficients c_j.

We expand the solutions for the x and z coordinates in terms of the perturbation indexes such that:

$$z_t = \sum_{l=0}^{\infty} z_{t,m,n} \tag{39}$$

$$p_{z_t} = \sum_{l=0}^{\infty} p_{z_t,m,n} \tag{40}$$

$$x_t = \sum_{l=0}^{\infty} x_{t,m,n} \tag{41}$$

$$p_{x_t} = \sum_{l=0}^{\infty} p_{x_t,m,n} \tag{42}$$

The indexes m and n denote the power of h and c_j, respectively. We also assume the coupling term $h^n c_j^n = 0, \quad for\ n = 1,2,....$The particle is assumed to be initiated at the time $-t_0$ with initial momentum (negative) $p_{z_i}$and the scattering event is over at t_0. The small parameters in the perturbation theory are the coupling constants c_j and h.

20.3.3 0th Order Equations of Motion

For the zero order terms, $m = n = 0$, we obtain the following equations of motion.

For the vertical direction:

$$M\ddot{z}_{t,0,0} = -\bar{V}'(z_{t,0,0}) \tag{43}$$

For the horizontal direction:

$$M\ddot{x}_{t,0,0} = 0 \tag{44}$$

We note that for x the zeroth order equation of motion is that for a free particle.

$$\frac{dx_{t,0,0}}{dt} = \frac{\partial H}{\partial p_{x_t}} = \frac{p_{x_i}}{M} \tag{45}$$

$$\frac{dp_{x_{t,0,0}}}{dt} = 0 \tag{46}$$

From that we see that the horizontal momentum is a constant.

$$p_{x_t,0,0} = constant \tag{47}$$

or using the action variable:

$$I_{x_t,0,0} = constant \tag{48}$$

20.3.4 Solution of 0th Order Equations of Motion

In the horizontal direction the motion is to zeroth order a free particle motion:

$$x_{t,0,0} = x_{-t_0} + \frac{p_{x_i}}{M}(t + t_0) \tag{49}$$

or , we define:

$$x_{t,0,0} = \left(x_{-t_0} + \frac{p_{x_i}}{M}t_0\right) + \frac{p_{x_i}}{M}t = x_0 + \frac{p_{x_i}}{M}t \tag{50}$$

20.3.5 1st Order Equations of Motion

We'd like to find the first order solution. For the horizontal momentum we have:

$$\frac{dp_{x_{t,1,0}}}{dt} = -\bar{V}'(z_{t,0,0})h'(x_{t,0,0}) \tag{51}$$

20.3.6 Solution of 1st Order Equations of Motion

We solve for the horizontal momentum

$$p_{x_t,1,0} = -\int_{-t_0}^{t} dt'[V'(z_{t',0,0})h'(x_{t',0,0})] \tag{52}$$

we substitute $x_{t,0,0}$from Eq. 49 and obtain:

$$p_{x_t,1,0} = -\int_{-t_0}^{t} dt'\left[V'(z_{t',0,0})h'\left(x_0 + \frac{p_{x_i}}{M}t'\right)\right] \tag{53}$$

We also substitute the derivative of the corrugation function:

$$h'(x) = \frac{2\pi h}{l}cos\left(\frac{2\pi x}{l}\right) \tag{54}$$

to obtain:

$$p_{x_t,1,0} = -\int_{-t_0}^{t} dt'\left[V'(z_{t',0,0})\frac{2\pi h}{l}cos\left(\frac{2\pi}{l}\left[x_0 + \frac{p_{x_i}}{M}t'\right]\right)\right] \tag{55}$$

We have a cosine of a sum:

$$p_{x_t,1,0} = -\int_{-t_0}^{t} dt' \left[V'(z_{t',0,0}) \frac{2\pi h}{l} cos\left(\frac{2\pi}{l} x_0 + \frac{2\pi}{l} \frac{p_{x_i}}{M} t' \right) \right] \tag{56}$$

We can split the cosine sum:

$$p_{x_t,1,0} = -\int_{-t_0}^{t} dt' \left[V'(z_{t',0,0}) \frac{2\pi h}{l} \left(\cos\left(\frac{2\pi}{l} x_0 \right) \cos\left(\frac{2\pi}{l} \frac{p_{x_i}}{M} t' \right) - \sin\left(\frac{2\pi}{l} x_0 \right) \sin\left(\frac{2\pi}{l} \frac{p_{x_i}}{M} t' \right) \right) \right] \tag{57}$$

we use the definition for the horizontal frequency:

$$\omega_x = \frac{2\pi p_{x_i}}{Ml}. \tag{58}$$

and of the action angle variable $q_{x_i} = q_{x_{-t_0}}$ to obtain:

$$p_{x_t,1,0} = -\int_{-t_0}^{t} dt' \left[V'(z_{t,0,0}) \frac{2\pi h}{l} \left(\cos\left(q_{x_i}\right) \cos\left(\omega_x t'\right) - \sin\left(q_{x_i}\right) \sin\left(\omega_x t'\right) \right) \right]. \tag{59}$$

The second integrand is an odd function (when the upper limit $t = t_0$) and evaluates to zero, so we have:

$$p_{x_{t_0},1,0} = -\frac{2\pi h}{l} \cos\left(q_{x_i}\right) \int_{-t_0}^{t_0} dt' \left[V'(z_{t',0,0}) \cos\left(\omega_x t'\right) \right] \tag{60}$$

20.3.7 Solution after the Collision is Over

$$I_{x_{\infty},1,0} = -h\hbar \cos\left(q_{x_i}\right) A(\omega_x) \tag{61}$$

and we used the definition:

$$A(\omega) = \frac{1}{\hbar} \int_{-\infty}^{\infty} dt [\cos(\omega t)\, \bar{V}'(z_{t,0,0})] \tag{62}$$

20.4 Equations of Motion for the Bath Variables

20.4.1 The Exact Equations of Motion for the Bath

The equations of motion are again derived using Hamilton's equations. Because the transformation of the position and momentum variables is canonical, Hamilton's equations apply to our new variables. We obtain the following equations for the action-angle variables of the j-th bath oscillator:

$$\frac{dq_{j_t}}{dt} = [\omega_j - c_j \bar{V}'(z_t)\sqrt{\frac{1}{2I_{j_t}M\omega_j}}\cos(q_{j_t})] \tag{63}$$

$$\frac{dI_{j_t}}{dt} = -c_j \bar{V}'(z)\sqrt{\frac{2I_{j_t}}{M\omega_j}}sin(q_{j_t}) \tag{64}$$

20.4.2 Perturbation Expansion

Again, we would like to solve the equations of motion using perturbation theory. The bath term has no powers of h in the equations of motion and so we can ignore the index m. We use only the index n to denote the powers of c_j.

We obtain the equations of motion for the bath variables:

$$x_{j_t} = \sum_{l=0}^{\infty} x_{j_t,n} \tag{65}$$

$$p_{j_t} = \sum_{l=0}^{\infty} p_{j_t,n} \tag{66}$$

20.4.3 0th Order Equations of Motion

For the zero-order terms, $n = 0$, we collect terms with zero power in c_j and obtain the equations of motion:

$$\frac{dq_{j_t,0}}{dt} = \omega_j \tag{67}$$

$$\frac{dI_{j_t,0}}{dt} = 0 \tag{68}$$

20.4.4 Solution to 0th Order Equations of Motion

We have the solutions:

$$q_{j_t,0} = q_j + \omega_j t \tag{69}$$

$$I_{j_t,0} = I_{j_i} = \hbar(n_{j_i} + \frac{1}{2}) \tag{70}$$

20.4.5 1st Order Equation of Motion

For the 1st-order terms, $n = 1$, we collect terms with power of 1 for c_j . For our 1st order solution we consider only $I_{j_t.1}$.

We obtain the equation of motion:

$$\frac{dI_{j_t.1}}{dt} = -c_j \bar{V}'(z) \sqrt{\frac{2I_{j_t}}{M\omega_j}} sin(q_{j_t}) \tag{71}$$

20.4.6 Solution to 1st Order Equation of Motion

The first order solution for the j-th oscillator is readily seen to be:

$$\begin{aligned} I_{j_t,1} &= -c_j \int_{-t_0}^{t} dt' V'(z_{t',0,0}) \sqrt{\frac{2I_{j_{t'}}}{M\omega_j}} \sin(q_{j_{t'},0,0}) \\ &= -c_j \sqrt{\frac{2I_{j_i}}{M\omega_j}} \int_{-t_0}^{t} dt' V'(z_{t',0}) \sin(q_{j_{t'},0,0}). \end{aligned} \tag{72}$$

20.4.7 Solution after the collision is over

We would like to solve for when the time $t_0$is very large, i.e. after the collision is over. For that we look at the limit when $t_0 \to \infty$.

We solve for $I_{j_t,1}$:

$$
\begin{aligned}
I_{j_t,1} &= -c_j\sqrt{\frac{2I_{j_i}}{M\omega_j}}\int_{-t_0}^{t} dt' V'(z_{t',0,0})\sin(q_{j_{t'},0}) \\
&= -c_j\sqrt{\frac{2I_{j_i}}{M\omega_j}}\int_{-t_0}^{t} dt' V'(z_{t',0,0})\sin(q_j+\omega_j t') \\
&= -c_j\sqrt{\frac{2I_{j_i}}{M\omega_j}}[\int_{-t_0}^{t} dt' V'(z_{t',0,0})\sin(q_j)\cos(\omega_j t') \\
&\quad +\int_{-t_0}^{t} dt' V'(z_{t',0,0})\cos(q_j)\sin(\omega_j t')]
\end{aligned}
\tag{73}
$$

So finally, for the 0th and 1st order contributions to I_j we obtain, at the limit $t_0 \to \infty$:

$$
I_{j_\infty,0} = I_{j_i} = \hbar(n_{j_i}+\frac{1}{2}) \tag{74}
$$

$$
I_{j_\infty,1} = -c_j\sqrt{\frac{2I_j}{M\omega_j}}sin(q_j)A(\omega_j) \tag{75}
$$

for the $\bar{q}_{j_\infty,0}$ variable we will only need the zero-th order contribution

$$
\bar{q}_{j_\infty,0} = \bar{q}_{j_{-t_0}} \tag{76}
$$

20.5 Separation of the S-Matrix Element to Bath and System

We now consider the S-matrix element as defined in Eq. 31. We note that looking at the 1st-order perturbation theory equations, that there are no terms that mix the perturbation parameters h and c_j. In the first-order solution for the system, Eq. 52 there is only h and in the first-order solution for the bath, Eq. 72 there is only c_j. We may therefore separate the S-matrix into a product of two separate contributions, one for the system and one for the bath. We begin by redefining the phase function φ_{t_0} as a sum of two phase functions:

$$
\varphi_{t_0} = \Psi_{t_0} + \Xi_{t_0} \tag{77}
$$

such that:

$$\Psi_{t_0} = -\int_{-t_0}^{t_0} dt\ [q_{x_t}\dot{I}_{x_t} + z_t\dot{p}_{z_t}]. \tag{78}$$

and

$$\Xi_{t_0} = -\int_{-t_0}^{t_0} dt\ [\sum_{j=1}^{N} q_{j_t}\dot{I}_{j_t}]. \tag{79}$$

And we obtain the new form for the S-matrix element:

$$\begin{aligned} S_{n_{x_f},n_f;0,n_i} &= \lim_{t_0\to\infty}\int_0^{2\pi}\frac{dq_{x_i}}{2\pi}\int_0^{2\pi}\prod_{j=1}^{N}\frac{dq_{j_i}}{2\pi}|\mathbf{D}|^{1/2} \\ &\cdot\exp\left(\frac{i}{\hbar}\left[\Psi_{t_0}+\Xi_{t_0}+\bar{q}_{x_{t_0}}(I_{x_{t_0}}-\hbar n_{x_f})+\sum_{j=1}^{N}\bar{q}_{j_{t_0}}\left(I_{j_{t_0}}-\hbar\left(n_{j_f}+\frac{1}{2}\right)\right)\right]\right) \end{aligned} \tag{80}$$

In our approximation we shall set the Jacobian of the transformation to the unity matrix ($|\mathbf{D}| = I$), as in Miller's papers, so that after some rearrangement of the terms we obtain:

$$\begin{aligned} S_{n_{x_f},n_f;0,n_i} &= \lim_{t_0\to\infty}\int_0^{2\pi}\frac{dq_{x_i}}{2\pi}exp\left(\frac{i}{\hbar}\left[\Psi_{t_0}+\bar{q}_{x_{t_0}}(I_{x_{t_0}}-\hbar n_{x_f})\right]\right) \\ &\quad \int_0^{2\pi}\prod_{j=1}^{N}\frac{dq_{j_i}}{2\pi}exp\left(\frac{i}{\hbar}\left[\Xi_{t_0}+\sum_{j=1}^{N}\bar{q}_{j_{t_0}}\left(I_{j_{t_0}}-\hbar\left(n_{j_f}+\frac{1}{2}\right)\right)\right]\right) \\ &= A\times B \end{aligned} \tag{81}$$

The terms are defined as:

$$A = \lim_{t_0\to\infty}\int_0^{2\pi}\frac{dq_{x_i}}{2\pi}exp\left(\frac{i}{\hbar}\left[\Psi_{t_0}+\bar{q}_{x_{t_0}}(I_{x_{t_0}}-\hbar n_{x_f})\right]\right) \tag{82}$$

and

$$B = \lim_{t_0\to\infty}\int_0^{2\pi}\prod_{j=1}^{N}\frac{dq_{j_i}}{2\pi}exp\left(\frac{i}{\hbar}\left[\Xi_{t_0}+\sum_{j=1}^{N}\bar{q}_{j_{t_0}}\left(I_{j_{t_0}}-\hbar\left(n_{j_f}+\frac{1}{2}\right)\right)\right]\right) \tag{83}$$

20.6 The System Term of the S-Matix Element

20.6.1 The Phase Function for the System

We now consider the phase function Ψ_{t_0}(Eq. 78) in the limit $t_0 \to \infty$.

Miller has shown [41] that:

$$\frac{\partial\Psi_{t_0}}{\partial q_{x_{-t_0}}} = -\bar{q}_{x_{t_0}}\frac{\partial I_{x_{t_0}}}{\partial q_{x_{-t_0}}} \tag{84}$$

For the first order contribution we have:

$$\frac{\partial\Psi_{t_0,1}}{\partial q_{x_{-t_0}}} = -\bar{q}_{x_{t_0},0}\frac{\partial I_{x_{t_0,1,0}}}{\partial q_{x_{-t_0}}} \tag{85}$$

(The term $\frac{\partial I_{x_{t_0,0,0}}}{\partial q_{x_{-t_0}}}$vanishes because we have shown that $I_{x_{t_0,0,0}}$ is a constant - Eq. 48).

We can integrate in the limit $t_0 \to \infty$ to obtain:

$$\Psi_{\infty,1} = -\int_{-\infty}^{+\infty} dq_{x_{-t_0}}\ \bar{q}_{x_{t_0},0,0}\frac{\partial I_{x_{t_0},1,0}}{\partial q_{x_{-t_0}}} \tag{86}$$

We use integration by parts ($\int udv = uv - \int vdu$) to obtain:

$$\Psi_{\infty,1} = -\ \bar{q}_{x_\infty,0,0}I_{x_\infty,1,0} + \int_{-\infty}^{+\infty} dq_{x_{-t_0}}\ I_{x_{t_0},1,0}\frac{\partial\bar{q}_{x_{t_0,0,0}}}{\partial q_{x_{-t_0}}} \tag{87}$$

we substitute the 0th order approximation for the horizontal coordinate, Eq. 49 (converted to the conjugate variable):

$$\Psi_{\infty,1} = -\ \bar{q}_{x_\infty,0,0}I_{x_\infty,1,0} + \int_{-\infty}^{+\infty} dq_{x_{-t_0}}\ I_{x_{t_0},1,0}\frac{\partial\left(\frac{2\pi}{l}\left(x_{-t_0}+\frac{p_{x_i}}{M}(t+t_0)\right)\right)}{\partial q_{x_{-t_0}}} \tag{88}$$

and we obtain:

$$\Psi_{\infty,1} = -\bar{q}_{x_\infty,0,0} I_{x_\infty,1,0} + \int_{-\infty}^{+\infty} dq_{x_{-t_0}}\, I_{x_{t_0},1,0} \frac{\partial\left(q_{x_{-t_0}} + \frac{2\pi}{l}\frac{p_{x_i}}{M}(t+t_0)\right)}{\partial q_{x_{-t_0}}}$$

so that

$$\begin{aligned} \Psi_{\infty,1} &= -\bar{q}_{x_\infty,0,0} I_{x_\infty,1,0} + \int_{-\infty}^{+\infty} dq_{x_{-t_0}}\, I_{x_{t_0},1,0} \\ &= -\bar{q}_{x_\infty,0,0} I_{x_\infty,1,0} - h\hbar\, \sin(q_{x_i}) A(\omega_x) \end{aligned} \tag{89}$$

20.6.2 The Final Term for the System

We now evaluate the term in the parenthesis in the equation for the term A (Eq. 82)

$$\Psi_{t_0} + \bar{q}_{x_{t_0}}(I_{x_{t_0}} - \hbar n_{x_f}) = \Psi_{t_0,0} + \Psi_{t_0,1} + (\bar{q}_{x_{t_0},0} + \bar{q}_{x_{t_0},1})(I_{x_{t_0},0,0} + I_{x_{t_0},1,0} - \hbar n_{x_f}) \tag{90}$$

By definition the initial Bragg number is $I_{x_{t_0},0,0} = \hbar n_{x_i} = 0$.
We then obtain, ignoring terms of higher order:

$$\begin{aligned} \Psi_{t_0} + \bar{q}_{x_{t_0}}(I_{x_{t_0}} - \hbar n_{x_f}) &= \Psi_{t_0,0} + \Psi_{t_0,1} + (\bar{q}_{x_{t_0},0} + \bar{q}_{x_{t_0},1})(I_{x_{t_0},1,0} - \hbar n_{x_f}) \\ &= \Psi_{t_0,0} + \Psi_{t_0,1} + \bar{q}_{x_{t_0},0} I_{x_{t_0},1,0} - \bar{q}_{x_{t_0},0}\hbar n_{x_f} \\ &+ \bar{q}_{x_{t_0},1} I_{x_{t_0},1,0} - \bar{q}_{x_{t_0},1}\hbar n_{x_f} \\ &= \Psi_{t_0,0} + \Psi_{t_0,1} + \bar{q}_{x_{t_0},0} I_{x_{t_0},1,0} - \bar{q}_{x_{t_0},0}\hbar n_{x_f} \end{aligned} \tag{91}$$

The terms $\bar{q}_{x_{t_0},1} I_{x_{t_0},1,0}$ and $\bar{q}_{x_{t_0},1}\hbar n_{x_f}$ are ignored because they are higher than 1st order.
In the end we obtain:

$$\Psi_{t_0} + \bar{q}_{x_{t_0}}(I_{x_{t_0}} - \hbar n_{x_f}) = \Psi_{t_0,0} + \Psi_{t_0,1} + \bar{q}_{x_{t_0},0} I_{x_{t_0},1,0} - \bar{q}_{x_{t_0},0}\hbar n_{x_f} \tag{92}$$

we substitute ∞ for t_0 and also put in the term for $\Psi_{\infty,1}$:

$$\begin{aligned}\Psi_\infty + \bar{q}_{x_\infty}(I_{x_\infty} - \hbar n_{x_f}) &= \Psi_{\infty,0} - \bar{q}_{x_\infty,0,0} I_{x_\infty,1,0} - h\hbar\, sin\,(q_{x_i}) A(\omega_x) + \bar{q}_{x_\infty,0} I_{x_\infty,1,0} - \bar{q}_{x_\infty,0}\hbar n_{x_f} \\ &= \Psi_{\infty,0} - h\hbar\, sin\,(q_{x_i}) A(\omega_x) - \bar{q}_{x_\infty,0}\hbar n_{x_f} \end{aligned} \tag{93}$$

We evaluate the term $\bar{q}_{x_\infty,0}$ using its definition in Eq. 29 :

$$\bar{q}_{x_\infty,0} = q_{x_{t_0},0} + \frac{M z_{t_0}\omega_x}{p_{z_i}} \tag{94}$$

We substitute the value for the 0th order approximation of $\bar{q}_{x_\infty,0}$:

$$\bar{q}_{x_\infty,0} = \frac{2\pi}{l}(x_0 + \frac{p_{x_i}}{M} t_0) + \frac{M z_{t_0}\omega_x}{p_{z_i}} \tag{95}$$

and use the definition $\omega_x = \frac{2\pi}{lM} p_{x_i}$ to obtain:

$$\bar{q}_{x_\infty,0} = q_{x_i} + \omega_x t_0 + \frac{M z_{t_0}\omega_x}{p_{z_i}} \tag{96}$$

We substitute $\bar{q}_{x_\infty,0}$ into the whole term in the parenthesis of A as shown above:

$$\begin{aligned}\Psi_\infty + \bar{q}_{x_\infty}(I_{x_\infty} - \hbar n_{x_f}) &= \Psi_{\infty,0} - h\hbar\, sin\,(q_{x_i}) A(\omega_x) \\ &- \left(q_{x_i} + \omega_x t_0 + \frac{M z_{t_0}\omega_x}{p_{z_i}} \right) \hbar n_{x_f} \\ &= \Upsilon_{\infty,0} - h\hbar\, sin\,(q_{x_i}) A(\omega_x) - q_{x_i}\hbar n_{x_f} \end{aligned} \tag{97}$$

where we defined a new constant phase term which we called $\Upsilon_{\infty,0}$:

$$\Upsilon_{\infty,0} = \Psi_{\infty,0} + \left(\omega_x t_0 + \frac{M z_{t_0} \omega_x}{p_{z_i}}\right) \hbar n_{x_f} \tag{98}$$

we plug this into the equation for A:

$$A = exp\left(\frac{i}{\hbar}\left[\Upsilon_{\infty,0}\right]\right) \int_0^{2\pi} \frac{dq_{x_i}}{2\pi} exp\left(i\left[-q_{x_i} n_{x_f} - hA(\omega_x)\, sin\left(q_{x_i}\right)\right]\right) \tag{99}$$

we use n for the final mode instead of n_{x_f},and use the definition of the Bessel function:

$$J_n(x) = \frac{1}{\pi} \int_0^{2\pi} exp(i(n\tau - x sin(\tau))\, d\tau \tag{100}$$

and also the identity:

$$J_{-n}(x) = (-1)^n J_n(x) \tag{101}$$

we obtain:

$$\begin{aligned} A &= exp\left(\frac{i}{\hbar}\left[\Upsilon_{\infty,0}\right]\right) \int_0^{2\pi} \frac{dq_{x_i}}{2\pi} exp\left(i\left[-q_{x_i} n - hA(\omega_x)\, sin\left(q_{x_i}\right)\right]\right) \\ &= exp\left(\frac{i}{\hbar}\left[\Upsilon_{\infty,0}\right]\right) (-1)^n J_n\left(hA(\omega_x)\right) \end{aligned} \tag{102}$$

We wish to evaluate the square of the absolute value of A:

$$|A|^2 = J_n^2\left(hA(\omega_x)\right) \tag{103}$$

and we finally obtain that the square of the absolute value of A is simply the square of a Bessel function.

20.7 The Bath Term of the S-Matrix Element

We continue with the treatment of the bath term B and its phase function Ξ_{t_0} (Eq. 83).

20.7.1 The Phase Function for the Bath

We now consider the phase function Ξ_{t_0}(Eq. 78) in the limit $t_0 \to \infty$.

$$\Xi_{t_0} = -\int_{-\infty}^{\infty} dt\ [\sum_{j=1}^{N} q_{j_t} \dot{I}_{j_t}]. \tag{104}$$

Miller has shown[41] that:

$$\frac{\partial \Xi_{t_0}}{\partial q_{k_i}} = -\sum_{j=1}^{N} \bar{q}_{j_{t_0}} \frac{\partial I_{j_{t_0}}}{\partial q_{k_i}}$$

We see that the derivative by one variable q_{k_i}will give us only one term, the term of the derivative of I_k, and all other terms will cancel. This is due to the separability of the bath oscillators (each oscillator is independent of all others).

We take the limit that $t \to \infty$and obtain the first-order term:

$$\frac{\partial \Xi_{\infty,1}}{\partial q_{k_i}} = \bar{q}_{k_\infty,0} \frac{\partial I_{k_\infty,1}}{\partial q_{k_i}} \tag{105}$$

$$\frac{\partial \Xi_{\infty,1}}{\partial q_{k_i}} = \bar{q}_{k_\infty,0} \frac{\partial I_{k_\infty,1}}{\partial q_k} \frac{\partial q_k}{\partial q_{k_i}}$$

$$\frac{\partial \Xi_{\infty,1}}{\partial q_{k_i}} = \bar{q}_{k_\infty,0} \frac{\partial I_{k_\infty,1}}{\partial q_k} \frac{\partial (q_{k_i} + \omega_k t_0}{\partial q_{k_i}}$$

$$\frac{\partial \Xi_{\infty,1}}{\partial q_{k_i}} = \bar{q}_{k_\infty,0} \frac{\partial I_{k_\infty,1}}{\partial q_k} \tag{106}$$

We integrate to obtain $\Xi_{\infty,1}$. We first look at the contribution for the k-th oscillator:

$$\int \frac{\partial \Xi_{\infty,1}}{\partial q_{k_i}} = -\int \partial q_k\ \bar{q}_{k_\infty,0} \frac{\partial I_{k_\infty,1}}{\partial q_k} \tag{107}$$

we use integration by parts to obtain

$$\Xi_{\infty,1} = \sum_{k=1}^{N} \left[-\bar{q}_{k_\infty,0} I_{k_{\infty,1}} + \int \partial q_k\ I_{k_\infty,1} \frac{\partial \bar{q}_{k_\infty,0}}{\partial q_k} \right] \tag{108}$$

we substitute the value for $\bar{q}_{k_\infty,0}$:

$$\Xi_{\infty,1} = \sum_{k=1}^{N} \left[-\bar{q}_{k_\infty,0} I_{k_{\infty,1}} + \int \partial q_k \, I_{k_{\infty,1}} \frac{\partial (q_{k_\infty,0} - \frac{M z_{\infty,0} \omega_k}{p_{z_{\infty,0}}})}{\partial q_k} \right] \tag{109}$$

and then:

$$\Xi_{\infty,1} = -\sum_{k=1}^{N} \bar{q}_{k_\infty,0} I_{k_{\infty,1}} + \sum_{k=1}^{N} \int \partial q_k \, I_{k_{\infty,1}} \tag{110}$$

Substituting the formula for $I_{k_{\infty,1}}$(Eq. 75):

$$\Xi_{\infty,1} = -\sum_{k=1}^{N} \bar{q}_{k_\infty,0} I_{k_{\infty,1}} - \sum_{k=1}^{N} c_k \sqrt{\frac{2I_k}{M\omega_k}} A(\omega_k) \int \partial q_k sin(q_k)$$

$$\Xi_{\infty,1} = -\sum_{k=1}^{N} \bar{q}_{k_\infty,0} I_{k_{\infty,1}} + \sum_{k=1}^{N} c_k \sqrt{\frac{2I_k}{M\omega_k}} A(\omega_k) cos(q_k). \tag{111}$$

We use the notation

$$\bar{A}_j \left(n_{j_{if}} \right) = c_j \sqrt{\frac{2\hbar \left(n_{j_{if}} + \frac{1}{2} \right)}{M\omega_j}} A \left(\omega_j \right) \tag{112}$$

where we have chosen:

$$n_{j_{if}} = \frac{n_{j_i} + n_{j_f}}{2} \tag{113}$$

to make the transition probability microscopically reversible, to obtain:

$$\Xi_{\infty,1} = -\sum_{k=1}^{N} \bar{q}_{k_\infty,0} I_{k_{\infty,1}} + \sum_{k=1}^{N} \bar{A}_k \left(n_{j_{if}} \right) cos(q_k). \tag{114}$$

The total contribution to Ξ_∞ is then

$$\Xi_\infty = \Xi_{\infty,0} + \Xi_{\infty,1} \tag{115}$$

We need to evaluate the all of the terms in the complex exponent of B. These terms are:

$$\Xi_{t_0} + \sum_{j=1}^{N} \bar{q}_{j_{t_0}} \left(I_{j_{t_0}} - \hbar \left(n_{j_f} + \frac{1}{2} \right) \right) \tag{116}$$

We evaluate these terms by first substituting the 0th and 1st order approximations for Ξ_{t_0}(and looking at$t \to \infty$):

$$\Xi_{\infty,0} - \sum_{k=1}^{N} \bar{q}_{k_\infty,0} I_{k_{\infty,1}} + \sum_{k=1}^{N} \bar{A}_k \left(n_{j_{if}}\right) cos(q_k) + \sum_{j=1}^{N} \bar{q}_{j_\infty} \left(I_{j_\infty} - \hbar \left(n_{j_f} + \frac{1}{2}\right)\right) \tag{117}$$

we expand the last term and put the different orders of $\bar{q}_{j_\infty}$:

$$\Xi_{\infty,0} - \sum_{k=1}^{N} \bar{q}_{k_\infty,0} I_{k_{\infty,1}} + \sum_{k=1}^{N} \bar{A}_k \left(n_{j_{if}}\right) cos(q_k) + \sum_{j=1}^{N} (\bar{q}_{j_{\infty,},0} I_{j_\infty,0} + \bar{q}_{j_{\infty,},1} I_{j_\infty,0} + \bar{q}_{j_{\infty,},0} I_{j_\infty,1}) - \sum_{j=1}^{N} (\bar{q}_{j_\infty,0} + \bar{q}_{j_\infty,1}) \hbar \left(n_{j_f} + \frac{1}{2}\right) \tag{118}$$

Noting that

$$I_{j_\infty,0} = I_{j_i} = \hbar(n_{j_i} + \frac{1}{2}) \tag{119}$$

we obtain that expression (118) reduces to:

$$\Xi_{\infty,0} + \sum_{k=1}^{N} \bar{A}_k \left(n_{j_{if}}\right) cos(q_k) + \sum_{j=1}^{N} (\bar{q}_{j_{\infty,},0} + \bar{q}_{j_{\infty,},1}) \hbar \left(n_{j_i} - n_{j_f}\right) \tag{120}$$

We neglect the 2nd-order term $\bar{q}_{j_{\infty,},1} \hbar \left(n_{j_i} - n_{j_f}\right)$ and obtain:

$$\Xi_{\infty,0} + \sum_{k=1}^{N} \bar{A}_k \left(n_{j_{if}}\right) cos(q_k) + \sum_{j=1}^{N} (\bar{q}_{j_{\infty,},0}) \hbar \left(n_{j_i} - n_{j_f}\right) \tag{121}$$

We use the definition of$\bar{q}_{j_{\infty,},0}$ (similar to the definition in Eq. 96, using Eq. 69 and Eq. 76), which is:

$$\bar{q}_{j_\infty,0} = q_j + \omega_j t_0 + \frac{M z_{t_0,0} \omega_j}{p_{z_{t_0},0,0}} \tag{122}$$

to find:

$$\Xi_{\infty,0} + \sum_{k=1}^{N} \bar{A}_k \left(n_{j_{if}}\right) cos(q_k) + \sum_{j=1}^{N} q_j \hbar \left(n_{j_i} - n_{j_f}\right) + \sum_{j=1}^{N} \left(\omega_j t_0 + \frac{M z_{t_0,0} \omega_j}{p_{z_{t_0},0,0}}\right) \hbar \left(n_{j_i} - n_{j_f}\right). \tag{123}$$

20.7.2 The Final Term for the Bath

We now look again at the term B, and substitute the term in the complex exponent:

$$B = \int_0^{2\pi} \prod_{j=1}^{N} \frac{dq_{j_i}}{2\pi} exp\left(\frac{i}{\hbar}\left[\Xi_{\infty,0} + \sum_{j=1}^{N}\left(\omega_j t_0 + \frac{M z_{t_0,0}\omega_j}{p_{z_{t_0},0,0}}\right)\hbar\left(n_{j_i} - n_{j_f}\right)\right]\right)$$
$$\cdot exp\left(\frac{i}{\hbar}\left[\sum_{k=1}^{N}\bar{A}_j\left(n_{j_{if}}\right)cos(q_j) + \sum_{j=1}^{N} q_j\hbar\left(n_{j_i} - n_{j_f}\right)\right]\right) \quad (124)$$

When we consider $|B|^2$ all the terms on the first line will cancel as they are independent of the integrand. We use this form of the Bessel function:

$$\frac{1}{2\pi}\int_0^{2\pi} dx\, exp(inx + iAcos\, x) = (-1)^n exp\left(-i\frac{n\pi}{2}\right) J_n(A) \quad (125)$$

to obtain:

$$|B|^2 = \prod_{j=1}^{N} J_{n_{j_i} - n_{j_f}}\left(\bar{A}_j(n_{j_{if}})\right) \quad (126)$$

(we remind ourselves that $n_{j_{if}}$ was previously defined in Eq. 113).

20.8 The Final S-Matrix Element

$$\left|S_{n,\mathbf{n}_f;0,\mathbf{n}_i}\right|^2 = |AB|^2 \quad (127)$$
$$= J_n^2\left(hA(\omega_x)\right)\prod_{j=1}^{N} J^2_{n_{j_f} - n_{j_i}}\left(\bar{A}_j\left(n_{j_{if}}\right)\right) \quad (128)$$

21 The Discretized Theory for the Bath

21.1 Thermal Averaging for the SCP

All that remains to be done is to perform the summation over final bath states and averaging over initial bath states to obtain the final momentum distribution and the related angular distribution. For this purpose, using the notation

$$\tan\theta\,(n) = \frac{2\pi\hbar n}{l\,|p_{z_i}|} \quad (129)$$

we note that energy conservation (Eq. 12) implies that the final vertical momentum is a function of the initial vertical momentum, the Bragg quantum number and the initial and final horizontal and bath actions:

$$p_{z_{t_0}}^2 = |p_{z_i}|^2 \left[\frac{\cos\left(|\theta_i| + 2\theta\left(n\right)\right)}{\cos|\theta_i|\cos^2\theta\left(n\right)} - \frac{2M\hbar\Delta\mathbf{n}\cdot\omega}{|p_{z_i}|^2} \right] \tag{130}$$

$$\equiv |p_{z_i}|^2 \zeta\left(n, \Delta\mathbf{n}\cdot\omega\right)^2 \tag{131}$$

and energy conservation imposes the condition that

$$\zeta\left(n, \Delta\mathbf{n}\cdot\omega\right) \geq 0. \tag{132}$$

Inserting unity as $1 = \int_{-\infty}^{\infty} d\bar{\Omega}\delta\left(\bar{\Omega} - \Delta\mathbf{n}\cdot\omega\right)$ and then using the Fourier representation of the Dirac delta function implies that the thermally averaged final momentum distribution may be rewritten as (with $H\left(x\right)$ denoting the unit step function):

$$\left\langle P(p_{x_f}, p_{z_f})\right\rangle_\beta = \sum_n \int_{-\infty}^{\infty} d\bar{\Omega}\delta(p_{x_f} - p_{x_i} - \frac{2\pi\hbar n}{l})\,\delta(p_{z_f} - |p_{z_i}|\,\zeta\left(n,\bar{\Omega}\right))H\left(\zeta\left(n,\bar{\Omega}\right)\right)\tilde{F}\left(\bar{\Omega},\beta,n\right) \tag{133}$$

$$\tag{134}$$

All the dynamical information is hidden within the "form factor" $F\left(\tau,\beta,n\right)$ defined as:

$$F\left(\tau,\beta,n\right) = \frac{1}{Z_B}\sum_{n_i=0}^{\infty}\sum_{n_f=0}^{\infty} P_{n,n_f;0,n_i} \exp\left[-i\tau\Delta\mathbf{n}\cdot\omega - \beta\hbar\left(\left(\mathbf{n}_i + \frac{1}{2}\mathbf{I}\right)\cdot\omega\right)\right] \tag{135}$$

with

$$\tilde{F}\left(\bar{\Omega},\beta,n\right) = \frac{1}{2\pi}\int_{-\infty}^{\infty} d\tau \exp\left(i\tau\bar{\Omega}\right) F\left(\tau,\beta,n\right). \tag{136}$$

21.2 The Thermally Averaged Angular Distribution

The associated angular distribution is

$$\left\langle P(\theta_f)\right\rangle_\beta = \sum_n \int_{-\infty}^{\infty} d\bar{\Omega}\delta\left(\theta_f - \tan^{-1}\left(\frac{p_{x_i} + \frac{2\pi\hbar n}{l}}{|p_{z_i}|\,\zeta\left(n,\bar{\Omega}\right)}\right)\right) H\left(\zeta\left(n,\bar{\Omega}\right)\right)\tilde{F}\left(\bar{\Omega},\beta,n\right). \tag{137}$$

We use the relations:

$$p_{z_i} = -\sqrt{2ME_i}cos\,|\theta_i| \tag{138}$$

$$p_{x_i} = \sqrt{2ME_i}sin\,|\theta_i| \tag{139}$$

and the definition of $tan\theta(n)$ in Eq. 129.
such that:

$$\begin{aligned} \frac{2\pi\hbar n}{l} &= |p_{z_i}|tan\theta(n) \\ &= \sqrt{2ME_i}cos\,|\theta_i|tan\theta(n) \end{aligned} \tag{140}$$

to see that:

$$\begin{aligned} p_{x_f} = x_i + \frac{2\pi\hbar n}{l} &= \sqrt{2ME_i}sin\,|\theta_i| + \sqrt{2ME_i}cos\,|\theta_i|tan\theta(n) \\ &= \sqrt{2ME_i}\left[sin\,|\theta_i| + cos\,|\theta_i|tan\theta(n)\right] \\ &= \sqrt{2ME_i}\left[sin\,|\theta_i| + cos\,|\theta_i|\,\frac{sin\theta(n)}{cos\theta(n)}\right] \\ &= \sqrt{2ME_i}\left[\frac{sin\,|\theta_i|cos\theta(n) + cos\,|\theta_i|sin\theta(n)}{cos\theta(n)}\right] \\ &= \sqrt{2ME_i}\left[\frac{sin(|\theta_i| + \theta(n))}{cos\theta(n)}\right] \end{aligned} \tag{141}$$

We also have from energy conservation:

$$\begin{aligned} p_{z_{t_0}}^2 &= |p_{z_i}|^2\left[\frac{\cos\left(|\theta_i| + 2\theta\left(n\right)\right)}{\cos|\theta_i|\cos^2\theta\left(n\right)} - \frac{2M\hbar\Delta\mathbf{n}\cdot\boldsymbol{\omega}}{|p_{z_i}|^2}\right] \\ &\equiv |p_{z_i}|^2\,\zeta\left(n, \Delta\mathbf{n}\cdot\boldsymbol{\omega}\right)^2 \end{aligned} \tag{142}$$

We take the square root to get $p_{z_{t_0}}$

$$
\begin{aligned}
p_{z_{t_0}} &= \sqrt{|p_{z_i}|^2}\sqrt{\frac{\cos\left(|\theta_i|+2\theta\left(n\right)\right)}{\cos|\theta_i|\cos^2\theta\left(n\right)}-\frac{2M\hbar\Delta\mathbf{n}\cdot\omega}{|p_{z_i}|^2}} \\
&= \sqrt{|p_{z_i}|^2\frac{\cos\left(|\theta_i|+2\theta\left(n\right)\right)}{\cos|\theta_i|\cos^2\theta\left(n\right)}-|p_{z_i}|^2\frac{2M\hbar\Delta\mathbf{n}\cdot\omega}{|p_{z_i}|^2}} \\
&= \sqrt{|p_{z_i}|^2\frac{\cos\left(|\theta_i|+2\theta\left(n\right)\right)}{\cos|\theta_i|\cos^2\theta\left(n\right)}-2M\hbar\Delta\mathbf{n}\cdot\omega} \\
&= \sqrt{\left[\sqrt{2ME_i}cos\,||\theta_i|\right]^2\frac{\cos\left(|\theta_i|+2\theta\left(n\right)\right)}{\cos|\theta_i|\cos^2\theta\left(n\right)}-2M\hbar\Delta\mathbf{n}\cdot\omega} \\
&= \sqrt{2ME_i cos\,||\theta_i|^2\frac{\cos\left(|\theta_i|+2\theta\left(n\right)\right)}{\cos|\theta_i|\cos^2\theta\left(n\right)}-2M\hbar\Delta\mathbf{n}\cdot\omega} \\
&= \sqrt{2M\hbar}\sqrt{E_i cos\,||\theta_i|\frac{\cos\left(|\theta_i|+2\theta\left(n\right)\right)}{\hbar\cos^2\theta\left(n\right)}-\Delta\mathbf{n}\cdot\omega}
\end{aligned}
\tag{143}
$$

We then define:

$$
\Omega(\theta_i,n)=E_i cos\,||\theta_i|\frac{\cos\left(|\theta_i|+2\theta\left(n\right)\right)}{\hbar\cos^2\theta\left(n\right)} \tag{144}
$$

to obtain:

$$
p_{z_{t_0}} = \sqrt{2M\hbar}\sqrt{\Omega(\theta_i,n)-\Delta\mathbf{n}\cdot\omega} \tag{145}
$$

We then make the substitution for $p_{z_{t_0}}$ and p_{x_f} and use the identities $\delta(\theta-tan^{-1}(\alpha))=\frac{1}{cos^2\theta}\delta(\alpha-tan\theta)$ and $\delta(\sqrt{x}-a)=2\sqrt{x}\delta(x-a^2)$ to see that:

$$
\begin{aligned}
\left\langle P(\theta_f)\right\rangle_\beta &= \sum_n \frac{2E_i\sin^2\left(|\theta_i|+\theta\left(n\right)\right)}{\hbar\cos^2\theta\left(n\right)\sin^2\theta_f\tan\theta_f} \\
&\quad\cdot\int_{-\infty}^{\infty}d\bar{\Omega}\delta\left(\bar{\Omega}-\frac{E_i}{\hbar}\left[1-\frac{\sin^2\left(|\theta_i|+\theta\left(n\right)\right)}{\sin^2\theta_f\cos^2\theta\left(n\right)}\right]\right)H\left(\zeta\left(n,\bar{\Omega}\right)\right)\tilde{F}\left(\bar{\Omega},\beta,n\right)
\end{aligned}
\tag{146}
$$

with

$$E_i = \frac{p_{x_i}^2 + p_{z_i}^2}{2M}. \tag{147}$$

and the δ-function enforces the definition:

$$\begin{aligned} \bar{\Omega}(\theta_f, \theta_i, n) &= \left[\Omega(\theta_i, n) - \frac{E_i sin^2(|\theta_i| + \theta(n))}{\hbar cos^2\theta(n) tan^2\left(\theta_f\right)}\right] \\ &= \frac{E_i}{\hbar}\left[1 - \frac{sin^2(|\theta_i| + \theta(n))}{cos^2\theta(n) sin^2\left(\theta_f\right)}\right] \end{aligned} \tag{148}$$

21.3 Factorization of the Transition Probability

Eq. 146 is exact in principle. However, within the semiclassical perturbation theory the transition probability factorizes so that one may rewrite the form factor in terms of a product of separate form factors for each bath oscillator:

$$F(\tau, \beta, n) = J_n^2(hA(\omega_x)) \prod_{j=1}^{N} f_j(\tau, \beta) \tag{149}$$

with

$$f_j(\tau, \beta) = \left[1 - \exp\left(-\hbar\beta\omega_j\right)\right] \sum_{n_{j_i}=0}^{\infty} \sum_{n_{j_f}=0}^{\infty} \exp\left[-n_{j_i}\hbar\beta\omega_j - i\tau\omega_j\left(n_{j_f} - n_{j_i}\right)\right] J_{n_{j_f}-n_{j_i}}^2\left(\bar{A}_j\left(n_{j_{if}}\right)\right). \tag{150}$$

Eqs. 149 and 150 are central to the numerical computations which will be presented below. However, first we consider their simplification resulting from the fact that the coupling to the bath modes is weak.

21.4 Perturbation Expansion

We start by making approximations to the Bessel functions, which we'll need later on. The definition of the zero-th and first order Bessel function are given by:

$$J_0(x) = \sum_{m=0}^{\infty} \frac{(-1)^m x^{2m}}{2^{2m}(m!)^2} \tag{151}$$

$$J_1(x) = \frac{x}{2} \sum_{m=0}^{\infty} \frac{(-1)^m x^{2m}}{2^{2m}(m+1)!m!} \tag{152}$$

We consider the term $J_0^2\left(hA(\omega_x)\right)$ and expand it to up to first order (m=0, m=1):

$$\begin{aligned} J_0^2\left(hA(\omega_x)\right) &\approx \left[\sum_{m=0}^{m=1}\frac{(-1)^m(hA(\omega_x))^{2m}}{2^{2m}(m!)^2}\right]^2 = \left[\frac{1}{1}+\frac{(-1)(hA(\omega_x))^2}{2^2(1!)^2}\right]^2 \\ &= \left[1-\frac{(hA(\omega_x))^2}{4}\right]^2 \end{aligned} \tag{153}$$

We expand the terms in the parenthesis, and keep terms up to first order:

$$\begin{aligned} J_0^2\left(hA(\omega_x)\right) &\approx 1-2\frac{(hA(\omega_x))^2}{4}+\left[\frac{(hA(\omega_x))^2}{4}\right]^2 \\ &\approx 1-\frac{h^2A(\omega_x)^2}{2} \end{aligned} \tag{154}$$

If the argument of the Bessel function is given as in $J_0^2\left(\bar{A}_j\left(n_{j_{if}}\right)\right)$ then we have:

$$J_0^2\left(\bar{A}_j\left(n_{j_{if}}\right)\right) \approx 1-\frac{\bar{A}_j\left(n_{j_{if}}\right)^2}{2} \tag{155}$$

We now consider the term $J_1^2\left(hA(\omega_x)\right)$ and expand it to up to first order (m=0, m=1):

$$
\begin{aligned}
J_1^2\left(hA(\omega_x)\right) &\approx \left\{\frac{hA(\omega_x)}{2}\sum_{m=0}^{m=1}\frac{(-1)^m(hA(\omega_x))^{2m}}{2^{2m}(m+1)!m!}\right\}^2 \\
&= \left\{\frac{hA(\omega_x)}{2}\left[1+\frac{(-1)(hA(\omega_x))^2}{2^2(1+1)!1!}\right]\right\}^2 \\
&= \left\{\frac{hA(\omega_x)}{2}\left[1-\frac{(hA(\omega_x))^2}{8}\right]\right\}^2 \\
&= \left\{\frac{hA(\omega_x)}{2}-\frac{hA(\omega_x)}{2}\frac{(hA(\omega_x))^2}{8}\right\}^2 \\
&= \left\{\frac{hA(\omega_x)}{2}-\frac{(hA(\omega_x))^3}{16}\right\}^2 \\
&= \frac{h^2A(\omega_x)^2}{4}-2\frac{hA(\omega_x)}{2}\frac{(hA(\omega_x))^3}{16}+\frac{(hA(\omega_x))^6}{16^2} \\
&\approx \frac{h^2A(\omega_x)^2}{4}
\end{aligned}
\tag{156}
$$

If the argument of the Bessel function is given as in $J_1^2\left(\bar{A}_j\left(n_{j_{if}}\right)\right)$ then we have:

$$
J_1^2\left(\bar{A}_j\left(n_{j_{if}}\right)\right) \approx \frac{\bar{A}_j\left(n_{j_{if}}\right)^2}{4} \tag{157}
$$

21.4.1 Zero Phonon Transitions

We first consider zero-phonon transitions, i.e. $n_{j_i}=n_{i_f}$, no change in the final state of the oscillator. From the factorization of the form factor we may treat separately the different contribution to the form factor from each oscillator. We substitute the $n_{j_i}-n_{j_f}=0$ to obtain:

$$
f_j(\tau,\beta,\Delta n=0)=\left[1-\exp\left(-\hbar\beta\omega_j\right)\right]\sum_{n_{j_i}=0}^{\infty}\sum_{n_{j_f}=0}^{\infty}\exp\left[-n_{j_i}\hbar\beta\omega_j\right]J_0^2\left(\bar{A}_j\left(n_{j_{if}}\right)\right). \tag{158}
$$

And approximate the Bessel function:

$$
f_j(\tau,\beta,\Delta n=0)=\left[1-\exp\left(-\hbar\beta\omega_j\right)\right]\sum_{n_{j_i}=0}^{\infty}\sum_{n_{j_f}=0}^{\infty}\exp\left[-n_{j_i}\hbar\beta\omega_j\right]\left[1-\frac{\bar{A}_j\left(n_{j_{if}}\right)^2}{2}\right]. \tag{159}
$$

We expand to two terms and reduce to one summation over n_j

$$\begin{aligned} f_j(\tau,\beta,\Delta n=0) &= \left[1-\exp\left(-\hbar\beta\omega_j\right)\right]\sum_{n_j=0}^{\infty}\exp\left[n_j(-\hbar\beta\omega_j)\right] \\ &\quad -\left[1-\exp\left(-\hbar\beta\omega_j\right)\right]\sum_{n_j=0}^{\infty}\exp\left[-n_j\hbar\beta\omega_j\right]\frac{\bar{A}_j\left(n_j\right)^2}{2} \end{aligned} \tag{160}$$

The first term is a sum of an infinite geometric series.

$$\begin{aligned} f_j(\tau,\beta,\Delta n=0) &= \left[1-\exp\left(-\hbar\beta\omega_j\right)\right]\sum_{n_j=0}^{\infty}\left\{\exp\left[(-\hbar\beta\omega_j)\right]\right\}^{n_j} \\ &\quad -\left[1-\exp\left(-\hbar\beta\omega_j\right)\right]\sum_{n_j=0}^{\infty}\exp\left[-n_j\hbar\beta\omega_j\right]\frac{\bar{A}_j\left(n_j\right)^2}{2} \end{aligned} \tag{161}$$

And the series is given by the series sum formula:

$$\begin{aligned} f_j(\tau,\beta,\Delta n=0) &= \left[1-\exp\left(-\hbar\beta\omega_j\right)\right]\frac{1}{1-\exp\left[(-\hbar\beta\omega_j)\right]} \\ &\quad -\left[1-\exp\left(-\hbar\beta\omega_j\right)\right]\sum_{n_j=0}^{\infty}\exp\left[-n_j\hbar\beta\omega_j\right]c_j^2\frac{\hbar\left(n_j+\frac{1}{2}\right)}{M\omega_j}A\left(\omega_j\right)^2 \end{aligned} \tag{162}$$

$$f_j(\tau,\beta,\Delta n=0) = 1-\frac{c_j^2\hbar A\left(\omega_j\right)^2\left[1-\exp\left(-\hbar\beta\omega_j\right)\right]}{M\omega_j}\sum_{n_j=0}^{\infty}\exp\left[-n_j\hbar\beta\omega_j\right]\left(n+\frac{1}{2}\right) \tag{163}$$

We expand $\left(n+\frac{1}{2}\right)$:

$$f_j(\tau,\beta,\Delta n=0) = 1-\frac{c_j^2\hbar A\left(\omega_j\right)^2\left[1-\exp\left(-\hbar\beta\omega_j\right)\right]}{M\omega_j}\left[\sum_{n_j=0}^{\infty}n_j\ \left\{\exp\left[-\hbar\beta\omega_j\right]\right\}^{n_j}+\frac{1}{2}\sum_{n_j=0}^{\infty}\left\{\exp\left[-\hbar\beta\omega_j\right]\right\}^{n_j}\right] \tag{164}$$

Again the first term is a series, of the form $\sum_{n=0}^{\infty} n\,x^n = \frac{x}{(1-x)^2}$ and the second is a series like before:

$$f_j(\tau,\beta,\Delta n=0) = 1-\frac{c_j^2\hbar A\left(\omega_j\right)^2\left[1-\exp\left(-\hbar\beta\omega_j\right)\right]}{M\omega_j}\left[\frac{\exp\left[-\hbar\beta\omega_j\right]}{(1-\exp\left[-\hbar\beta\omega_j\right])^2}+\frac{1}{2}\,\frac{1}{1-\exp\left[-\hbar\beta\omega_j\right]}\right] \quad (165)$$

We simplify to get:

$$f_j(\tau,\beta,\Delta n=0) = 1-\frac{c_j^2\hbar A\left(\omega_j\right)^2}{2M\omega_j}\left[\frac{2\exp\left[-\hbar\beta\omega_j\right]+1-\exp\left[-\hbar\beta\omega_j\right]}{(1-\exp\left[-\hbar\beta\omega_j\right])}\right] \quad (166)$$

And simplify some more:

$$f_j(\tau,\beta,\Delta n=0) = 1-\frac{c_j^2\hbar A\left(\omega_j\right)^2}{2M\omega_j}\left[\frac{1+\exp\left[-\hbar\beta\omega_j\right]}{1-\exp\left[-\hbar\beta\omega_j\right]}\right] \quad (167)$$

We use the definition of coth(x):

$$coth(x)=\frac{1+exp(-2x)}{1-exp(-2x)} \quad (168)$$

To get:

$$f_j(\tau,\beta,\Delta n=0) = 1-\frac{c_j^2\hbar A\left(\omega_j\right)^2}{2M\omega_j}coth(\hbar\beta\omega_j/2) \quad (169)$$

21.4.2 One Phonon Transitions

For one phonon transitions we have two options: an oscillator losing a phonon, and an oscillator gaining a phonon.

We will consider both options. Again, from the factorization of the form factor we may treat separately the different contribution to the form factor from each oscillator. We substitute $n_{j_f}-n_{j_i}=1$ to obtain the following, and follow steps similar to the above for zero-phonon contributions:

$$
\begin{aligned}
f_j(\tau,\beta,\Delta n=1) &= \left[1-\exp\left(-\hbar\beta\omega_j\right)\right]\sum_{n_{j_i}=0}^{\infty}\sum_{n_{j_f}=0}^{\infty}\exp\left[-n_{j_i}\hbar\beta\omega_j-i\tau\omega_j\right]J_1^2\left(\bar{A}_j\left(n_{j_{if}}\right)\right). \\
&= \left[1-\exp\left(-\hbar\beta\omega_j\right)\right]\sum_{n_{j_i}=0}^{\infty}\sum_{n_{j_f}=0}^{\infty}\exp\left[-n_{j_i}\hbar\beta\omega_j-i\tau\omega_j\right]\frac{\bar{A}_j\left(n_{j_{if}}\right)^2}{4} \\
&= \left[1-\exp\left(-\hbar\beta\omega_j\right)\right]\sum_{n_{j_i}=0}^{\infty}\sum_{n_{j_f}=0}^{\infty}\exp\left[-n_{j_i}\hbar\beta\omega_j-i\tau\omega_j\right]\frac{\left[\frac{2c_j^2\hbar\left(\frac{n_{j_i}+n_{j_f}}{2}+\frac{1}{2}\right)A^2\left(\omega_j\right)}{M\omega_j}\right]}{4} \\
&= \left[1-\exp\left(-\hbar\beta\omega_j\right)\right]\frac{c_j^2\hbar A^2\left(\omega_j\right)}{2M\omega_j}\exp\left[-i\tau\omega_j\right]\sum_{n_{j_i}=0}^{\infty}\sum_{n_{j_f}=0}^{\infty}\exp\left[-n_{j_i}\hbar\beta\omega_j\right]\left(n_{j_i}+\frac{1}{2}+\frac{1}{2}\right) \\
&= \left[1-\exp\left(-\hbar\beta\omega_j\right)\right]\frac{c_j^2\hbar A^2\left(\omega_j\right)}{2M\omega_j}\exp\left[-i\tau\omega_j\right]\sum_{n_{j_i}=0}^{\infty}\left\{n_{j_i}\,\exp\left[-n_{j_i}\hbar\beta\omega_j\right]+\exp\left[-n_{j_i}\hbar\beta\omega_j\right]\right\} \\
&= \left[1-\exp\left(-\hbar\beta\omega_j\right)\right]\frac{c_j^2\hbar A^2\left(\omega_j\right)}{2M\omega_j}\exp\left[-i\tau\omega_j\right]\sum_{n_{j_i}=0}^{\infty}\left\{n_{j_i}\,\left\{\exp\left[-\hbar\beta\omega_j\right]\right\}^{n_{j_i}}+\left\{\exp\left[-\hbar\beta\omega_j\right]\right\}^{n_{j_i}}\right\} \\
&= \left[1-\exp\left(-\hbar\beta\omega_j\right)\right]\frac{c_j^2\hbar A^2\left(\omega_j\right)}{2M\omega_j}\exp\left[-i\tau\omega_j\right]\left\{\frac{\exp\left[-\hbar\beta\omega_j\right]}{\left(1-\exp\left[-\hbar\beta\omega_j\right]\right)^2}+\frac{1}{1-\exp\left[-\hbar\beta\omega_j\right]}\right\} \\
&= \frac{c_j^2\hbar A^2\left(\omega_j\right)}{2M\omega_j}\exp\left[-i\tau\omega_j\right]\left\{\frac{\exp\left[-\hbar\beta\omega_j\right]}{\left(1-\exp\left[-\hbar\beta\omega_j\right]\right)}+1\right\} \\
&= \frac{c_j^2\hbar A^2\left(\omega_j\right)}{2M\omega_j}\exp\left[-i\tau\omega_j\right]\left\{\frac{\exp\left[-\hbar\beta\omega_j\right]+1-\exp\left[-\hbar\beta\omega_j\right]}{1-\exp\left[-\hbar\beta\omega_j\right]}\right\} \\
&= \frac{c_j^2\hbar A^2\left(\omega_j\right)}{2M\omega_j\left(1-\exp\left[-\hbar\beta\omega_j\right]\right)}\exp\left[-i\tau\omega_j\right] \qquad (170)
\end{aligned}
$$

We can also find a representation using the $coth(x)$ function:

$$
\begin{aligned}
f_j(\tau,\beta,\Delta n=1) &= \exp\left[-i\tau\omega_j\right]\frac{c_j^2\hbar A^2\left(\omega_j\right)}{2M\omega_j}2\left[\frac{2+\exp\left[-\hbar\beta\omega_j\right]-\exp\left[-\hbar\beta\omega_j\right]}{\left(1-\exp\left[-\hbar\beta\omega_j\right]\right)}\right] \\
&= \exp\left[-i\tau\omega_j\right]\frac{c_j^2\hbar A^2\left(\omega_j\right)}{2M\omega_j}2\left[\frac{1+\exp\left[-\hbar\beta\omega_j\right]+1-\exp\left[-\hbar\beta\omega_j\right]}{\left(1-\exp\left[-\hbar\beta\omega_j\right]\right)}\right] \\
&= \exp\left[-i\tau\omega_j\right]\frac{c_j^2\hbar A^2\left(\omega_j\right)}{2M\omega_j}2\left[\frac{1+\exp\left[-\hbar\beta\omega_j\right]}{\left(1-\exp\left[-\hbar\beta\omega_j\right]\right)}+1\right] \\
&= \exp\left[-i\tau\omega_j\right]\frac{c_j^2\hbar A^2\left(\omega_j\right)}{M\omega_j}\left[coth\left(\frac{\hbar\beta\omega_j}{2}\right)+1\right]
\end{aligned}
$$

Next, we substitute $n_{j_f}-n_{j_i}=-1$ to obtain the following, and follow steps similar to the above:

$$
f_j(\tau,\beta,\Delta n=-1) = \left[1-\exp\left(-\hbar\beta\omega_j\right)\right]\sum_{n_{j_i}=0}^{\infty}\sum_{n_{j_f}=0}^{\infty}\exp\left[-n_{j_i}\hbar\beta\omega_j+i\tau\omega_j\right]J_1^2\left(\bar{A}_j\left(n_{j_{if}}\right)\right).
$$

$$
f_j(\tau,\beta,\Delta n=-1) = \left[1-\exp\left(-\hbar\beta\omega_j\right)\right]\sum_{n_{j_i}=0}^{\infty}\sum_{n_{j_f}=0}^{\infty}\exp\left[-n_{j_i}\hbar\beta\omega_j+i\tau\omega_j\right]\frac{\bar{A}_j\left(n_{j_{if}}\right)^2}{4}
$$

$$
\begin{aligned}
f_j(\tau,\beta,\Delta n=-1) &= \left[1-\exp\left(-\hbar\beta\omega_j\right)\right]\sum_{n_{j_i}=0}^{\infty}\sum_{n_{j_f}=0}^{\infty}\exp\left[-n_{j_i}\hbar\beta\omega_j+i\tau\omega_j\right]\frac{\frac{2c_j^2\hbar\left(n_{j_i}-\frac{1}{2}+\frac{1}{2}\right)A^2\left(\omega_j\right)}{M\omega_j}}{4} \\
&\quad \left[1-\exp\left(-\hbar\beta\omega_j\right)\right]\sum_{n_{j_i}=0}^{\infty}\sum_{n_{j_f}=0}^{\infty}\exp\left[-n_{j_i}\hbar\beta\omega_j+i\tau\omega_j\right]\frac{2c_j^2\hbar n_{j_i}A^2\left(\omega_j\right)}{4M\omega_j} \qquad (171)
\end{aligned}
$$

We are left with only n_{j_i}, and so can remove the sum over n_{j_f},noting that since $n_{j_f}+1=n_{j_i}$, the sum over n_{j_i}must start from 1, or else n_{j_f}will have a negative value.

$$
\begin{aligned}
f_j(\tau,\beta,\Delta n=-1) &= \left[1-\exp\left(-\hbar\beta\omega_j\right)\right]\sum_{n_{j_i}=1}^{\infty}\exp\left[-n_{j_i}\hbar\beta\omega_j+i\tau\omega_j\right]\frac{2c_j^2\hbar n_{j_i}A^2\left(\omega_j\right)}{4M\omega_j} \\
&= \left[1-\exp\left(-\hbar\beta\omega_j\right)\right]\frac{2c_j^2\hbar A^2\left(\omega_j\right)}{4M\omega_j}\exp\left[i\tau\omega_j\right]\sum_{n_{j_i}=1}^{\infty}n_{j_i}\left\{\exp\left[-\hbar\beta\omega_j\right]\right\}^{n_{j_i}} \\
&= \left[1-\exp\left(-\hbar\beta\omega_j\right)\right]\frac{c_j^2\hbar A^2\left(\omega_j\right)}{2M\omega_j}\exp\left[i\tau\omega_j\right]\sum_{n_{j_i}=1}^{\infty}n_{j_i}\left\{\exp\left[-\hbar\beta\omega_j\right]\right\}^{n_{j_i}} \\
&= \left[1-\exp\left(-\hbar\beta\omega_j\right)\right]\frac{c_j^2\hbar A^2\left(\omega_j\right)}{2M\omega_j}\exp\left[i\tau\omega_j\right]\left\{\frac{\exp\left[-\hbar\beta\omega_j\right]}{\left(1-\exp\left[-\hbar\beta\omega_j\right]\right)^2}\right\} \\
&= \frac{c_j^2\hbar A^2\left(\omega_j\right)}{2M\omega_j}\exp\left[i\tau\omega_j\right]\left\{\frac{\exp\left[-\hbar\beta\omega_j\right]}{\left(1-\exp\left[-\hbar\beta\omega_j\right]\right)}\right\} \qquad (172)
\end{aligned}
$$

Allowing then only up to a change of one photon during the collision process implies that:

$$
F(\tau,\beta,n)\simeq J_n^2\left(hA(\omega_x)\right)\prod_{j=1}^{N}f_j(\tau,\beta,\Delta n=0)\left[1+\sum_{j=1}^{N}\frac{f_j(\tau,\beta,\Delta n=1)+f_j(\tau,\beta,\Delta n=-1)}{f_j(\tau,\beta,\Delta n=0)}\right]. \qquad (173)
$$

21.5 The Debye-Waller Factor

Using the definition of the spectral density (Eq. 9) and the exponentiation $1-x\simeq\exp(-x)$ one readily finds that

$$
\prod_{j=1}^{N}f_j(\tau,\beta,\Delta n=0)=\exp(-2W) \qquad (174)
$$

and the Debye Waller factor [56] is

$$
W = \frac{1}{2\pi\hbar M}\int_{-\infty}^{+\infty}dt_1\int_{-\infty}^{+\infty}dt_2\bar{V}'(z_{t_1,0})\bar{V}'(z_{t_2,0})\int_0^{\infty}d\omega J_z(\omega)\cos\left[\omega\left(t_1-t_2\right)\right]\coth\left(\frac{\hbar\beta\omega}{2}\right) \qquad (175)
$$

The same expression has been derived previously for neutron scattering through surfaces in Ref. [57] and for surface scattering in Ref. [56].

21.6 Modeling of the Spectral Density

A central purpose of this work is to compute the thermal angular distribution within the semiclassical perturbation theory framework but without restricting the theory to only a few phonon transitions. To achieve this, we discretize the problem, that is instead of using continuum limit expressions, we assume a continuum limit spectral density and then approximate it with a finite sum over harmonic oscillators. Then for each oscillator we compute its form factor as given in Eq. 150.

The discretization is carried out following the methodology of Refs. [45, 46]. The spectral density is modeled as Ohmic with an exponential cutoff, that is:

$$J_z(\omega) = \gamma\omega \exp\left(-\frac{\omega}{\omega_c}\right). \tag{176}$$

γ is the friction coefficient and ω_c is referred to as the cutoff frequency, although in fact it is the frequency at which the spectral density reaches its maximum value.

21.7 Bath Discretization

To evaluate the angular distribution the bath oscillator frequencies ω_j and coupling coefficients c_j are needed. Following the suggestion of Ref. [45] for N_B+1 bath oscillators, the discretized frequencies for the first N_B oscillators are determined as

$$\omega_j = -\omega_c ln\left(1-\frac{j}{N_B+1}\right), \quad j=1,...,N_B \tag{177}$$

and the associated coupling coefficients as:

$$c_j = \sqrt{\frac{2\omega_j^2\gamma\omega_c}{\pi(N_B+1)}}, \quad j=1,...,N_B \tag{178}$$

21.8 Evaluating the Fourier Transform of the Form Factor

The Fourier transform of the form factor is computed by introducing a Gaussian smoothing:

$$\left\langle \tilde{F}\left(\bar{\Omega},\beta,n\right)\right\rangle = \frac{1}{2\pi\sqrt{2\pi T_{sm}^2}}\int_{-\infty}^{\infty} d\tau \exp\left(-\frac{\tau^2}{2T_{sm}^2}+i\tau\bar{\Omega}\right) F(\tau,\beta,n) \tag{179}$$

the smoothing period T_{sm} is chosen to be:

$$T_{sm} = \frac{2\pi}{\Delta\omega} \tag{180}$$

where $\Delta\omega$ is taken to be a typical spacing between adjacent frequencies of the discretized oscillators.

22 The Morse Potential Model

To apply the theory, we choose the vertical interaction potential to be the Morse potential

$$\bar{V}(z) = V_0[(\exp(-\alpha z) - 1)^2 - 1] \tag{181}$$

which is characterized by the well depth V_0 and the stiffness parameter α. The advantage of the Morse form is that the arguments of the Bessel functions may be evaluated analytically. One readily finds ([61]) that:

$$A(\omega) = -\frac{2\pi M\omega}{\alpha\hbar}\frac{\cosh(\Phi\frac{\omega}{\Omega})}{\sinh(\pi\frac{\omega}{\Omega})} \tag{182}$$

with

$$\Omega^2 = \frac{2\alpha^2 E_z}{M} \tag{183}$$

and

$$\cos(\Phi) = -\sqrt{\frac{V_0}{E_z + V_0}}. \tag{184}$$

23 The Continuum Theory for the Bath

23.1 Derivation of the Continuum Theory

Next we shall introduce the full continuum theory. This derivation follows our paper S. Daon, E. Pollak, and S. Miret-Artés. J. Chem. Phys. 137, 201103 (2012).

23.1.1 Derivation of the Angular Distribution

We start from the definition of the angular distribution, Eq. 13:

$$P(\theta_f) = \int_{-\infty}^{\infty} dp_{x_f} \int_0^{\infty} dp_{z_f} \delta\left(\theta_f - \tan^{-1}\left(\frac{p_{x_f}}{p_{z_f}}\right)\right) \sum_{n,n_f} \delta(p_{x_f} - p_{x_i} - \frac{2\pi\hbar n}{l})\, \delta(p_{z_f} - p_{z_{t_0}}) P_{n,n_f;0,n_i} \tag{185}$$

and the momentum distribution:

$$P(p_{x_f}, p_{z_f}; n_i) = \sum_{n=-\infty}^{\infty} \sum_{\mathbf{n_f}} \delta(p_{x_f} - p_{x_i} - \frac{2\pi\hbar n}{l})\, \delta(p_{z_f} - p_{z_{t_0}}) P_{n,n_f;0,n_i} \tag{186}$$

We plug the values of the transition probability and momentum distribution into the angular distribution to obtain:

$$\begin{aligned} P(\theta_f) &= \int_{-\infty}^{\infty} dp_{x_f} \int_0^{\infty} dp_{z_f} \delta\left(\theta_f - \tan^{-1}\left(\frac{p_{x_f}}{p_{z_f}}\right)\right) \sum_{n=-\infty}^{\infty} \sum_{\mathbf{n_f}} \delta(p_{x_f} - p_{x_i} - \frac{2\pi\hbar n}{l}) \\ &\quad \delta(p_{z_f} - p_{z_{t_0}}) J_n^2\left(hA(\omega_x)\right) \prod_{j=1}^{N} J^2_{n_{j_f} - n_{j_i}}\left(\bar{A}_j\left(n_{j_{if}}\right)\right) \end{aligned} \tag{187}$$

We can then eliminate the the integrations over p_{x_f} and p_{z_f} by making the substitutions according to the delta functions:

$$\begin{aligned} P(\theta_f) &= \sum_{n=-\infty}^{\infty} \sum_{\mathbf{n_f}} \delta\left(\theta_f - \tan^{-1}\left(\frac{p_{x_i} + \frac{2\pi\hbar n}{l}}{p_{z_{t_0}}}\right)\right) \\ &\quad J_n^2\left(hA(\omega_x)\right) \prod_{j=1}^{N} J^2_{n_{j_f} - n_{j_i}}\left(\bar{A}_j\left(n_{j_{if}}\right)\right) \end{aligned} \tag{188}$$

We substitute $p_{z_{t_0}}$ and p_{x_f} as defined in Eqs. 143 and 141, use the definition of $\Omega(\theta_i, n)$ (Eq. 144) and follow a similar derivation as in Section 21.2 to obtain:

$$\begin{aligned} P(\theta_f) &= \sum_{n=-\infty}^{\infty} \sum_{\mathbf{n_f}} \delta\left(\theta_f - \tan^{-1}\left(\frac{\sqrt{2ME_i}\left[\frac{sin(|\theta_i| + \theta(n))}{cos\theta(n)}\right]}{\sqrt{2M\hbar}\sqrt{\Omega(\theta_i, n) - \Delta\mathbf{n}\cdot\omega}}\right)\right) \\ &\quad J_n^2\left(hA(\omega_x)\right) \prod_{j=1}^{N} J^2_{n_{j_f} - n_{j_i}}\left(\bar{A}_j\left(n_{j_{if}}\right)\right) H(\Omega(\theta_i, n) - \Delta\mathbf{n}\cdot\omega) \end{aligned} \tag{189}$$

Where we added to the product the term $H(\Omega(\theta_i, n) - \Delta\mathbf{n}\cdot\omega)$ to enforce that the term inside the square root is positive. We then see that:

$$P(\theta_f) = \sum_{n=-\infty}^{\infty} \sum_{\mathbf{n_f}} \delta\left(\theta_f - \tan^{-1}\left(\sqrt{\frac{E_i}{\hbar cos^2\theta(n)}} \frac{\sqrt{sin^2(|\theta_i| + \theta(n))}}{\sqrt{\Omega(\theta_i, n) - \Delta\mathbf{n}\cdot\omega}}\right)\right)$$
$$J_n^2\left(hA(\omega_x)\right) \prod_{j=1}^{N} J^2_{n_{j_f} - n_{j_i}}\left(\bar{A}_j\left(n_{j_{if}}\right)\right) H(\Omega(\theta_i, n) - \Delta\mathbf{n}\cdot\omega) \quad (190)$$

We use the identity $\delta(\theta - tan^{-1}(\alpha)) = \frac{1}{cos^2\theta}\delta(\alpha - tan\theta)$ to see that:

$$P(\theta_f) = \sum_{n=-\infty}^{\infty} \sum_{\mathbf{n_f}} \frac{1}{cos^2\theta_f} \delta\left(\sqrt{\frac{E_i sin^2(|\theta_i| + \theta(n))}{\hbar cos^2\theta(n)\left(\Omega(\theta_i, n) - \Delta\mathbf{n}\cdot\omega\right)}} - tan\left(\theta_f\right)\right)$$
$$J_n^2\left(hA(\omega_x)\right) \prod_{j=1}^{N} J^2_{n_{j_f} - n_{j_i}}\left(\bar{A}_j\left(n_{j_{if}}\right)\right) H(\Omega(\theta_i, n) - \Delta\mathbf{n}\cdot\omega) \quad (191)$$

We divide inside and outside the delta function by $tan(\theta_f)$:

$$P(\theta_f) = \sum_{n=-\infty}^{\infty} \sum_{\mathbf{n_f}} \frac{1}{cos^2\theta_f \tan\theta_f} \delta\left(\sqrt{\frac{E_i sin^2(|\theta_i| + \theta(n))}{\hbar cos^2\theta(n)\left(\Omega(\theta_i, n) - \Delta\mathbf{n}\cdot\omega\right) tan^2\left(\theta_f\right)}} - 1\right)$$
$$J_n^2\left(hA(\omega_x)\right) \prod_{j=1}^{N} J^2_{n_{j_f} - n_{j_i}}\left(\bar{A}_j\left(n_{j_{if}}\right)\right) H(\Omega(\theta_i, n) - \Delta\mathbf{n}\cdot\omega) \quad (192)$$

We then use the identity $\delta(\sqrt{x} - a) = 2\sqrt{x}\delta(x - a^2)$ to see that:

$$P(\theta_f) = \sum_{n=-\infty}^{\infty} \sum_{\mathbf{n_f}} \frac{1}{cos^2\theta_f \tan\theta_f} 2\sqrt{\frac{E_i sin^2(|\theta_i| + \theta(n))}{\hbar cos^2\theta(n)\left(\Omega(\theta_i, n) - \Delta\mathbf{n}\cdot\omega\right) tan^2\left(\theta_f\right)}}$$
$$\delta\left(\frac{E_i sin^2(|\theta_i| + \theta(n))}{\hbar cos^2\theta(n)\left(\Omega(\theta_i, n) - \Delta\mathbf{n}\cdot\omega\right) tan^2\left(\theta_f\right)} - 1\right) J_n^2\left(hA(\omega_x)\right) \prod_{j=1}^{N} J^2_{n_{j_f} - n_{j_i}}\left(\bar{A}_j\left(n_{j_{if}}\right)\right)$$
$$H(\Omega(\theta_i, n) - \Delta\mathbf{n}\cdot\omega) \quad (193)$$

And after some simplification:

$$P(\theta_f) = \sum_{n=-\infty}^{\infty} \sum_{\mathbf{n_f}} \frac{1}{\left|cos\theta_f\right| \left|sin\theta_f\right|} 2\left(\Omega(\theta_i,n) - \Delta\mathbf{n}\cdot\omega\right) \delta\left(\Delta\mathbf{n}\cdot\omega - \left[\Omega(\theta_i,n) - \frac{E_i sin^2(|\theta_i| + \theta(n))}{\hbar cos^2\theta(n) tan^2\left(\theta_f\right)}\right]\right)$$
$$J_n^2\left(hA(\omega_x)\right) \prod_{j=1}^{N} J_{n_{j_f}-n_{j_i}}^2\left(\bar{A}_j\left(n_{j_{if}}\right)\right) H(\Omega(\theta_i,n) - \Delta\mathbf{n}\cdot\omega) \quad (194)$$

We then use the definition of $\bar{\Omega}(\theta_f,\theta_i,n)$ in Eq. 148 to see that:

$$P(\theta_f) = \sum_{n=-\infty}^{\infty} \sum_{\mathbf{n_f}} \frac{2\left(\Omega(\theta_i,n) - \Delta\mathbf{n}\cdot\omega\right)}{\left|cos\theta_f\right| \left|sin\theta_f\right|} \delta\left(\Delta\mathbf{n}\cdot\omega - \bar{\Omega}(\theta_f,\theta_i,n)\right)$$
$$J_n^2\left(hA(\omega_x)\right) \prod_{j=1}^{N} J_{n_{j_f}-n_{j_i}}^2\left(\bar{A}_j\left(n_{j_{if}}\right)\right) H(\Omega(\theta_i,n) - \Delta\mathbf{n}\cdot\omega) \quad (195)$$

23.1.2 The Zero-Phonon Contribution

We start by considering the contribution to the angular distribution which comes from only those transitions in which there is no change in the quantum number of any of the oscillators. To evaluate the value of $\Delta\mathbf{n}\cdot\omega$ we look at this table:

Oscillator #→	1	2	...	...	...	j	...	...	...	...	N
Final Occupation # $\mathbf{n_f}$→	n_{1_f}	n_{2_f}	...	...	...	...	...	...	...	...	n_{N_f}
Initial Occupation # $\mathbf{n_i}$→	n_{1_i}	n_{2_i}	...	...	...	...	...	...	...	...	n_{N_i}
$\Delta\mathbf{n}$→	0	0	0	0	0	0	0	0	0	0	0
ω→	ω_1	ω_2	...	...	...	ω_j	...	...	...	...	ω_N

Since $\Delta\mathbf{n} = \mathbf{0}$ we have that $\Delta\mathbf{n}\cdot\omega = 0$, and $n_{j_f} - n_{j_i} = 0$ for any j.

The contribution to the angular distribution then takes the form:

$$P(\theta_f;\Delta\mathbf{n}=\mathbf{0}) = \sum_{n=-\infty}^{\infty} \sum_{\mathbf{n_f}} \frac{2\Omega(\theta_i,n)}{\left|cos\theta_f\right| \left|sin\theta_f\right|} \delta\left(\bar{\Omega}(\theta_f,\theta_i,n)\right)$$
$$J_n^2\left(hA(\omega_x)\right) \prod_{j=1}^{N} J_0^2\left(\bar{A}_j\left(n_{j_{if}}\right)\right) H(\Omega(\theta_i,n)) \quad (196)$$

Next we would like to take the thermal average due to a surface at temperature T (with $\beta = 1/k_B T$). This is obtained by averaging over the thermal distribution of the initial oscillator states.

$$\left\langle P(\theta_f;\Delta\mathbf{n}=\mathbf{0})\right\rangle = \sum_{n=-\infty}^{\infty} J_n^2\left(hA(\omega_x)\right)\left[1-\exp\left(-\hbar\beta\omega_j\right)\right]\sum_{n_{j_i}=0}^{\infty}\sum_{n_{j_f}=0}^{\infty}\exp\left[-n_{j_i}\hbar\beta\omega_j\right]\frac{2\Omega(\theta_i,n)}{\left|cos\theta_f\right|\left|sin\theta_f\right|}\delta\left(\bar{\Omega}(\theta_f,\theta_i,n)\right)$$
$$\prod_{j=1}^{N} J_0^2\left(\bar{A}_j\left(n_{j_{if}}\right)\right)H(\Omega(\theta_i,n)) \tag{197}$$

We can reorder the terms:

$$\left\langle P(\theta_f;\Delta\mathbf{n}=\mathbf{0})\right\rangle = \sum_{n=-\infty}^{\infty}\frac{2J_n^2\left(hA(\omega_x)\right)}{\left|cos\theta_f\right|\left|sin\theta_f\right|}\Omega(\theta_i,n)\delta\left(\bar{\Omega}(\theta_f,\theta_i,n)\right)H(\Omega(\theta_i,n))$$
$$\prod_{j=1}^{N}\left[1-\exp\left(-\hbar\beta\omega_j\right)\right]\sum_{n_{j_i}=0}^{\infty}\sum_{n_{j_f}=0}^{\infty}\exp\left[-n_{j_i}\hbar\beta\omega_j\right]J_0^2\left(\bar{A}_j\left(n_{j_{if}}\right)\right) \tag{198}$$

Such that we note that the last product is a product of the function $f_j(\tau,\beta,\Delta n=0)$ defined earlier (Eq. X) for the zero-phonon contributions in the discretized theory. We then have:

$$\left\langle P(\theta_f;\Delta\mathbf{n}=\mathbf{0})\right\rangle = \sum_{n=-\infty}^{\infty}\frac{2J_n^2\left(hA(\omega_x)\right)}{\left|cos\theta_f\right|\left|sin\theta_f\right|}\Omega(\theta_i,n)\delta\left(\bar{\Omega}(\theta_f,\theta_i,n)\right)H(\Omega(\theta_i,n))$$
$$\prod_{j=1}^{N} f_j(\tau,\beta,\Delta n=0) \tag{199}$$

and after substituting the analytical value for $f_j(\tau,\beta,\Delta n=0)$ we have:

$$\left\langle P(\theta_f;\Delta\mathbf{n}=\mathbf{0})\right\rangle = \sum_{n=-\infty}^{\infty}\frac{2J_n^2\left(hA(\omega_x)\right)}{\left|cos\theta_f\right|\left|sin\theta_f\right|}\Omega(\theta_i,n)\delta\left(\bar{\Omega}(\theta_f,\theta_i,n)\right)H(\Omega(\theta_i,n))$$
$$\prod_{j=1}^{N}\left[1-\frac{c_j^2\hbar A\left(\omega_j\right)^2}{2M\omega_j}coth(\hbar\beta\omega_j/2)\right] \tag{200}$$

We use the approximation:

$$1-x\approx exp(-x) \tag{201}$$

to obtain:

$$\left\langle P(\theta_f;\Delta\mathbf{n}=\mathbf{0})\right\rangle = \sum_{n=-\infty}^{\infty}\frac{2J_n^2\left(hA(\omega_x)\right)}{\left|cos\theta_f\right|\left|sin\theta_f\right|}\Omega(\theta_i,n)\delta\left(\bar{\Omega}(\theta_f,\theta_i,n)\right)H(\Omega(\theta_i,n)) \prod_{j=1}^{N} exp\left[-\frac{c_j^2\hbar A\left(\omega_j\right)^2}{2M\omega_j}coth(\hbar\beta\omega_j/2)\right] \tag{202}$$

and we identify the Debye-Waller factor as:

$$exp(-2W)=\prod_{j=1}^{N} exp\left[-\frac{c_j^2\hbar A\left(\omega_j\right)^2}{2M\omega_j}coth(\hbar\beta\omega_j/2)\right]=exp\left[-\sum_{j=1}^{N}\frac{c_j^2\hbar A\left(\omega_j\right)^2}{2M\omega_j}coth(\hbar\beta\omega_j/2)\right] \tag{203}$$

And it is given by Eq. 174 defined previously. The final expression for the zero-phonon contribution is then:

$$\left\langle P(\theta_f;\Delta\mathbf{n}=\mathbf{0})\right\rangle = \sum_{n=-\infty}^{\infty}\frac{2J_n^2\left(hA(\omega_x)\right)}{\left|cos\theta_f\right|\left|sin\theta_f\right|}\Omega(\theta_i,n)\delta\left(\bar{\Omega}(\theta_f,\theta_i,n)\right)H(\Omega(\theta_i,n))exp(-2W) \tag{204}$$

23.1.3 The Single Phonon Contribution

We would like to evaluate the contribution to the angular distribution arising from single-phonon transitions only. We distinguish between two cases. One is when a phonon gains one quantum, the other is when a phonon loses one quantum. For the first case, when one phonon exactly gains exactly one quantum of energy, we have the state in the following table:

Oscillator #→	1	2	...	...	...	j	...	...	...	...	N
Final Occupation # $\mathbf{n_f}$→	n_{1_f}	n_{2_f}	...	...	...	...	...	...	...	...	n_{N_f}
Initial Occupation # $\mathbf{n_i}$→	n_{1_i}	n_{2_i}	...	...	...	...	...	...	...	...	n_{N_i}
$\Delta\mathbf{n}$→	0	0	...	...	0	1	0	...	...	...	0
ω→	ω_1	ω_2	...	...	...	ω_j	...	...	...	...	ω_N

We see that for N oscillators, there's just one bath oscillator, the j-th bath oscillator, which has a change in the occupation number. Therefore the total vector Δn is zero at all slots at the index k ($n_{k_f}-n_{k_i}=0$) except for one, at the index j, in which it is one ($n_{j_f}-n_{j_i}=1$). Therefore the total value of the scalar product is given by:

$$\Delta\mathbf{n}\cdot\omega = (\mathbf{n_f}-\mathbf{n_i})\cdot\omega = 1*\omega_j = \omega_j$$

We substitute this value into our expression for the angular distribution:

$$\begin{aligned} P(\theta_f;\Delta\mathbf{n}=1) &= \sum_{n=-\infty}^{\infty} J_n^2\left(hA(\omega_x)\right)\sum_{\mathbf{n_f}}\frac{2\left(\Omega(\theta_i,n)-\omega_j\right)}{\left|cos\theta_f\right|\left|sin\theta_f\right|}\prod_{j=1}^{N}J_0^2\left(\bar{A}_j\left(n_{j_i}\right)\right) \\ &\quad \sum_{j=1}^{N}\frac{J_1^2\left(\bar{A}_j\left(n_{j_i}+\frac{1}{2}\right)\right)}{J_0^2\left(\bar{A}_j\left(n_{j_i}\right)\right)}\delta\left(\omega_j-\bar{\Omega}(\theta_f,\theta_i,n)\right)H(\Omega(\theta_i,n)-\omega_j) \end{aligned} \tag{205}$$

Noting that from $\delta\left(\omega_j-\bar{\Omega}(\theta_f,\theta_i,n)\right)$ we have that $\omega_j=\bar{\Omega}(\theta_f,\theta_i,n)$, we make this substitution:

$$\begin{aligned} P(\theta_f;\Delta\mathbf{n}=1) &= \sum_{n=-\infty}^{\infty} J_n^2\left(hA(\omega_x)\right)\sum_{\mathbf{n_f}}\frac{2\left(\Omega(\theta_i,n)-\bar{\Omega}(\theta_f,\theta_i,n)\right)}{\left|cos\theta_f\right|\left|sin\theta_f\right|}\prod_{j=1}^{N}J_0^2\left(\bar{A}_j\left(n_{j_i}\right)\right) \\ &\quad \sum_{j=1}^{N}\frac{J_1^2\left(\bar{A}_j\left(n_{j_i}+\frac{1}{2}\right)\right)}{J_0^2\left(\bar{A}_j\left(n_{j_i}\right)\right)}\delta\left(\omega_j-\bar{\Omega}(\theta_f,\theta_i,n)\right)H(\bar{\Omega}(\theta_f,\theta_i,n)) \end{aligned} \tag{206}$$

We note that:

$$2\left(\Omega(\theta_i,n)-\bar{\Omega}(\theta_f,\theta_i,n)\right) = \frac{2E_i sin^2(|\theta_i|+\theta(n))}{\hbar cos^2\theta(n)tan^2\left(\theta_f\right)} \tag{207}$$

to obtain:

$$\begin{aligned} P(\theta_f;\Delta\mathbf{n}=1) &= \sum_{n=-\infty}^{\infty} J_n^2\left(hA(\omega_x)\right)\sum_{\mathbf{n_f}}\frac{2E_i sin^2(|\theta_i|+\theta(n))}{\hbar cos^2\theta(n)tan^2\left(\theta_f\right)}\frac{1}{\left|cos\theta_f\right|\left|sin\theta_f\right|}\prod_{j=1}^{N}J_0^2\left(\bar{A}_j\left(n_{j_i}\right)\right) \\ &\quad \sum_{j=1}^{N}\frac{J_1^2\left(\bar{A}_j\left(n_{j_i}+\frac{1}{2}\right)\right)}{J_0^2\left(\bar{A}_j\left(n_{j_i}\right)\right)}\delta\left(\omega_j-\bar{\Omega}(\theta_f,\theta_i,n)\right)H(\Omega(\theta_f,\theta_i,n)) \end{aligned} \tag{208}$$

$$P(\theta_f;\Delta\mathbf{n}=1) = \sum_{n=-\infty}^{\infty} J_n^2\left(hA(\omega_x)\right)\sum_{\mathbf{n_f}}\frac{2E_i sin^2(|\theta_i|+\theta(n))cos^2\left(\theta_f\right)}{\hbar cos^2\theta(n)sin^2\left(\theta_f\right)}\frac{1}{\left|cos\theta_f\right|\left|sin\theta_f\right|}\prod_{j=1}^{N}J_0^2\left(\bar{A}_j\left(n_{j_i}\right)\right)$$
$$\sum_{j=1}^{N}\frac{J_1^2\left(\bar{A}_j\left(n_{j_i}+\frac{1}{2}\right)\right)}{J_0^2\left(\bar{A}_j\left(n_{j_i}\right)\right)}\delta\left(\omega_j-\bar{\Omega}(\theta_f,\theta_i,n)\right)H(\bar{\Omega}(\theta_f,\theta_i,n)) \tag{209}$$

$$P(\theta_f;\Delta\mathbf{n}=1) = \sum_{n=-\infty}^{\infty} J_n^2\left(hA(\omega_x)\right)\frac{2E_i sin^2(|\theta_i|+\theta(n))cos\left(\theta_f\right)}{\hbar cos^2\theta(n)sin^3\left(\theta_f\right)}\sum_{\mathbf{n_f}}\prod_{j=1}^{N}J_0^2\left(\bar{A}_j\left(n_{j_i}\right)\right)$$
$$\sum_{j=1}^{N}\frac{J_1^2\left(\bar{A}_j\left(n_{j_i}+\frac{1}{2}\right)\right)}{J_0^2\left(\bar{A}_j\left(n_{j_i}\right)\right)}\delta\left(\omega_j-\bar{\Omega}(\theta_f,\theta_i,n)\right)H(\bar{\Omega}(\theta_f,\theta_i,n)) \tag{210}$$

We perform the thermal average on the angular distribution and use the approximation $\frac{J_1^2(x)}{J_0^2(x)}\simeq\frac{x^2}{4}$ to obtain:

$$\left\langle P(\theta_f;\Delta\mathbf{n}=1)\right\rangle = \sum_{n=-\infty}^{\infty} J_n^2\left(hA(\omega_x)\right)\frac{2E_i sin^2(|\theta_i|+\theta(n))cos\left(\theta_f\right)}{\hbar cos^2\theta(n)sin^3\left(\theta_f\right)}\sum_{n_{j_i}=0}^{\infty}\sum_{n_{j_f}=0}^{\infty}\prod_{j=1}^{N}\left[1-\exp\left(-\hbar\beta\omega_j\right)\right]$$
$$\exp\left[-n_{j_i}\hbar\beta\omega_j\right]J_0^2\left(\bar{A}_j\left(n_{j_i}\right)\right)$$
$$\sum_{j=1}^{N}\frac{\bar{A}_j\left(n_{j_i}+\frac{1}{2}\right)^2}{4}\delta\left(\omega_j-\bar{\Omega}(\theta_f,\theta_i,n)\right)H(\bar{\Omega}(\theta_f,\theta_i,n)) \tag{211}$$

from Eq. 170, we can get the relation

$$\frac{f_j(\tau,\beta,\Delta n=1)}{\exp\left[-i\tau\omega_j\right]} = \left[1-\exp\left(-\hbar\beta\omega_j\right)\right]\sum_{n_{j_i}=0}^{\infty}\sum_{n_{j_f}=0}^{\infty}\exp\left[-n_{j_i}\hbar\beta\omega_j\right]\frac{\bar{A}_j\left(n_{j_{if}}\right)^2}{4} \tag{212}$$

such that we see that:

$$\frac{f_j(\tau,\beta,\Delta n=1)}{\exp\left[-i\tau\omega_j\right]} = \frac{c_j^2\hbar A^2\left(\omega_j\right)}{M\omega_j}\left[coth\left(\frac{\hbar\beta\omega_j}{2}\right)+1\right] \tag{213}$$

So that we obtain:

$$\left\langle P(\theta_f;\Delta\mathbf{n}=1)\right\rangle = \sum_{n=-\infty}^{\infty} J_n^2\left(hA(\omega_x)\right)\frac{2E_i sin^2(|\theta_i|+\theta(n))cos\left(\theta_f\right)}{\hbar cos^2\theta(n)sin^3\left(\theta_f\right)}$$
$$exp(-2W)\sum_{j=1}^{N}\frac{c_j^2\hbar A^2\left(\omega_j\right)}{M\omega_j}\left[coth\left(\frac{\hbar\beta\omega_j}{2}\right)+1\right]$$
$$\delta\left(\omega_j-\bar{\Omega}(\theta_f,\theta_i,n)\right)H(\bar{\Omega}(\theta_f,\theta_i,n)) \quad (214)$$

$$\left\langle P(\theta_f;\Delta\mathbf{n}=1)\right\rangle = \sum_{n=-\infty}^{\infty} J_n^2\left(hA(\omega_x)\right)\frac{2E_i sin^2(|\theta_i|+\theta(n))cos\left(\theta_f\right)}{Mcos^2\theta(n)sin^3\left(\theta_f\right)}$$
$$exp(-2W)\frac{2}{\pi}\frac{\pi}{2}\sum_{j=1}^{N}\frac{c_j^2}{\omega_j}A^2\left(\omega_j\right)\left[coth\left(\frac{\hbar\beta\omega_j}{2}\right)+1\right] \quad (215)$$
$$\delta\left(\omega_j-\bar{\Omega}(\theta_f,\theta_i,n)\right)H(\bar{\Omega}(\theta_f,\theta_i,n)) \quad (216)$$

$$\left\langle P(\theta_f;\Delta\mathbf{n}=1)\right\rangle = \sum_{n=-\infty}^{\infty} J_n^2\left(hA(\omega_x)\right)\frac{2E_i sin^2(|\theta_i|+\theta(n))cos\left(\theta_f\right)}{Mcos^2\theta(n)sin^3\left(\theta_f\right)}$$
$$exp(-2W)\frac{2}{\pi}\frac{\pi}{2}\sum_{j=1}^{N}\frac{c_j^2}{\omega_j}\delta\left(\omega_j-\bar{\Omega}(\theta_f,\theta_i,n)\right)A^2\left(\omega_j\right)\left[coth\left(\frac{\hbar\beta\omega_j}{2}\right)+1\right]$$
$$H(\bar{\Omega}(\theta_f,\theta_i,n)) \quad (217)$$

We use the definition of the spectral density, Eq. 9 to obtain the continuum limit expression to lowest order in c_j^2 :

$$\left\langle P(\theta_f;\Delta\mathbf{n}=1)\right\rangle = \sum_{n=-\infty}^{\infty} J_n^2\left(hA(\omega_x)\right)\frac{2E_i sin^2(|\theta_i|+\theta(n))cos\left(\theta_f\right)}{Mcos^2\theta(n)sin^3\left(\theta_f\right)}$$
$$exp(-2W)\frac{2}{\pi}J_z\left(\bar{\Omega}(\theta_f,\theta_i,n)\right)A^2\left(\bar{\Omega}(\theta_f,\theta_i,n)\right)\left[coth\left(\frac{\hbar\beta\bar{\Omega}(\theta_f,\theta_i,n)}{2}\right)+1\right]$$
$$H(\bar{\Omega}(\theta_f,\theta_i,n)) \quad (218)$$

$$\begin{aligned}\left\langle P(\theta_f;\Delta\mathbf{n}=1)\right\rangle &= \sum_{n=-\infty}^{\infty} J_n^2\left(hA(\omega_x)\right)\frac{4E_i sin^2(|\theta_i|+\theta(n))cos\left(\theta_f\right)}{\pi M cos^2\theta(n) sin^3\left(\theta_f\right)} \\ & exp(-2W)J_z\left(\bar{\Omega}(\theta_f,\theta_i,n)\right)A^2\left(\bar{\Omega}(\theta_f,\theta_i,n)\right)\left[coth\left(\frac{\hbar\beta\bar{\Omega}(\theta_f,\theta_i,n)}{2}\right)+1\right] \\ & H(\bar{\Omega}(\theta_f,\theta_i,n))\end{aligned} \tag{219}$$

For the second case, when one phonon exactly loses one quantum of energy, we have the state in the following table:

Oscillator #→	1	2	...	...	...	j	...	...	...	...	N
Final Occupation # $\mathbf{n_f}$→	n_{1_f}	n_{2_f}	...	...	...	...	...	...	...	...	n_{N_f}
Initial Occupation # $\mathbf{n_i}$→	n_{1_i}	n_{2_i}	...	...	...	...	...	...	...	...	n_{N_i}
$\Delta\mathbf{n}$→	0	0	...	...	0	-1	0	...	...	...	0
ω→	ω_1	ω_2	...	...	...	ω_j	...	...	...	...	ω_N

We we see, for N oscillators, there's just one bath oscillator, the j-th bath oscillator, which has a change in the occupation number. Therefore the total vector Δn is zero at all slots at the index k ($n_{k_f}-n_{k_i}=0$) except for one, at the index j, in which it is one ($n_{j_f}-n_{j_i}=-1$). Therefore the total value of the scalar product is given by:

$$\Delta\mathbf{n}\cdot\omega=(\mathbf{n_f}-\mathbf{n_i})\cdot\omega=-1*\omega_j=-\omega_j$$

In the same way as for the +1 transition, we then have for the thermally averaged contribution, to lowest order in c_j^2 :

$$\begin{aligned}\left\langle P(\theta_f;\Delta\mathbf{n}=-1)\right\rangle &= \sum_{n=-\infty}^{\infty} J_n^2\left(hA(\omega_x)\right)\frac{4E_i sin^2(|\theta_i|+\theta(n))cos\left(\theta_f\right)}{\pi M cos^2\theta(n) sin^3\left(\theta_f\right)} \\ & exp(-2W)\,J_z\left(\left|\bar{\Omega}(\theta_f,\theta_i,n)\right|\right)A^2\left(\bar{\Omega}(\theta_f,\theta_i,n)\right)\left[coth\left(\frac{\hbar\beta\left|\bar{\Omega}(\theta_f,\theta_i,n)\right|}{2}\right)-1\right] \\ & H(-\bar{\Omega}(\theta_f,\theta_i,n))\end{aligned} \tag{220}$$

The total contribution from one-phonon transitions is:

$$\begin{aligned}\left\langle P(\theta_f;\Delta\mathbf{n}=1)\right\rangle &= \sum_{n=-\infty}^{\infty} J_n^2\left(hA(\omega_x)\right)\frac{4E_i sin^2(|\theta_i|+\theta(n))cos\left(\theta_f\right)}{\pi M cos^2\theta(n) sin^3\left(\theta_f\right)} \\ & exp(-2W)\, J_z\left(\left|\bar{\Omega}(\theta_f,\theta_i,n)\right|\right) A^2\left(\bar{\Omega}(\theta_f,\theta_i,n)\right) \\ & \left[coth\left(\frac{\hbar\beta\left|\bar{\Omega}(\theta_f,\theta_i,n)\right|}{2}\right)+H\left(\bar{\Omega}(\theta_f,\theta_i,n)\right)-H\left(-\bar{\Omega}(\theta_f,\theta_i,n)\right)\right] \end{aligned} \tag{221}$$

23.1.4 Two Phonon Contributions

For the two-phonon contributions we must take into consideration five possibilities. 1 - single mode absorbing two phonons. 2 - two different modes, each absorbing a single phonon. 3 - two different modes, one absorbing a phonon, the other emitting a phonon. 4 - two different modes, each emitting a phonon. 5 - one mode, emitting two phonons.

We define:

$$\Gamma_j^2 = \frac{2\hbar c_j^2 A\left(\omega_j\right)^2}{M\omega_j} \tag{222}$$

First possibility - single mode absorbing two phonons:

Oscillator #→	1	2	...	...	...	j	...	...	...	...	N
Final Occupation # $\mathbf{n_f}$→	n_{1_f}	n_{2_f}	...	...	...	...	...	...	...	...	n_{N_f}
Initial Occupation # $\mathbf{n_i}$→	n_{1_i}	n_{2_i}	...	...	...	...	...	...	...	...	n_{N_i}
$\Delta\mathbf{n}$→	0	...	0	0	0	2	0	0	0	...	0
ω→	ω_1	ω_2	...	...	...	ω_j	...	...	...	...	ω_N

We have for the scalar product:

$$\Delta\mathbf{n}\cdot\omega = 2\omega_j$$

We start from the general definition of the angular distribution, and make this substitution

$$\begin{aligned} P(\theta_f;\Delta n=2) &= \sum_{n=-\infty}^{\infty}\sum_{\mathbf{n_f}}\frac{2\left(\Omega(\theta_i,n)-\Delta\mathbf{n}\cdot\omega\right)}{\left|cos\theta_f\right|\left|sin\theta_f\right|}\delta\left(\Delta\mathbf{n}\cdot\omega-\bar{\Omega}(\theta_f,\theta_i,n)\right) \\ & J_n^2\left(hA(\omega_x)\right)\prod_{j=1}^{N} J_{n_{j_f}-n_{j_i}}^2\left(\bar{A}_j\left(n_{j_{if}}\right)\right) H(\bar{\Omega}(\theta_f,\theta_i,n)) \end{aligned} \tag{223}$$

$$P(\theta_f;\Delta n=2) = \sum_{n=-\infty}^{\infty}\sum_{\mathbf{n_f}}\frac{2\left(\Omega(\theta_i,n)-\Delta\mathbf{n}\cdot\omega\right)}{\left|cos\theta_f\right|\left|sin\theta_f\right|}\delta\left(2\omega_j-\bar{\Omega}(\theta_f,\theta_i,n)\right)$$
$$J_n^2\left(hA(\omega_x)\right)\prod_{j=1}^{N}J^2_{n_{j_f}-n_{j_i}}\left(\bar{A}_j\left(n_{j_{if}}\right)\right)H(\bar{\Omega}(\theta_f,\theta_i,n)) \quad (224)$$

We note that in this case we will have a contribution of the order Γ_j^4,just like we had Γ_j^2 for the one-phonon contribution. This contribution is of order c_j^4 and will therefore be neglected in the continuum limit. We will therefore have no contribution from this term.

Second possibility - two different modes, each absorbing a single phonon.

Oscillator #→	1	2	...	j	...	...	...	k	...	...	N
Final Occupation # $\mathbf{n_f}$→	n_{1_f}	n_{2_f}	...	...	...	...	...	...	...	...	n_{N_f}
Initial Occupation # $\mathbf{n_i}$→	n_{1_i}	n_{2_i}	...	...	...	...	...	...	...	...	n_{N_i}
$\Delta\mathbf{n}$→	0	...	0	1	0	...	0	1	0	...	0
ω→	ω_1	ω_2	...	ω_j	...	...	...	ω_k	...	...	ω_N

We have for the scalar product:

$$\Delta\mathbf{n}\cdot\omega=\omega_j+\omega_k$$

We start from the general expression for the angular distribution, making this substitution:

$$P(\theta_f;\Delta n=1,1) = \sum_{n=-\infty}^{\infty}\sum_{\mathbf{n_f}}\frac{2\left(\Omega(\theta_i,n)-\bar{\Omega}(\theta_f,\theta_i,n)\right)}{\left|cos\theta_f\right|\left|sin\theta_f\right|}\delta\left(\omega_j+\omega_k-\bar{\Omega}(\theta_f,\theta_i,n)\right)$$
$$J_n^2\left(hA(\omega_x)\right)\prod_{j=1}^{N}J^2_{n_{j_f}-n_{j_i}}\left(\bar{A}_j\left(n_{j_{if}}\right)\right)H(\bar{\Omega}(\theta_f,\theta_i,n)) \quad (225)$$

Such that we have that: $\omega_j+\omega_k=\bar{\Omega}(\theta_f,\theta_i,n)$

We then make the thermal average like before, to lowest order in c_j^2 :

$$\begin{aligned}\left\langle P(\theta_f;\Delta n=1,1)\right\rangle &= \sum_{n=-\infty}^{\infty} J_n^2\left(hA(\omega_x)\right) exp(-2W)\frac{2\left(\Omega(\theta_i,n)-\bar{\Omega}(\theta_f,\theta_i,n)\right)}{\left|cos\theta_f\right|\left|sin\theta_f\right|}H(\bar{\Omega}(\theta_f,\theta_i,n)) \\ &\sum_{\substack{j=1\\k>j}}^{N}\sum_{k=1}^{N}\frac{\Gamma_j^2\Gamma_k^2}{128}\left[coth\left(\frac{\hbar\beta\omega_j}{2}\right)+1\right]\left[coth\left(\frac{\hbar\beta\omega_k}{2}\right)+1\right] \\ &\delta\left(\omega_j+\omega_k-\bar{\Omega}(\theta_f,\theta_i,n)\right) \end{aligned} \tag{226}$$

And we make the continuum limit form:

$$\begin{aligned}\left\langle P(\theta_f;\Delta n=1,1)\right\rangle &= \sum_{n=-\infty}^{\infty} J_n^2\left(hA(\omega_x)\right) exp(-2W)\frac{2\left(\Omega(\theta_i,n)-\bar{\Omega}(\theta_f,\theta_i,n)\right)}{\left|cos\theta_f\right|\left|sin\theta_f\right|}H(\bar{\Omega}(\theta_f,\theta_i,n)) \\ &\sum_{\substack{j=1\\k>j}}^{N}\sum_{k=1}^{N}\frac{1}{128}\frac{2\hbar c_j^2 A\left(\omega_j\right)^2}{M\omega_j}\frac{2\hbar c_k^2 A\left(\omega_k\right)^2}{M\omega_k}\delta\left(\omega_j+\omega_k-\bar{\Omega}(\theta_f,\theta_i,n)\right) \\ &\left[coth\left(\frac{\hbar\beta\omega_j}{2}\right)+1\right]\left[coth\left(\frac{\hbar\beta\omega_k}{2}\right)+1\right] \end{aligned} \tag{227}$$

$$\begin{aligned}\left\langle P(\theta_f;\Delta n=1,1)\right\rangle &= \sum_{n=-\infty}^{\infty} J_n^2\left(hA(\omega_x)\right) exp(-2W)\frac{2\left(\Omega(\theta_i,n)-\bar{\Omega}(\theta_f,\theta_i,n)\right)}{\left|cos\theta_f\right|\left|sin\theta_f\right|}H(\bar{\Omega}(\theta_f,\theta_i,n)) \\ &\frac{4\hbar^2}{128M^2}\sum_{j=1}^{N}\frac{c_j^2}{\omega_j}A\left(\omega_j\right)^2\sum_{\substack{k=1\\k>j}}^{N}\frac{c_k^2}{\omega_k}A\left(\omega_k\right)^2\delta\left(\omega_j+\omega_k-\bar{\Omega}(\theta_f,\theta_i,n)\right) \\ &\left[coth\left(\frac{\hbar\beta\omega_j}{2}\right)+1\right]\left[coth\left(\frac{\hbar\beta\omega_k}{2}\right)+1\right] \end{aligned} \tag{228}$$

$$\left\langle P(\theta_f;\Delta n=1,1)\right\rangle = \sum_{n=-\infty}^{\infty} J_n^2\left(hA(\omega_x)\right) exp(-2W)\frac{2^2}{\pi^2}\frac{4\hbar^2}{128M}\frac{2\left(\Omega(\theta_i,n)-\bar{\Omega}(\theta_f,\theta_i,n)\right)}{\left|cos\theta_f\right|\left|sin\theta_f\right|}H(\bar{\Omega}(\theta_f,\theta_i,n))$$
$$\frac{\pi}{2}\sum_{j=1}^{N}\frac{c_j^2}{\omega_j}A\left(\omega_j\right)^2\frac{\pi}{2}\frac{c_k^2}{\omega_k}A\left(\omega_k\right)^2\delta\left(\omega_j+\omega_k-\bar{\Omega}(\theta_f,\theta_i,n)\right)$$
$$\left[coth\left(\frac{\hbar\beta\omega_j}{2}\right)+1\right]\left[coth\left(\frac{\hbar\beta\omega_k}{2}\right)+1\right] \tag{229}$$

We have that $\omega_j=\bar{\Omega}(\theta_f,\theta_i,n)-\omega_k$ and use the definition of the spectral density to obtain:

$$\left\langle P(\theta_f;\Delta n=1,1)\right\rangle = \sum_{n=-\infty}^{\infty} J_n^2\left(hA(\omega_x)\right) exp(-2W)\frac{\hbar^2}{4\pi M^2}\frac{\left(\Omega(\theta_i,n)-\bar{\Omega}(\theta_f,\theta_i,n)\right)}{\left|cos\theta_f\right|\left|sin\theta_f\right|}H(\bar{\Omega}(\theta_f,\theta_i,n))$$
$$\int_0^{\bar{\Omega}} d\omega\, J_z(\omega)J_z(\bar{\Omega}(\theta_f,\theta_i,n)-\omega)A\left(\omega\right)^2A\left(\bar{\Omega}(\theta_f,\theta_i,n)-\omega\right)^2$$
$$\left[coth\left(\frac{\hbar\beta\omega}{2}\right)+1\right]\left[coth\left(\frac{\hbar\beta\left(\bar{\Omega}(\theta_f,\theta_i,n)-\omega\right)}{2}\right)+1\right] \tag{230}$$

Third possibility - two different modes, one absorbing a phonon, the other emitting a phonon.

Oscillator #→	1	2	...	j	...	...	...	k	...	...	N
Final Occupation # $\mathbf{n_f}$→	n_{1_f}	n_{2_f}	...	...	...	...	...	...	...	...	n_{N_f}
Initial Occupation # $\mathbf{n_i}$→	n_{1_i}	n_{2_i}	...	...	...	...	...	...	...	...	n_{N_i}
$\Delta\mathbf{n}$→	0	...	0	-1	0	...	0	1	0	...	0
ω→	ω_1	ω_2	...	ω_j	...	...	...	ω_k	...	...	ω_N

We have for the scalar product:

$$\Delta\mathbf{n}\cdot\omega=-\omega_j+\omega_k$$

And for the thermal average we have, similiar to the case of 1,1, to lowest order in c_j^2 :

$$\left\langle P(\theta_f;\Delta n=-1,1)\right\rangle = \sum_{n=-\infty}^{\infty} J_n^2\left(hA(\omega_x)\right) exp(-2W)\frac{2\left(\Omega(\theta_i,n)-\bar{\Omega}(\theta_f,\theta_i,n)\right)}{\left|cos\theta_f\right|\left|sin\theta_f\right|}$$
$$\sum_{j=1}^{N}\sum_{k=1}^{N}\frac{\Gamma_j^2\Gamma_k^2}{64}\left[coth\left(\frac{\hbar\beta\omega_j}{2}\right)-1\right]\left[coth\left(\frac{\hbar\beta\omega_k}{2}\right)+1\right]$$

$$\delta\left(-\omega_j+\omega_k-\bar{\Omega}(\theta_f,\theta_i,n)\right) \tag{231}$$

Such that we have that: $\omega_j+\omega_k=\bar{\Omega}(\theta_f,\theta_i,n)$

And in the continuum limit:

$$\left\langle P(\theta_f;\Delta n=-1,1)\right\rangle = \sum_{n=-\infty}^{\infty} J_n^2\left(hA(\omega_x)\right) exp(-2W)\frac{\hbar^2}{2\pi^2M^2}\frac{\left(\Omega(\theta_i,n)-\bar{\Omega}(\theta_f,\theta_i,n)\right)}{\left|cos\theta_f\right|\left|sin\theta_f\right|}$$
$$\int_0^{\infty} d\omega\, J_z(\omega)J_z(\bar{\Omega}(\theta_f,\theta_i,n)+\omega)A\left(\omega\right)^2A\left(\bar{\Omega}(\theta_f,\theta_i,n)+\omega\right)^2H(\bar{\Omega}(\theta_f,\theta_i,n)+\omega) \tag{232}$$

$$\left[coth\left(\frac{\hbar\beta\omega}{2}\right)-1\right]\left[coth\left(\frac{\hbar\beta\left(\bar{\Omega}(\theta_f,\theta_i,n)+\omega\right)}{2}\right)+1\right] \tag{233}$$

Fourth possibility - two different modes, each emitting a phonon

Oscillator #→	1	2	...	j	...	...	...	k	...	...	N
Final Occupation # $\mathbf{n_f}$→	n_{1_f}	n_{2_f}	...	...	...	...	...	...	...	...	n_{N_f}
Initial Occupation # $\mathbf{n_i}$→	n_{1_i}	n_{2_i}	...	...	...	...	...	...	...	...	n_{N_i}
$\Delta\mathbf{n}$→	0	...	0	-1	0	...	0	-1	0	...	0
ω→	ω_1	ω_2	...	ω_j	...	...	...	ω_k	...	...	ω_N

We have that:

$$\Delta\mathbf{n}\cdot\omega=-\omega_j-\omega_k=-(\omega_j+\omega_k)$$

And as the same way as in the 1,1 case we have to lowest order in c_j^2 :

$$\begin{aligned}\left\langle P(\theta_f;\Delta n=-1,-1)\right\rangle &= \sum_{n=-\infty}^{\infty} J_n^2\left(hA(\omega_x)\right) exp(-2W)\frac{2\left(\Omega(\theta_i,n)-\bar{\Omega}(\theta_f,\theta_i,n)\right)}{\left|cos\theta_f\right|\left|sin\theta_f\right|}H(-\bar{\Omega}(\theta_f,\theta_i,n))\\ &\sum_{\substack{j=1\\k>j}}^{N}\sum_{k=1}^{N}\frac{\Gamma_j^2\Gamma_k^2}{128}\left[coth\left(\frac{\hbar\beta\omega_j}{2}\right)-1\right]\left[coth\left(\frac{\hbar\beta\omega_k}{2}\right)-1\right]\\ &\delta\left(-\omega_j-\omega_k-\bar{\Omega}(\theta_f,\theta_i,n)\right)\end{aligned} \tag{234}$$

And for the continuum limit:

$$\begin{aligned}\left\langle P(\theta_f;\Delta n=-1,-1)\right\rangle &= \sum_{n=-\infty}^{\infty} J_n^2\left(hA(\omega_x)\right) exp(-2W)\frac{\hbar^2}{4\pi^2M^2}\frac{\left(\Omega(\theta_i,n)-\bar{\Omega}(\theta_f,\theta_i,n)\right)}{\left|cos\theta_f\right|\left|sin\theta_f\right|}H(-\bar{\Omega}(\theta_f,\theta_i,n))\\ &\int_0^{|\bar{\Omega}|} d\omega\, J_z(\omega)J_z(\left|\bar{\Omega}(\theta_f,\theta_i,n)\right|-\omega)A\left(\omega\right)^2A\left(\left|\bar{\Omega}(\theta_f,\theta_i,n)\right|-\omega\right)^2\\ &\left[coth\left(\frac{\hbar\beta\omega}{2}\right)-1\right]\left[coth\left(\frac{\hbar\beta\left(\left|\bar{\Omega}(\theta_f,\theta_i,n)\right|-\omega\right)}{2}\right)-1\right]\end{aligned} \tag{235}$$

Fifth possibility - one mode, emitting two phonons.

Oscillator #→	1	2	...	...	...	j	...	...	...	...	N
Final Occupation # $\mathbf{n_f}$→	n_{1_f}	n_{2_f}	...	...	...	...	...	...	...	...	n_{N_f}
Initial Occupation # $\mathbf{n_i}$→	n_{1_i}	n_{2_i}	...	...	...	...	...	...	...	...	n_{N_i}
$\Delta\mathbf{n}$→	0	...	...	...	0	-2	0	...	...	...	0
ω→	ω_1	ω_2	...	...	...	ω_j	...	...	...	...	ω_N

We have that:

$$\Delta\mathbf{n}\cdot\omega=-2\omega_j$$

We note again that in this case we will have a contribution of the order Γ_j^4,just like we had Γ_j^2 for the one-phonon contribution. This contribution is of order c_j^4 and will therefore be neglected in the continuum limit. We will therefore have no contribution from this term.

23.2 The Total Angular Distribution for 0,1 and 2-phonon Contributions

The angular distribution is then given by the sum of all the contributions given above:

$$\begin{aligned}\left\langle P(\theta_f;\Delta n=-2,-1,0,1,2)\right\rangle &= \left\langle P(\theta_f;\Delta n=0)\right\rangle + \left\langle P(\theta_f;\Delta n=1)\right\rangle \\ &+ \left\langle P(\theta_f;\Delta n=-1)\right\rangle + \left\langle P(\theta_f;\Delta n=-1,-1)\right\rangle \\ &+ \left\langle P(\theta_f;\Delta n=1,1)\right\rangle + \left\langle P(\theta_f;\Delta n=-1,1)\right\rangle\end{aligned}$$

24 Beam collimation

24.1 The Model System

In this section we will again use the SCP theory, to study how collimation affects the measured angular distribution. For the study of collimation, we use the same model system, but take out the bath by taking N=0 oscillators, thereby removing the sum over the bath variables from the Hamiltonian. The Hamiltonian for the scattering of mass M from a corrugated surface is then written as:

$$\hat{H} = \frac{\hat{p}_x^2 + \hat{p}_z^2}{2M} + \bar{V}(\hat{z}) + \bar{V}'(\hat{z})h(\hat{x}) \tag{236}$$

By making the substitution N=0 for the S-matrix element we obtain the simplified expression for the S-matrix squared:

$$\left|S_{n,0}\right|^2 = J_n^2\left(hA(\omega_x)\right) \tag{237}$$

And the diffraction probability becomes:

$$P_{n,0} = \left|S_{n,0}\right|^2 \tag{238}$$

The final momentum distribution simplifies to:

$$P(p_{x_f}, p_{z_f}) = \sum_{n=-\infty}^{\infty} \delta(p_{x_f} - p_{x_i} - \frac{2\pi\hbar n}{l})\,\delta(p_{z_f} - p_{z_{t_0}})P_{n,0} \tag{239}$$

24.2 Averaging over Initial Velocities

Typically the incident beam has a Gaussian distribution of velocities centered about some average values. We may assume that this distribution takes the form

$$P(p_{||}, p_{\perp}, \bar{p}_{||}) = \frac{1}{\pi\sigma_{||}\sigma_{\perp}} exp\left(-\frac{(p_{||}-\bar{p}_{||})^2}{\sigma_{||}^2} - \frac{p_{\perp}^2}{\sigma_{\perp}^2}\right) \tag{240}$$

where $p_{||}$ is the (negative) incident momentum in the direction of the average propagation of the beam while $p_{\perp}$ is the incident momentum perpendicular to the average direction of propagation. The average incident (negative) scattering angle $\bar{\theta}_i$ is by definition the angle between the average (negative) parallel momentum $\bar{p_{||}}$and the z axis. We then have that the parallel and perpendicular momenta may be expressed in terms of the vertical and horizontal incident momenta as,

$$p_{||} = p_{z_i} cos(\bar{\theta}_i) + p_{x_i} sin(\bar{\theta}_i) = -p_i cos(\theta_i - \bar{\theta}_i) \tag{241}$$

$$p_{\perp} = -p_{z_i} sin(\bar{\theta}_i) + p_{x_i} cos(\bar{\theta}_i) = p_i sin(\theta_i - \bar{\theta}_i) \tag{242}$$

with

$$p_i^2 = p_{x_i}^2 + p_{z_i}^2 = \sqrt{2ME_i} \tag{243}$$

We insert these expressions into the momentum distribution:

$$P(p_{||}, p_{\perp}; \bar{p}_{||}, \bar{\theta}_i) = \frac{1}{\pi\sigma_{||}\sigma_{\perp}} exp\left(-\frac{(-p_i cos(\theta_i - \bar{\theta}_i) - \bar{p_{||}})^2}{\sigma_{||}^2} - \frac{\left[p_i sin(\theta_i - \bar{\theta}_i)\right]^2}{\sigma_{\perp}^2}\right) \tag{244}$$

$$= \frac{1}{\pi\sigma_{||}\sigma_{\perp}} exp\left(-\frac{(p_i cos(\theta_i - \bar{\theta}_i) + \bar{p_{||}})^2}{\sigma_{||}^2} - \frac{p_i^2 sin^2(\theta_i - \bar{\theta}_i)}{\sigma_{\perp}^2}\right) \tag{245}$$

We now assume "good" collimation in the perpendicular direction such that

$$P(p_{||}, p_{\perp}; \bar{p}_{||}, \bar{\theta}_i) = \frac{1}{\pi\sigma_{||}\sigma_{\perp}} exp\left(-\frac{(p_i + \bar{p_{||}})^2}{\sigma_{||}^2} - \frac{p_i^2 sin^2(\theta_i - \bar{\theta}_i)}{\sigma_{\perp}^2}\right) \tag{246}$$

24.3 The Angular Distribution

One may now derive an expression for the angular distribution.

We use the notation

$$B_n(\theta_i) = \frac{2\pi\hbar n}{l p_i cos\theta_i}$$

and replacing $B_n(\theta_i)$ with its value at the maximum, $B_n(\bar{\theta}_i)$ and similarly for $|S_{n,0}|^2$we find that the final angular distribution is [52]:

$$P(\theta;\bar{p}_{||},\bar{\theta}_i) \simeq \sum_{n=-\infty}^{\infty} \int_0^{\infty} dp_i\, p_i\, \frac{|S_{n,0}(p_i,\bar{\theta}_i|^2}{\pi\sigma_{||}\sigma_{\perp}} exp\left(-\frac{(p_i+\bar{p}_{||})^2}{\sigma_{||}^2} - \frac{p_i^2(tan^{-1}[B_n(\bar{\theta}_i)]-\theta-\bar{\theta}_i)^2}{\sigma_{\perp}^2}\right)$$

and the remaining integral over the initial momentum has to be carried out numerically.

This result is instructive. We note that the uncertainty in the parallel momentum only serves to average out the magnitude of the separate diffraction probabilities, but it does not affect the diffraction pattern itself. Each separate diffraction peak is smeared only through the uncertainty in the perpendicular momentum, as expressed by the angular width $\sigma_{\perp}/(\sqrt{2}\ p_i)$. This demonstrates that sufficient collimation will reveal the underlying diffraction structure of the angular momentum distribution. It also provides a quick estimate for the collimation needed to expose the diffraction pattern.

The angular distance between successive diffraction peaks is

$$\Delta\theta_n = tan^{-1}[B_{n+1}(\bar{\theta}_i)] - tan^{-1}[B_n(\bar{\theta}_i)] \tag{247}$$

Thus, the condition for the observation of the n-th diffraction peak is

$$\frac{\sigma_{\perp}}{p_i} \ll \Delta\theta_n$$

We note that the angle difference between diffraction peaks is not linear in the diffraction number. As the diffraction number increases, the angle difference decreases and a better angular resolution is needed to resolve the peak. As is well-known, the angle difference decreases with increasing momentum of the projectile and with increasing mass.

If we further replace p_i with its average value $-\bar{p}_{||}$ in the argument of the S-matrix element and the term $tan^{-1}[B_n(\bar{\theta}_i)]$ we readily find that the angular distribution reduces to a sum over error functions: [52]

$$P(\theta;\bar{p}_{||},\bar{\theta}_i) =\simeq \sum_{n=-\infty}^{\infty} \frac{\sigma_{||}\sigma_{\perp}|S_{n,0}(\bar{p}_{||},\bar{\theta}_i)|^2}{2\pi C_n^2}\left(exp\left[-\frac{\bar{p}_{||}^2}{\sigma_{||}^2}\right] - \frac{\bar{p}_{||}\sqrt{\pi}\sigma_{\perp}}{\sigma_{||}C_n} exp\left[-\frac{\bar{p}_{||}^2}{\sigma_{||}^2}\left\{\frac{C_n^2-\sigma_{\perp}^2}{C_n^2}\right\}\right] erfc\left[\frac{\bar{p}_{||}\sigma_{\perp}}{\sigma_{||}C_n}\right]\right)$$

and we used the notation:

$$C_n^2 = \left[\sigma_{\perp}^2 + \sigma_{||}^2(tan^{-1}[B_n(\bar{\theta}_i)] - \theta - \bar{\theta}_i)^2\right]$$

This equation provides us with a closed expression for the angular distribution after averaging over the gaussian profile of the incident beam.

24.4 The Classical Angular Distribution

It is of interest to us to also derive an expression for the classical angular distribution, to facilitate comparison between the SCP theory and classical theory.

We define the rainbow shift angle function K which arises in the classical perturbation theory defined by Pollak and co-workers: [55, 36, 38, 39]

$$K(p_{x_i}, p_{z_i}) = \frac{2\pi}{l p_{z_i}} h\hbar A(\omega_x)$$

For the model sine corrugation function, we find that:

$$p_{x_f} - p_{x_i} = -p_{z_i} K(p_{x_i}, p_{z_i}) cos\frac{2\pi x_0}{l}$$

The classical angular distribution is found to be [52]:

$$P(\theta_f) = \frac{1}{\pi\sqrt{K(p_{x_i}, p_{z_i})^2 cos^2(\theta_i+\theta_f) - sin^2(\theta_i+\theta_f)}} H\left[K(p_{x_i}, p_{z_i})^2 - tan^2(\theta_i+\theta_f)\right]$$

Averaging over the profile of the incident beam is then readily approximated as:

$$\begin{aligned}\left\langle P(\theta_f)\right\rangle \quad \simeq \quad & \frac{\bar{p}_{||}}{\pi\sqrt{\pi}\,\sigma_{\perp}} \int_{-\pi/2}^{\pi/2} du \frac{1}{\sqrt{1+K(p_{x_i}, p_{z_i})^2 - K(p_{x_i}, p_{z_i})^2 sin^2 u}} \\ & exp\left(\frac{\bar{p}_{||}^2}{\sigma_{\perp}^2}\left[sin^{-1}\left(\frac{K(p_{x_i}, p_{z_i})}{\sqrt{1+K(p_{x_i}, p_{z_i})^2}} sin\, u\right) - \bar{\theta}_i - \theta_f\right]^2\right)\end{aligned}$$

The averaging over the angular width of the incident beam smooths the classical divergence at the rainbow angles.

Part VI

Results

In the following section we will use the SCP theory to analyze the measured low temperature angular distribution of Ne, Ar and Kr scattered from a Cu(111) surface, and compare to experimental results [49, 50]. We will use the continuum theory as described in Part V. We use the Morse potential model as the particle potential, this allows us to obtain closed analytic expressions for the trajectory. We will start by reviewing the experimental setup. We end the discussion with some results demonstrating the effects of beam collimation for a different system, the Ar-LiF(100) system.

24.5 Experimental Setup

We will compare our theory to experimental results provided by Andersson et al. [49, 50]. The basic experimental setup is depicted in Fig. 3.

The experiments conducted by Andersson and co-workers facilitate a fairly sophisticated setup for gas-scattering. To observe quantum effects, it was to necessary to observe the low-temperature behavior of the angular distribution. This required measurements to be performed at such low incident energy that the probe particles, with few exceptions, stick permanently and accumulate on the target surface. Adsorbed particles will then quickly blur the results of the coherent scattering and the data collection time becomes too short. They had to devise a remedy for this complication. Their solution was to desorb the particles by laser pulses of short duration so that the mean surface temperature is marginally affected. For this purpose they used a Lambda Physik XeCl excimer laser operating at a laser power $< 3\ MW/cm^2$ and 20ns pulse duration. It was found that repetition rates of around a few Hertz are in general sufficient to keep the surface clean. The laser beam used hit the surface close to normal incidence and the reflected beam exits via the entrance window. Under the relevant temperatures the surface ordering was found to be unaffected by laser irradiation as revealed by specular elastic scattering measurements with and without laser heating.

The scattering experiments were carried out in a cryopumped ultrahigh vacuum chamber operating at a base pressure of $2 * 10^{-11}$Torr and attached to a differentially pumped nozzle beam source. The incident and scattered beam intensities were measured using a rotatable stagnation detector with an angular resolution of 0.8^0. The angular divergence of the incident beam was about 0.1^0.

The x-ray aligned and polished Cu(111) surface was cleaned in a ultrahigh vacuum chamber by standard methods involving argon-ion bombardment and heating cycles.

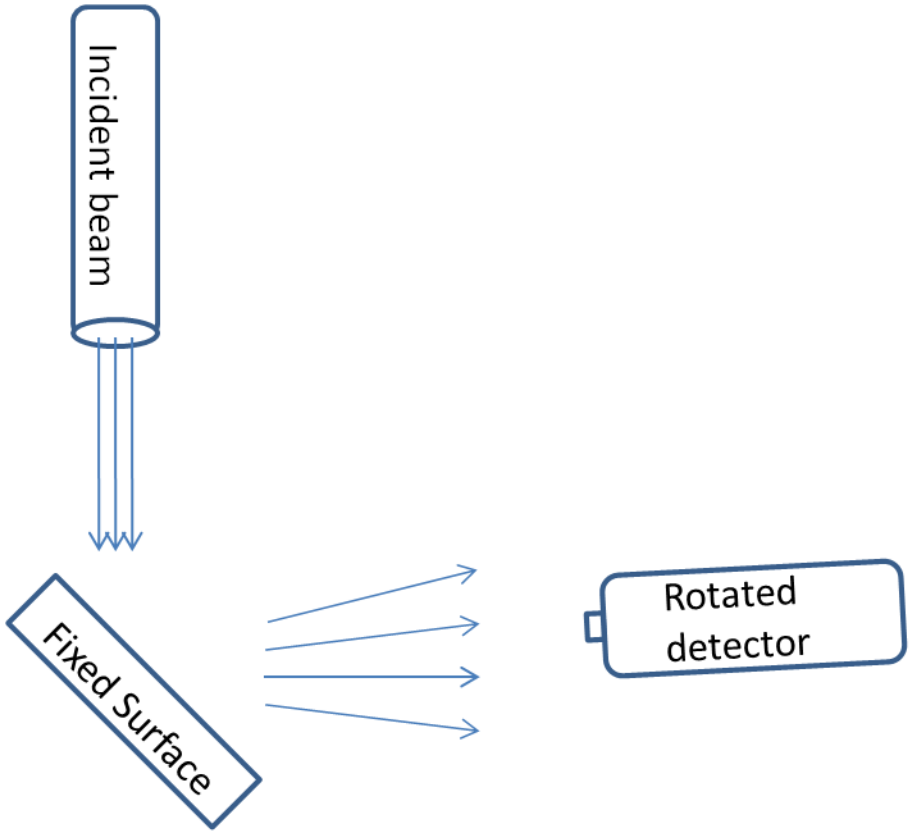

Figure 3: The Experimental Settings for all scattering experiments described in this work. The surface and particle incident angle is fixed. The detector is rotating, thereby able to measure the reflected particle intensity from different particle reflection angles.

25 Parametrization

As we explained, our theory uses a Morse potential, and so we need parameters for the potential - the stiffness parameter α, the well-depth V_0, the friction coefficient $\bar{\gamma}$ as well as the corrugation height h.

Table 1: Parameters used for Ne,Ar and Kr scattered on a Cu(111) surface.

	$\alpha \cdot l$	$V_0[meV]$	$\bar{\gamma}[dimensionless]$	$h[a.u.]$
Kr	4.2	134.0	0.1205	$2.82 \cdot 10^{-3}$
Ar	3.3	70.0	0.05782	$1.98 \cdot 10^{-3}$
Ne	3.0	31.6	0.01234	$1.10 \cdot 10^{-3}$

The well depths are taken from recent ab-initio computations [65] and presented in Table 1. The lattice length is 3.61 Angstrom [66]. The "corrugation height" is determined from the measured ratio of the $n = 0$ to $n = -1$ Bragg peaks, which determines the magnitude of the phase amplitude $hA(\omega_x)$ appearing in the argument of the respective Bessel functions. The spectral density is chosen to be Ohmic (for a theoretical justification see Ref. [67]) with an exponential cutoff $J(\omega) = \gamma\omega \exp(-\omega/\omega_c)$. The cutoff frequency is considered here to be a property of the surface and is the same for all the atoms. The friction coefficient $\bar{\gamma}$ is fit separately for each atom. The theory thus involves only two parameters for each atom $(\bar{\gamma}, \alpha)$ and the cutoff frequency ω_c, common to all cases. The parameters are given in Table 1 ($\bar{\gamma} = M^2\omega_0^3\gamma$ where $\omega_0^2 = 2V_0\alpha^2/M$).

The Debye-Waller factor was calculated using equations 174 and 175[51]. It leaves very little freedom in the fitting procedure, except for the cutoff frequency $\hbar\omega_c$ chosen to be 6 meV.

26 Results for the Continuum Theory (only 0,1 and 2-phonon Transitions)

As we will see, the theory provides a good description of the quantum dominated low energy and low surface temperature measurement of the scattering of Ne, Ar and Kr on a Cu(111) surface [49, 50]. We will also address this specific system to provide predictions concerning the effect of beam collimation[49, 50].

26.1 The Debye-Waller Factor

We first present results for the Debye-Waller factor using the continuum theory (Eq. 175) and its comparison to the experiment of Andersson and co-workers. This first test of the theory demonstrates how it fits the

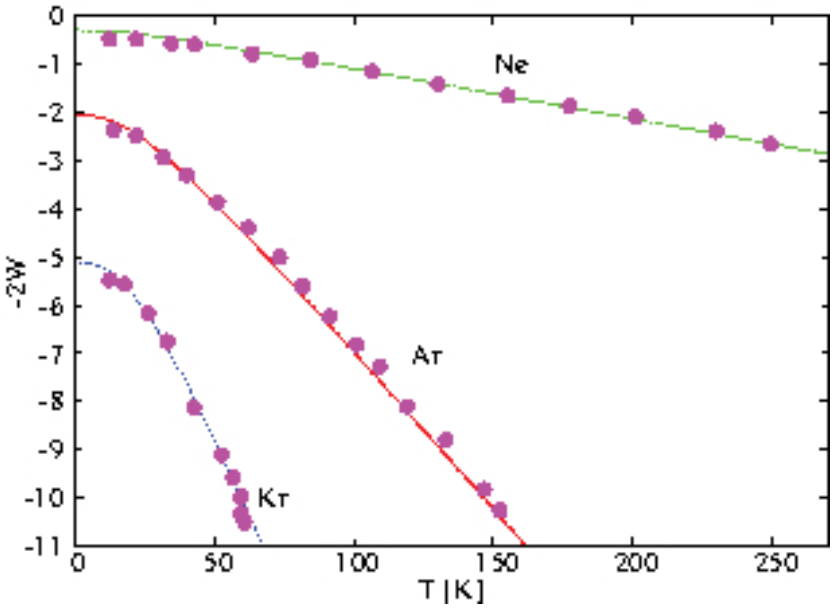

Figure 4: The Semiclassical Perturbation approximation (continuum theory) fit to the measured temperature dependence of the Debye-Waller factor for Ne, Ar and Kr scattered from Cu(111). The solid circles represent the experimental results of [49, 50]while solid lines are the fits obtained with our theory. The parameters are given in Table 1.

temperature changes of the experiment. We use the fitting parameters given above in Table I.

26.2 The Angular Distribution

Next, we wish to use our theory to obtain the angular distribution, and compare to experiment. Results are provided in figure 5.

In all cases that will be presented using this model, the elastic peaks were Gaussian broadened ($\Delta\theta = 0.4^o$), to agree with the experimental broadening, as also detailed in Ref. [50]. For Ne scattering at 10K, the two phonon contribution is negligible. This provides an objective criterion for determining that at this temperature only single phonon scattering takes place. The fit to experiment indicates that the chosen Ohmic spectral density provides a good description for the coupling of the Ne atom to the surface phonons. The minuscule Bragg peak at $n = -1$ which cannot be seen on the scale of the figure, implies that the corrugation is very weak.

From all these findings we gained a better understanding of the diffraction process, especially when dominated by few-phonon transitions. When only few (say, 0, 1 or 2) phonon transitions take place, such as at very low temperatures we have shown that it is possible to attribute the different contributions in the angular distribution to each type of phonon transition. For zero-phonon transitions we have elastic scattering which

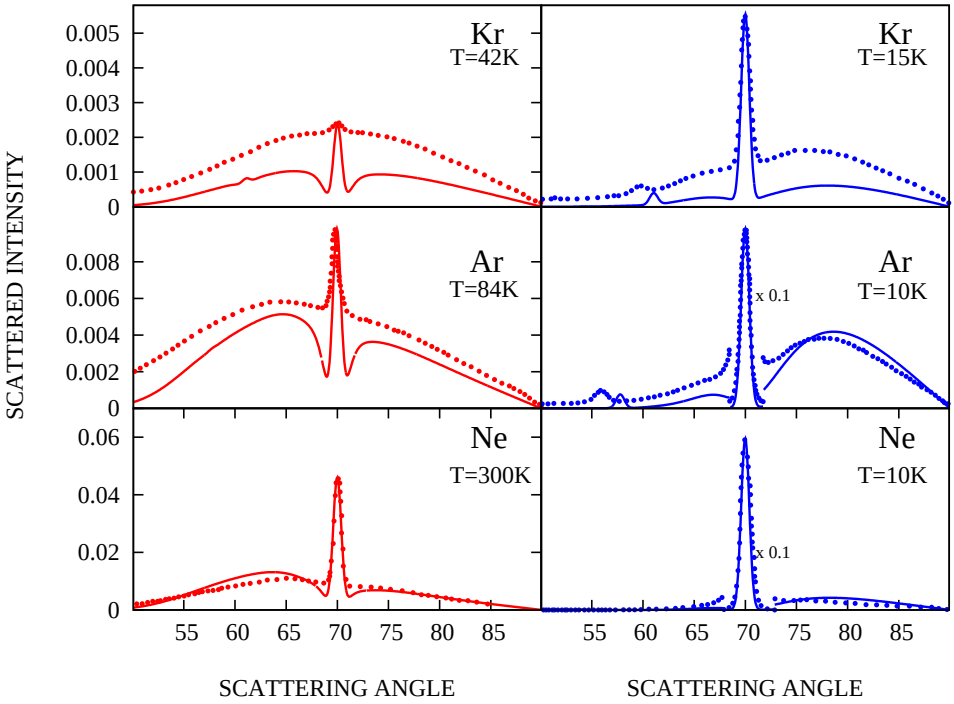

Figure 5: Comparison of the Semiclassical Perturbation theory (continuum theory) generated (solid lines) angular distributions and the experimental measurements (dotted lines) for low (right panel) and high (left panel) surface temperatures. The low temperature experimental and theoretical specular peaks for Ne and Ar are multiplied by 0.1 to fit them into the scale of the plots (the plots were scaled so as to fit the maxima of the reported experimental unnormalized distributions).

leads to sharp Bragg peaks, among them the specular peak. For 1-phonon transition and in a lesser extent to 2 and higher phonons, we obtain a broad background which is composed of many small contributions resulting from energy transfer to and from the surface.[49]

27 Results for Discretized Multiphonon Theory - for All Phonon Transitions

27.1 The Debye-Waller Factor and Its Comparison for Both Theories

A first check on the discretized multi-phonon theory is to determine how well the continuum limit expression for the Debye-Waller factor (Eq.175) (obtained by expansion of the Bessel functions to lowest order and exponentiation) agrees with its discretized form which is a sum of thermally averaged Bessel functions (Eq. 174)The results are presented in Fig. 6 and show good agreement between the two theories. The agreement with experiment has already been presented above and in [51].

27.2 The Angular Distribution

A second check of the present theory is to compare the results for the discretized theory (dashed lines) with the continuum limit expressions (solid lines) for up to two phonon contributions. This is shown in Fig. 7. One notes, that apart from the oscillations due to the finite discretization, there is good agreement between the various computations.

In the continuum theory, only up to two phonon contributions were included, using the continuum form. The comparison with the experimental results showed good agreement at very low temperature, but as the temperature was increased, especially for Ar and Kr scattering, there were deviations which we attributed to higher order phonon scattering contributions. That this is so, is shown in Fig. 8 where we plot the angular distributions obtained using one, two and multi-phonon contributions. As the temperature is increased, the all phonon contribution becomes larger relative to the continuum one and two phonon results. At the higher temperature, one should not ignore multi-phonon contributions.

Finally, in Fig. 9 we compare the discretized theory, including all multi-phonon contributions with the experimental results of Ref. [50]. The parameters used are the same as those used for the analytic theory, that is they were based only on fitting the low temperature distributions. We find good agreement between experiment and theory for the scattering of Ne and Ar. From Fig. 8 it is clear that for Ne, more than two phonon transitions are not important, even at room temperature. This is not the case for the scattering of Ar,

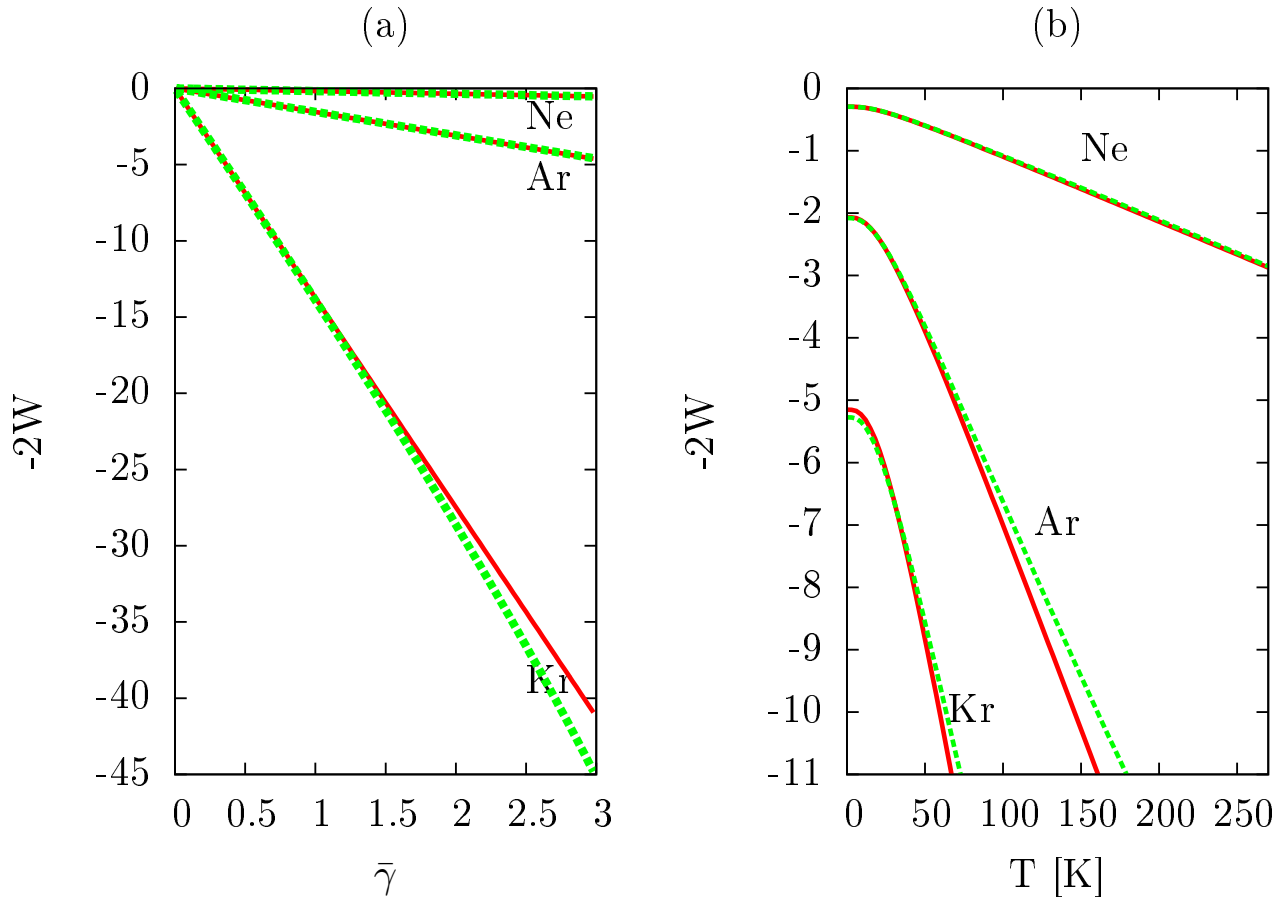

Figure 6: Comparison of the continuum limit expression for the Debye-Waller factor (Eq. 175) and its estimate as the discretized sum of Bessel functions (Eq. 174) . The results are presented (continuum limit - dashed, green line, discretized expression - solid, red line) for the scattering of Ne, Ar and Kr as a function of the reduced friction coefficient in panel (a) and as a function of the surface temperature in panel (b). The number of oscillators used was 40.

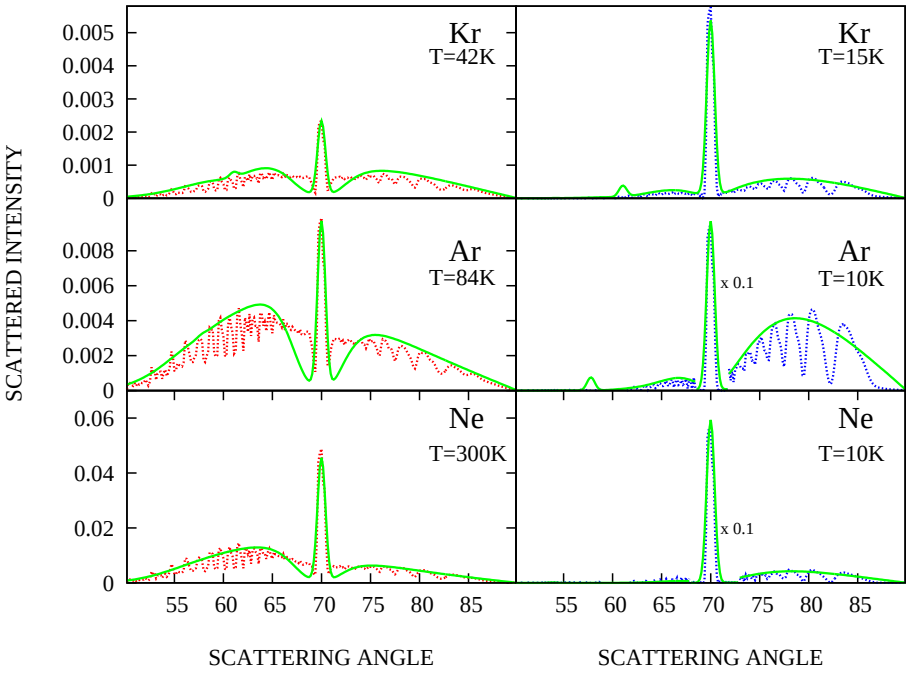

Figure 7: Comparison between the discretized theory and the continuum angular distributions when only one and two phonon contributions are allowed. Apart from the oscillatory character of the discretized results, there is good agreement between the two computations. The number of oscillators used for the discretization was 20.

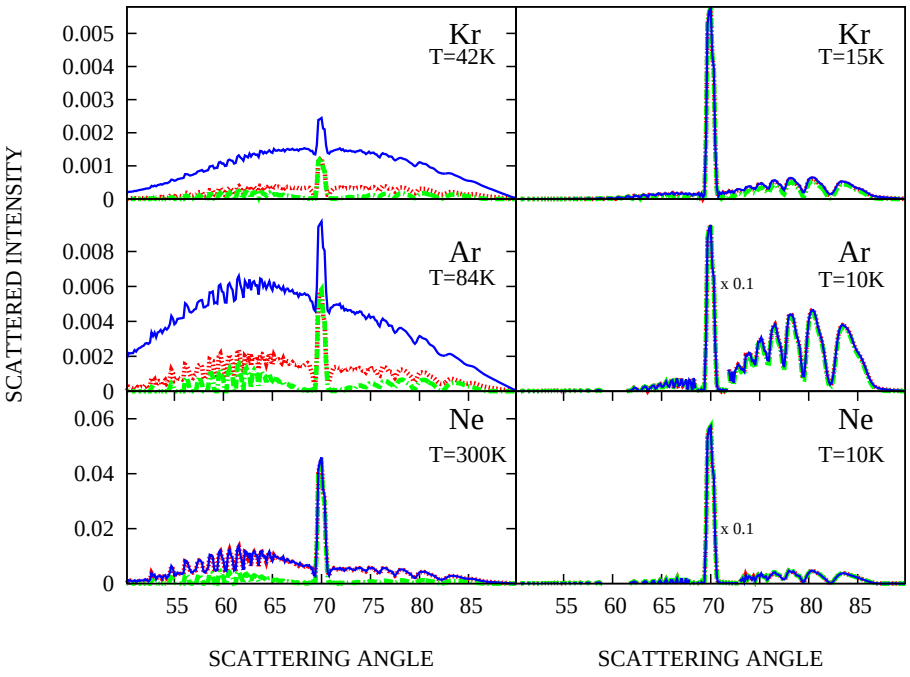

Figure 8: The contributions of multi-phonon transitions as the surface temperature is increased. The one (dash-dotted line), one+two (dotted) and all phonon (solid) contributions are shown for the angular distributions of Ne, Ar, and Kr, scattered on the Cu(100) surface. Note the increased contribution from multi-phonon transitions as the temperature is increased. The number of oscillators used in the discretized computation is 20.

where only inclusion of the multi-phonon transitions at T=84 K gives quantitative agreement with experiment. Finally, for Kr scattering, the results, especially at the higher temperature (T=42K) where the multi-phonon contributions are significant are in better agreement with experiment than the previous results based on only up to two phonon transitions. We do note that already the low temperature theoretical results, presented in Ref. [51] were a bit low, so the lack of quantitative agreement is not surprising.

We note the change in the location of the background peaks as we change the surface temperature. For both the discretized and continuum theory, we can observe a shift of the maximum of the background from the left (scattering angle smaller than specular) to the right (scattering angle larger than specular). This can be attributed to the existence of a phonon bath in the z direction only (no x-bath). That happens because as we strengthen the bath (by raising the temperature) the scattering angle tends to go to angles higher than specular. The experimental results further confirm this assumption.

27.3 Assessment of Convergence of the Discretized Theory

The discretized theory is presented in figure 9 for 20 oscillators and infinite phonon contributions. To assess whether 20 oscillators are enough, we also made the same calculation using 10 oscillators. This is presented in Figure 10. Careful scrutiny reveals that for 10 oscillators, we observe more oscillatory behavior than for 20 oscillators. We expect that as we go to higher number of oscillators, our result will become smoother. For 20 oscillators the picture is relatively satisfactory, although it could be improved for more oscillators. We do not expect any surprises by using more oscillators, and the reason that we used 20 oscillators only is due to the limited computing power available to us. We also provide a plot showing the different phonon orders for 10 oscillators in Fig. 11. It is similar to the figure for 20 oscillators (Fig. 8), though somewhat more oscillatory.

28 Demonstration of Beam Collimation Effects for the Ar-LiF(100) System

Kondo et al. [68] have measured an angular distribution for the scattering of Ar on the LiF(100) surface. In their experiment, the incidence energy was varied between 300 and 700 meV. The angle between the incident beam and the detector was kept fixed at 90^0 and the final intensity was measured as a function of the angle of incidence which was varied about 45^o . The angular distribution measured in this way is qualitatively similar to the angular distribution measured when the incident angle is fixed at 45^o relative to the vertical axis and the final angle is measured. To simplify then we will discuss here only the final angular distribution measured

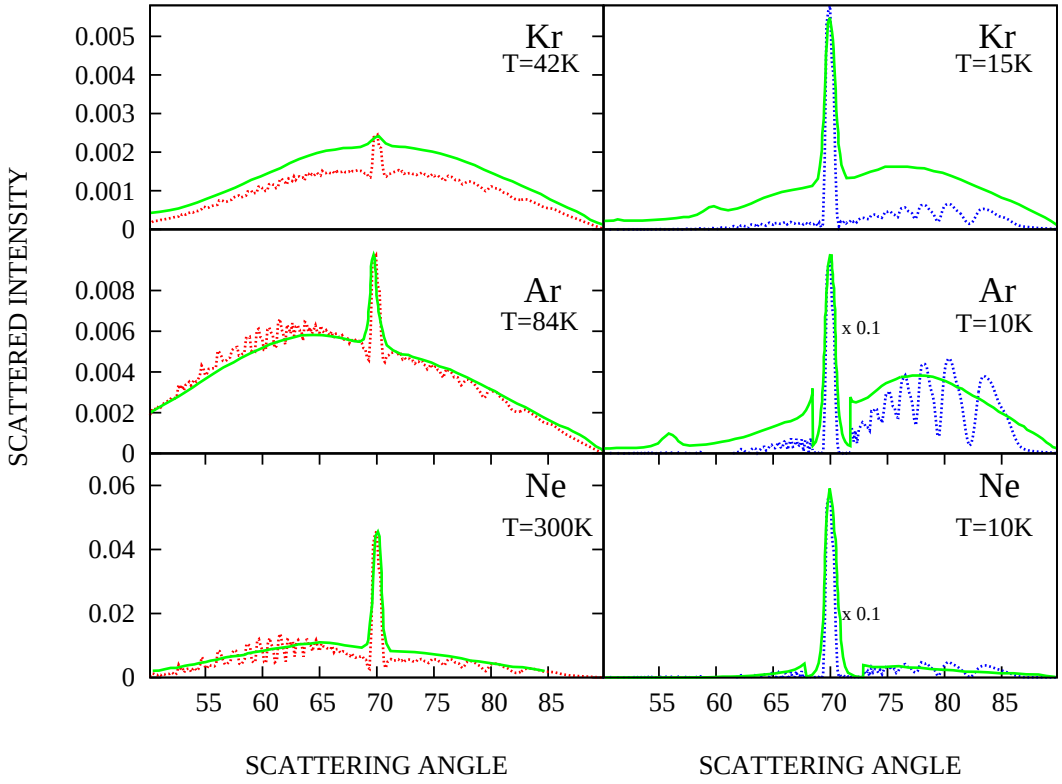

Figure 9: Comparison of the theoretically generated (dashed lines) angular distributions using the multi-phonon discretized theory with the experimental measurements (solid lines) of Ref. [50] for the scattering of Ne, Ar and Kr on the Cu(100) surface. The experimental and theoretical distributions were scaled to agree with each other at the specular peak. The discretized theory is based on 20 oscillators.

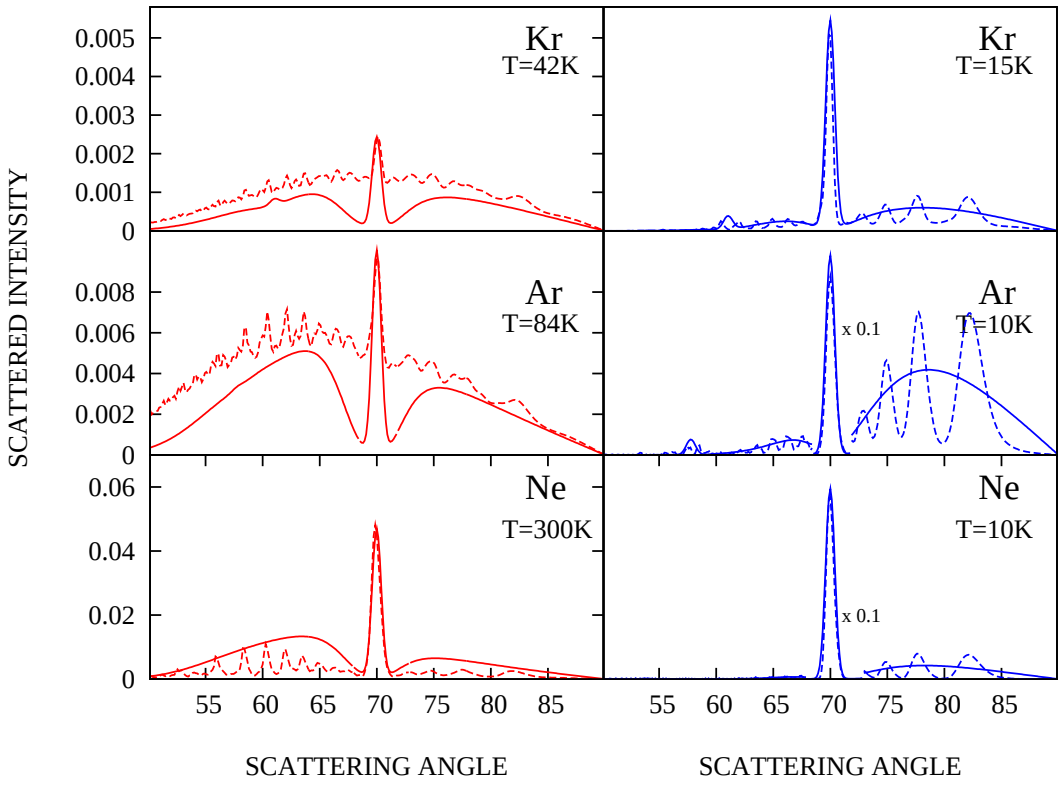

Figure 10: Comparison of the continuum theory (solid lines) - final angular distributions and the discretized theory (dotted lines) for low (right panel) and high (left panel) surface temperatures. Continuous model takes into account only 0,1,2 phonon contributions. Discretized theory results account for infinite phonon contributions for $N_B = 10$ harmonic oscillators, using a beam width of 0.2^o. The low temperature specular peaks for Ne and Ar are multiplied by 0.1 so as to fit them into the scale of the plots. It can be clearly seen that for 10 oscillators the discretized bath model resembles the continuous model using discrete phonon peaks, and even outperforms it in its resemblance to the experiment [50] for Kr and Ar at high temperatures (where high phonon contributions count the most).

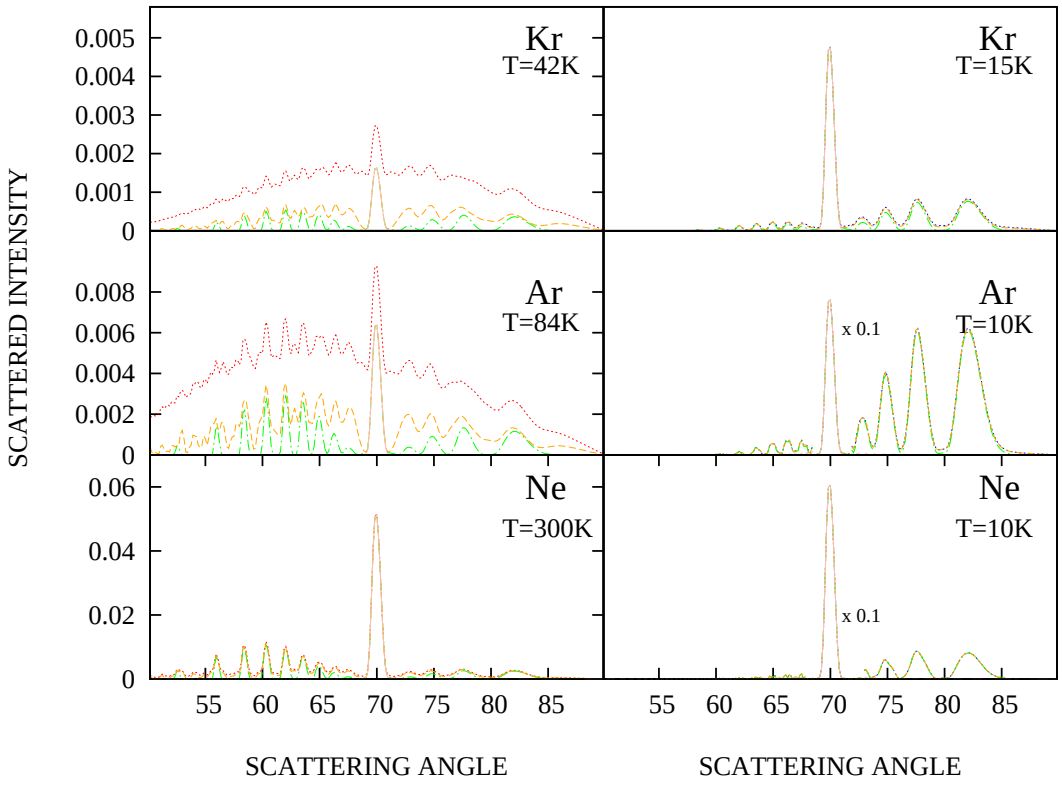

Figure 11: Comparison of the theoretically generated angular distributions obtained using the discretized theory (10 oscillators) for different numbers of phonon contributions. Zero-phonon contributions (solid pink) provide us only with the specular peak, while zero-and-one phonon contributions (solid-dashed green) provide some additional background. Zero, one and two-phonon contributions (dashed yellow) enlarge the background and infinite phonon contributions (red) provide a picture that resembles the experimental distributions, especially for Kr and Ar at high temperatures.

at the fixed angle of incidence of 45^o. Pollak and co-workers[36, 38, 39]have used a Morse potential and a sinusoidal corrugation to fit the experimentally measured results. Here we will use the same model, with a single corrugation function with corrugation height $h = 0.2\ a.u.$. The lattice length of the surface is $l = 4$, the Morse potential well depth was chosen as $V_0 = 88meV$ and the stiffness parameter α was chosen such that $\alpha l = 3$. The various analytic expressions for this model are given by:

$$K(p_{x_i}, p_{z_i}) = \frac{4\pi^2 h}{l} \frac{\bar{\Omega} cosh(\Phi\bar{\Omega})}{sinh(\pi\bar{\Omega})},$$

where the dimensionless parameter:

$$\bar{\Omega} = \frac{2\pi}{\alpha l} |tan\theta_i|$$

and the energy dependent angle Φ varies from $\pi/2$ at high incidence energies to π at low energies and is defined as,

$$cos\Phi = -\sqrt{\frac{V_0}{V_0 + E_i cos^2\theta_i}}$$

In the experiment the uncertainty in the incidence energy ($\frac{\Delta E_i}{E_i}$) was roughly 20% at all energies, implying a momentum uncertainty for the parallel incident momentum of 10%. The experimental paper does not report the angular resolution for the Ar beam, here we use a 2^0 angular width as our base line. We thus have that at all energies studied experimentally we choose the Gaussian widths of the incident beam as

$$\frac{\sigma_{||}}{\sqrt{2}\ p_i} = 0.1 x_{||}$$

and

$$\frac{\sigma_{\perp}}{\sqrt{2}\ p_i} = \frac{\pi}{90} x_{\perp}$$

where it is understood that the experimental conditions are assumed to correspond to the scaling parameters $x_{||}$ and $x_{\perp}$equaling unity.

In Figure 12 we plot the dependence of the angle difference function as defined in Eq. 247 as a function of the quantum number n of the nth diffraction peak at two incident energies. At the lower energy (E = 315 meV), the angle difference function is of the order of 1.5^0 over the whole region in which one finds measurable scattering amplitude. At the higher energy (E = 705 meV) the angular difference in the experimentally relevant region is roughly 1^0 . Clearly a higher angular resolution is needed for the higher energy, as expected from

theory and from the observation that as the projectile's energy increases, one may expect it to be closer to the classical limit.

The angular distributions predicted by our model are shown in Figure 13 for the low energy case (315 meV) and in Figure 14 for the high energy case (705 meV). The uncertainty in the parallel momentum is kept fixed in all computations at 10%. In each of the plots, we show four results. The SCP angular distributions are plotted for three values of the perpendicular variance parameter $x_{\perp}$ - 1, 0.25, 0.1 corresponding to angular widths of 2^0 , 0.5^0 and 0.1^0 , respectively. We also show the classical distribution averaged with an angular width of 2^0. We first note that the SCP angular distribution is almost identical to the classical one when the angular width is 2^0. This is to be expected, since as one can see from Figure 12, the angular difference between successive peaks is at most 1.6^0 at this energy. It is also evident that increasing the resolution by an order of magnitude is sufficient for resolving the complete diffraction pattern. At the higher energy, the angular difference between successive peaks is smaller. Although all diffraction peaks are resolved with a width of 0.2^0 , one notes that the base line is not zero as it is in the lower energy. One would need to decrease the angular width of the incident beam a bit more. This analysis also explains why typically, one should expect that the diffraction peaks will be less noticeable around the classical rainbow angles. These angles are at the edge of the observable distribution, where the diffraction number is higher, so that a higher angular resolution of the incident beam is needed to resolve the separate diffraction peaks appearing under the envelope.

The collimation results show clearly the emergence and disappearance of the diffraction peak as the beam width is increased. Reducing the beam width from 2^o to 0.2^o,a factor of 10, is found to be sufficient for observing the full diffraction pattern. The results presented for this case ignore the effect on phonons on the scattering.

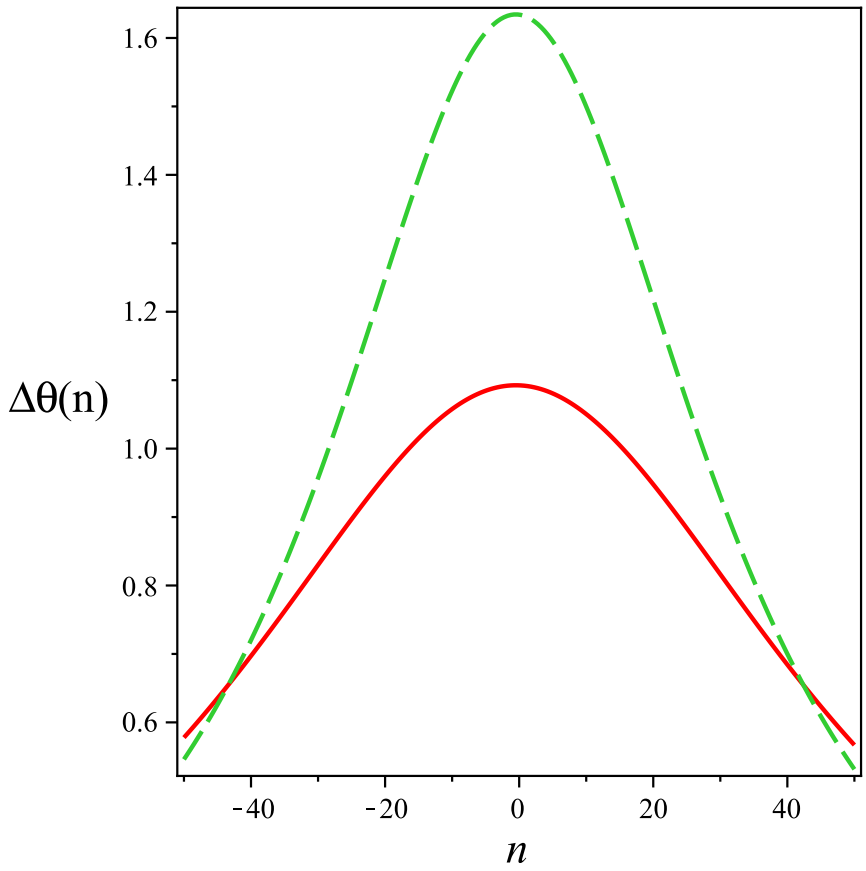

Figure 12: The angle difference function θ(n) (in degrees) needed to resolve individual diffraction peaks is plotted versus the diffraction number n for a model of Ar scattered on a LiF(100) surface at two energies of incidence. The green (dashed) line is at an energy of 315meV, the red (solid) line as at E=705 meV.

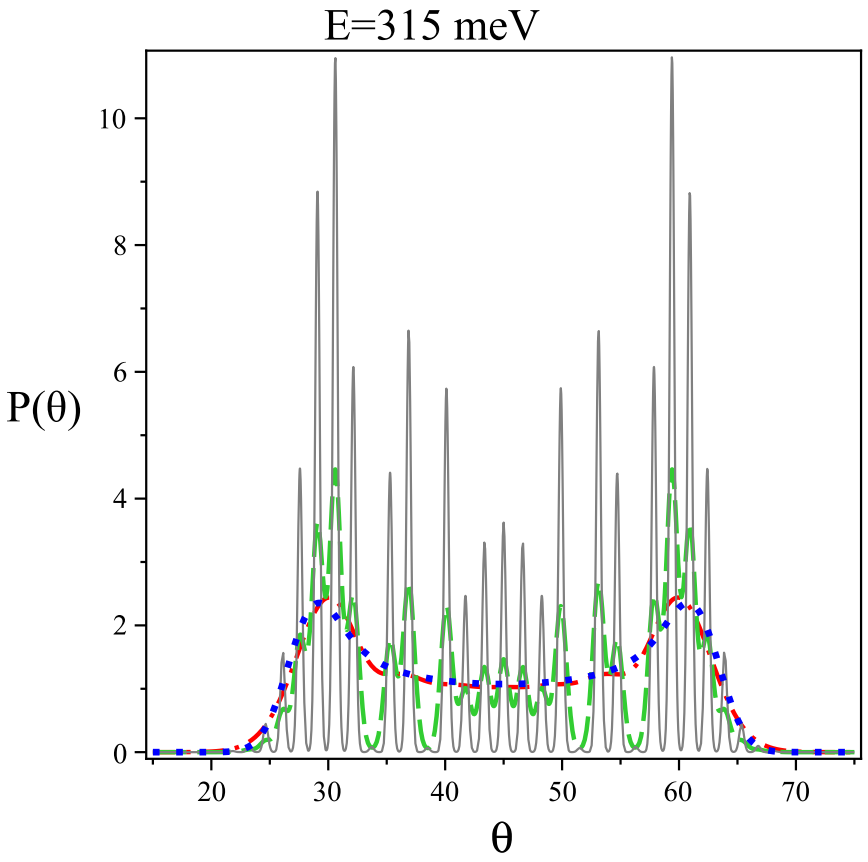

Figure 13: The SemiClassical angular distributions for scattering of Ar on LiF(100) at E=315meV is plotted for different angular widths of the incident beam. The gray (solid), green (dashed) and red (dashed-dotted) lines correspond to angular widths of $0.2^o, 0.5^o, 2^o$,respectively. The blue (dotted) line is the classical distribution obtained with an angular width of 2^o.Note the well resolved diffraction peaks for a beam width of 0.2^o,while for a beam width of $2^o$the SemiClassical and classical distributions are almost identical.

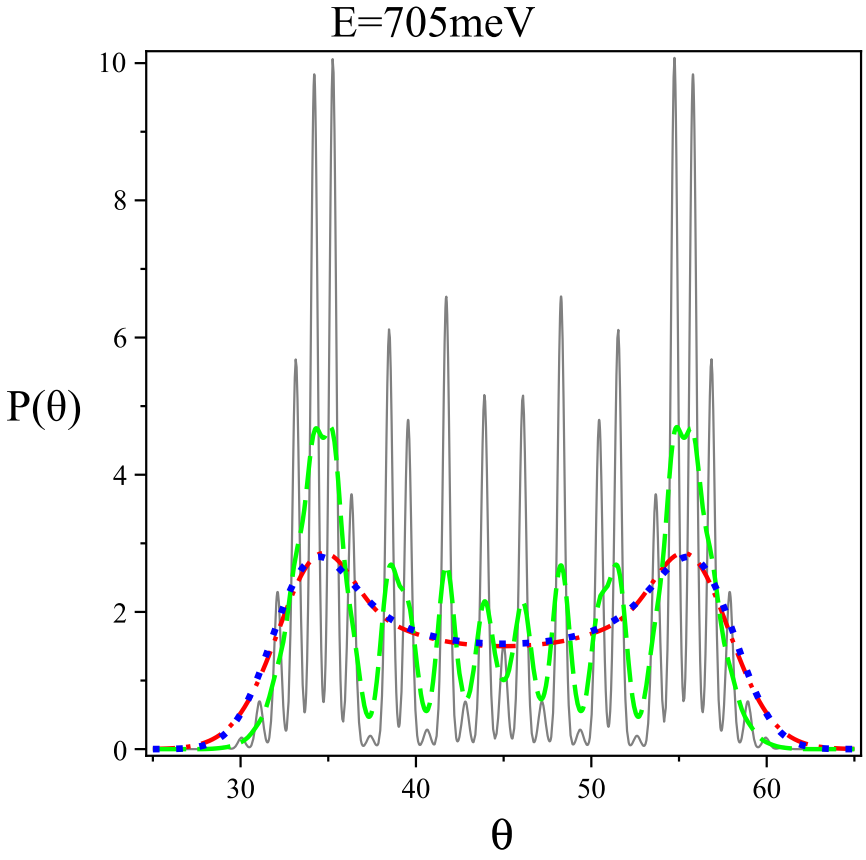

Figure 14: The SemiClassical angular distributions for scattering of Ar on LiF(100) at E=705meV is plotted for different angular widths of the incident beam. Legend as in figure 13. Note that due to the higher energy, the resolution in this figure is somewhat poorer that the resolution with the same beam characteristics as in figure 13 at a lower energy.

Part VII

Discussion

In this work we analyzed experimental results of atom-surface scattering using an extension of SCP theory. The SCP theory allows for a simplified description of the scattering process, which allowed us to obtain closed analytical expressions which also provide a lot of intution into the processes involved. An advantage of the SCP is that it provides a direct route between the spectral density and the observed measured angular distribution. As we saw, it was found to be possible to deduce the parameters of the spectral density from the diffraction pattern. The effects of surface temperature are another topic which is well-described by our theory. As we have shown, higher temperatures cause more phonon excitations to occur, which may have drastic effects over the resulting angular distribution. More phonon transitions may cause the specular peak to become lower while the "background" may become more noticeable.

We have split our discussion in this work into the two formulations of the SCP theory. One is the continuum theory and the second is the discretized theory. A last, third expression was derived for a continuum limit of a bath of classical harmonic oscillators. These expressions can be readily computed when using simple potentials such as Morse oscillator potential for the vertical potential and a periodic cosine or sine potential for the horizontal motion. We discussed and provided examples of the use of all theories and showed their performance in comparison to experiment.

We start with a discussion of the continuum theory. It was shown in Fig 5 that at the elevated temperature of 300K, for Ne, the complete angular distribution is well described by adding only the two phonon contribution. The quantitative agreement is striking. This is a reflection of the weak friction coefficient, which effectively disallows higher order phonon transitions. Even at this elevated surface temperature, the angular distribution is dominated by the elastic quantum diffraction peak. The results for Ar are of similar quality, though there the reduced friction coefficient was larger so that at the higher temperature three or more phonons were also excited. Finally, for Kr even at a surface temperature of 15K multiphonon transitions couldn't be neglected and the theoretical distribution remained somewhat lower than the measured one.

We continue with a discussion of the discretized theory. So far we compared continuum theory, and observed good agreement for most experimental results. However there remains some more to be desired, especially for Kr at a surface temperature of 15K, where it is clear from the results that multiphonon transitions can not be ignored. Therefore, an expression was derived for the angular distribution for any discrete number of bath harmonic oscillators. In our results we use the number $N_B = 20$ for the number of oscillators. In Figure 7, to assess the discretized theory, we first compared the results of the continuum theory to the discretized theory,

but still using only up to two phonon transitions for both theories. The results are very similar, except for the oscillations in the discretized model, which are expected due to the use of a finite number of oscillators. Next, in figure 8 we split the different contributions arising from one, one+two and all-phonon contributions in separate curves, so as to see the individual contributions that are added at each stage. From the results we can see that for low temperatures, there are hardly any contributions from two phonons, and most contributions are from either zero or one phonon. For high temperatures the pictures is different, as there are many contributions from phonon transitions higher than 2. We can clearly separate the different levels of contributions. Next, we compared the discretized results with experiment, in Figure 9. We can see nearly full agreement for all temperatures for Ar and Ne. Our calculation for the discretized bath confirmed our assumption: the broad background of the angular distribution indeed stems from the multiphonon transitions. By solving for the discretized bath it was clearly observable how the different peaks come together and build the broad background. It also confirmed our previous continuum limit expression for the bath, which assumed an infinite number of oscillators. The discretized results were shown to be in good agreement with the continuum results, both for the Debye-Waller factor as well as for low temperature scattering when only up to two phonon transitions are important. The multi-phonon theory accounts well for the measured features of the angular distribution which are the superposition of elastic "delta" function peaks on a smooth and broad background whose intensity increases as the surface temperature is increased.

Lastly in this work, we have shown the effect of beam collimation on the angular distribution[52]. Representing the angular spread of the incoming beam of atoms in terms of a Gaussian distribution, we demonstrated how good collimation of the incident beam may resolve the quantum diffraction peaks even for heavy atom scattering, or high energies. The critical parameter which determines whether one may observe diffraction is the angular width of the incident beam as compared to the angular distance between successive diffraction peaks. This distance, depends inversely on the speed of the projectile and decreases as the square root of the incident particle mass is increased. Finally, we showed how the quantum diffraction pattern decoheres and reduces to the classical angular distribution when the angular spread of the incident beam is sufficiently large. The theory was applied to a model for the scattering of Ar on the LiF(100) surface. Assuming a 2^0 angular spread of the incident beam, we showed that this would prevent observation of quantum diffraction, even if the surface is rigid. However, reducing the angular width by a factor of 10 to 0.2^0 is sufficient for observing the full diffraction pattern. Of course, the results presented for the collimation effects ignore the effects of phonons on the scattering. At room temperature one may assume that the phonon interaction is sufficiently strong so as to destroy the quantum coherence and even with a 0.2^0 resolution one would not observe diffraction. However, in this analysis we limited ourselves only to consideration of the angular spread, without taking into account additional effects. To conclude the effects of collimation, the collimation of the incident beam sharpened the

diffraction peaks, while the opposite effect caused them to smear out. As observed in Fig. 13, for high energy beams the individual phonon contributions were partly smeared out.

In summary, we demonstrated by application of the semiclassical perturbation theory to experimentally measured data, how the broad background is obtained by phonon scattering. The theory was also applied to the effect of beam collimation. A discretized theory was also formulated and compared to the continuous, analytical model.

29 Summary of Results as a Whole, and Main Conclusions

The semiclassical perturbation theory of Hubbard and Miller was explored and generalized for the study of atom-surface scattering. The theory was utilized to derive the angular distribution in several ways. First, we derived a continuum-limit theory for the angular distribution. The theory accounted for the Debye-Waller Factor as well as the angular distribution for phonon transitions up to two. Second, a discretized theory was derived and compared to the continuum theory. Expressions for the Debye-Waller factor and the angular distribution were also derived. Lastly, we also showed results for beam collimation for a simple system with no phonon bath.

The theory was applied to measured angular distributions of Ne, Ar and Kr scattered from a Cu(111) surface. It was shown that the numerical solution for all surface modes substantially improved the solution that is based on only the zero-,one-,and two-phonon contributions. It provides a good description of the angular distribution for Argon and Neon beams at high and low temperatures. The effect of beam collimation is found to smear out the features in the resulting angular distribution, such that some of the diffraction peaks become indistinguishable.

We find that the multi-phonon theory substantially improves the agreement between experiment and theory, especially at the higher surface temperatures. This provides evidence for the importance of multi-phonon transitions in determining the angular distribution as the surface temperature is increased.

The multi-phonon theory confirms our conjecture given in Ref. [51] that the broad background measured in the angular distribution at increased surface temperature comes from multi-phonon transitions. Comparison of the discretized theory with the experimentally measured results was favorable, using the same parameters as with the continuous-bath theory (as in [51]).

30 Implications of Our Work

The theory developed here is applicable to many experimental systems and can be used as a theoretical tool for the analysis of experimental data. Provided that we provide the proper guidance and support, the theory can provide experimental predictions for many experiments. It can also guide the experimentalist in choosing experimental parameters when one wants or doesn't want to, for example, observe quantum diffraction effects in the experiment.

31 Possible Future Developments

The same theory developed here now may be used to describe many other surface phenomena, such as quantum energy transfer to the surface, and quantum sticking probabilities. It may be generalized to include the full three dimensions of the scattered particle as well as coupling to horizontal phonons. Another direction is extension to include second order surface corrugation effects [48]. Finally, the theory should be readily applicable to many experimental results on atom surface scattering.

Part VIII

Literature

References

[1] A. Kundt, E. Warburg, Philos. Mag. 50 (1875) 53.

[2] J.C. Maxwel, Philos. Mag. 19 (1860) 20.

[3] M. Knudsen, The Kinetic Theory of Gases, Methuen, London, 1934.

[4] M.S. Smoluchowski, Philos. Mag. 46 (1898) 192; Ann. Phys. 35 (1911) 983.

[5] I. Estermann and O. Stern, Z. Phys. **61**, 95 (1930).

[6] A. Schueller, S. Wethekam, and H. Winter, Phys. Rev. Lett. 98, 016103 (2007).

[7] T.H. Johnson, Phys. Rev. 35 (1930) 1299; ibid. 37 (1931) 847.

[8] G. Benedek and J.P. Toennies, Surf. Sci. **299/300**, 587 (1994).

[9] N. Cabrera, V. Celli, F.O. Goodman, R. Manson, Surf. Sci. 19, 67 (1970).

[10] N. Cabrera, V. Celli, and R. Manson. Phys. Rev. Lett. 22, 346 (1969).

[11] J. R. Manson, Phys. Rev. B **43**, 6924 (1991).

[12] G.D. Billing. Chem. Phys. 70, 223 (1982)

[13] G.D. Billing. Chem. Phys. 74, 143 (1983)

[14] R. Guantesa, A.S. Sanzb, J. Margalef-Roiga, S. Miret-Artés. Surf. Sci. Rep. 53, 199 (2004)

[15] A.S. Sanz , S. Miret-Artés. Phys. Rep. 451, 37 (2007).

[16] R. Martinez-Casado, S. Miret-Artés, B. Meyer, F. Traeger and C. Wöll. Journal of Physics: Condensed Matter, 22(30), 304011 (2010).

[17] M. Mayrhofer-Reinhartshuber, P. Kraus, A. Tamtögl, S. Miret-Artés, and W. E. Ernst. Physical Review B 88, no. 20 (2013): 205425.

[18] P. Kraus, M. Mayrhofer-Reinhartshuber, C. Gösweiner, F. Apolloner, S. Miret-Artés and W.E. Ernst. Surface Science, 630, 208-215 (2014).

[19] B. Jackson, J. Chem. Phys. 90 (1989) 140; ibid. 92 (1990) 1458.

[20] B. Jackson, H. Metiu, J. Chem Phys. 86 (1987).

[21] B. Gumhalter, *Single and multiphonon atom surface scattering in the quantum regime*, Phys. Rep. **351**, 1 (2001).

[22] K. Burke, B. Gumhalter, D.C. Langreth, Phys. Rev. B 47 (1993) 12852

[23] B. Gumhalter, K. Burke, D.C. Langreth, Surf. Rev. Lett. 1 (1994) 133.

[24] A. Gross, *Quantum theory of reactive scattering and adsorption at surfaces*, Handbook of Material Modeling, edited by S. Yip, (Springer, 2005), p 1713.

[25] A. Gross, M. Scheffler. Chem. Phys. Lett. 263, 567 (1996).

[26] Geert-Jan Kroes, Axel Gross, Evert-Jan Baerends, Matthias Scheffler, and Drew A. McCormack. Acc. Chem. Res., 35 (2002).

[27] S. Miret-Artés and E. Pollak, Surf. Sci. Rep. **67**, 161 (2012).

[28] R. M. Logan and R. E. Stickney, J. Chem. Phys. 44, 195 (1966).

[29] R. M. Logan and J. C. Keck, J. Chem. Phys. 49, 860 (1968).

[30] J. C. Tully, J. Chem. Phys. 92, 680 (1990).

[31] W. A. Steele, Surf. Sci. 38, 1 (1973).

[32] U. Garibaldi, A. C. Levi, R. Spadacini, and G. E. Tommei, Surf. Sci. 48, 649 (1975).

[33] E. F. Greene and E. A. Mason, Surf. Sci. 75, 549 (1978)

[34] J. R. Klein and M. W. Cole, Surf. Sci. 79, 269 (1979).

[35] E. Pollak, S. Santanu, and S. Miret-Artés, J. Chem. Phys. 129, 054107 (2008).

[36] E. Pollak, J. M. Moix, and S. Miret-Artés, Phys. Rev. B 80, 165420 (2009); E. Pollak, J. M. Moix, and S. Miret-Artés, Phys. Rev. B 81, 039902 (2010) (Erratum).

[37] E. Pollak and J. Tatchen, Phys. Rev. B 80, 115404 (2009);E. Pollak and J. Tatchen, Phys. Rev. B 81, 049903 (2010) (Erratum)

[38] E. Pollak and S. Miret-Artés, J. Chem. Phys. 130, 194710 (2009); E. Pollak and S. Miret-Artés, J. Chem. Phys. 132, 049901 (2010) (Erratum)

[39] E. Pollak and S. Miret-Artés, Chem. Phys. 375, 337 (2010).

[40] Y. Zhou, E. Pollak and S. Miret-Artés. J. Chem. Phys. 140, 024709 (2014)

[41] W. H. Miller and F. T. Smith. Phys. Rev. A 17, 939 (1978).

[42] W. H. Miller. J. Chem. Phys. 53, 3578 (1970).

[43] W.H. Miller. J. Chem. Phys. 53, 1949 (1970).

[44] L. M. Hubbard and W. H. Miller, J. Chem. Phys. 78, 1801 (1983).

[45] H. Wang, M. Thoss, and W.H. Miller. J. Chem. Phys. 112, 47 (2000).

[46] M. Thoss, H. Wang, and W.H. Miller. J. Chem. Phys. 114, 9220 (2001).

[47] L. M. Hubbard and W. H. Miller, J. Chem. Phys. **80**, 5827 (1984).

[48] E. Pollak and S. Miret-Artés. J. Phys. Chem. C. doi: 10.1021/jp509500v

[49] F. Althoff, T. Andersson and S. Andersson, Phys. Rev. Lett. **79**, 4429 (1997).

[50] T. Andersson, F. Althoff, P. Linde, S. Andersson and K. Burke, Phys. Rev. B **65**, 045409 (2002).

[51] S. Daon, E. Pollak and S. Miret-Artés, J. Chem. Phys. **137**, 201103 (2012).

[52] S. Miret-Artés, S. Daon, and E. Pollak. J. Chem. Phys. **136**, 204707 (2012).

[53] M. Minniti, C. Díaz C, J.L.Fernández Cuñado, A. Politano, D. Maccariello, F. Martín, D. Farías, R.J. Miranda. Chem. Phys. **136**, 204707 (2012).

[54] Jeremy M. Moix and Eli Pollak. J. Chem. Phys. 134, 011103 (2011).

[55] E. Pollak, S. Sengupta, and S. Miret-Artés, J. Chem. Phys. **129**, 054107 (2008).

[56] Eqs. 4.35 and 4.36 of A.C. Levi and H. Suhl, Surf. Sci. Vol. 88, 221 (1979); K. Burke and W. Kohn, Phys. Rev. B, **43**, 2477 (1991).

[57] Eq. 2 of V.F. Sears and S.A. Shelley, Acta. Cryst. Vol. **A47**, 441 (1996).

[58] A. Azuri and E. Pollak. J. Chem. Phys. 139, 044707 (2013).

[59] E. Pollak, S. Sengupta, and S. Miret-Artés, J. Chem. Phys. 129, 054107 (2008)

[60] E. Pollak and S. Miret-Artés, J. Chem. Phys. 130, 194710 (2009).

[61] E. Pollak, J. M. Moix, and S. Miret-Artés, Phys. Rev. B 80, 165420 (2009)

[62] E. Pollak, J. M. Moix, and S. Miret-Artés, Phys. Rev. Lett. 104, 116103 (2010).

[63] E. Pollak and S. Miret-Artés, Chem. Phys. 375, 337 (2010).

[64] See the comment and response in A. Siber and B. Gumhalter, Phys. Rev. lett. **81**, 1742 (1998); F. Althoff, T. Andersson and S. Andersson, ibid. **81**, 1743 (1998).

[65] P.L. Silvestrelli, A. Ambrosetti, S. Grubisic and F. Ancilotto, Phys. Rev. B **85** 165405 (2012).

[66] M. Wilms, P. Broekman, C. Stuhlmann and K. Wandelt, Surf. Sci. **416**, 121 (1998).

[67] Y. Georgievskii, M.A. Kozhushner and E. Pollak, J. Chem. Phys. **102**, 6908 (1995).

[68] T. Kondo, H.S. Kato, T. Yamada, S. Yamamoto, and M. Kawai. Eur. Phys. J. D **38**, 129 (2006).

32 List of Papers Published As Part of This Thesis

The papers published as a part of this work are fully enclosed as Appendices.

These are:

1. Salvador Miret-Artés , Shauli Daon , and Eli Pollak. **"Semiclassical perturbation theory for diffraction in heavy-atom surface scattering"**. J. Chem. Phys. 136 , 204707 (2012)

2. Shauli Daon, Eli Pollak, and S. Miret-Artés. **"Communication: Semiclassical perturbation theory for the quantum diffractive scattering of atoms on thermal surfaces"**. J. Chem. Phys. 137, 201103 (2012)

3. Shauli Daon and Eli Pollak. **"Semiclassical multi-phonon theory for atom-surface scattering: Application to the Cu(111) system"**. Accepted for publication in J. Chem. Phys. (2015).

Part IX

Declaration

This thesis summarizes my own independent research, as conducted under the guidance of Prof. Eli Pollak.

Some parts were done in collaboration with Prof. Salvador Miret-Artés. We benefitted from dicussions with him and he is credited as the first author of the first paper published, and last author of our second paper.

Part X

Acknowledgements

This work was supported by grants from the Israel Science Foundation, the German Israel Foundation for Basic Research and the Minerva Foundation (Munich).

Part XI

Appendices

33 Appendix 1: Full Text of Published Paper: "Semiclassical perturbation theory for diffraction in heavy-atom surface scattering"

Full text of:

Salvador Miret-Artés , Shauli Daon , and Eli Pollak. J. Chem. Phys. 136 , 204707 (2012)

Semiclassical perturbation theory for diffraction in heavy atom surface scattering

Salvador Miret-Artés,[1,a)] Shauli Daon,[2] and Eli Pollak[2,b)]
[1]*Instituto de Física Fundamental, Consejo Superior de Investigaciones Científicas, Serrano 123, 28006 Madrid, Spain*
[2]*Chemical Physics Department, Weizmann Institute of Science, 76100 Rehovoth, Israel*

(Received 26 March 2012; accepted 11 May 2012; published online 31 May 2012)

The semiclassical perturbation theory formalism of Hubbard and Miller [J. Chem. Phys. **78**, 1801 (1983)] for atom surface scattering is used to explore the possibility of observation of heavy atom diffractive scattering. In the limit of vanishing $\hbar$ the semiclassical theory is shown to reduce to the classical perturbation theory. The quantum diffraction pattern is sensitive to the characteristics of the beam of incoming particles. Necessary conditions for observation of quantum diffraction are derived for the angular width of the incoming beam. An analytic expression for the angular distribution as a function of the angular and momentum variance of the incoming beam is obtained. We show both analytically and through some numerical results that increasing the angular width of the incident beam leads to decoherence of the quantum diffraction peaks and one approaches the classical limit. However, the incoherence of the beam in the parallel direction does not destroy the diffraction pattern. We consider the specific example of Ar atoms scattered from a rigid LiF(100) surface.
 [http://dx.doi.org/10.1063/1.4722339]

I. INTRODUCTION

A variety of experiments have been carried out during the past few decades in which one observed quantum diffraction effects in the scattering of heavy atoms from surfaces. The seminal diffraction peaks observed by Estermann and Stern in their observations of scattering of He atoms from a LiF surface have led to further studies of scattering from surfaces.[2] The observation of diffraction in atoms heavier than He was discovered for Ne when scattered from a LiF surface by Williams[3] and Boato *et al.*[4] Diffraction in Ne scattering on metallic surfaces was then observed by Rieder and Stocker.[5] Schweizer *et al.*[6,7] were the first to measure diffractive scattering of Ar atoms from a hydrogen covered tungsten surface. Very sharp diffraction features were measured for the scattering of Ne, Ar, and Kr atoms as well as diatomics such as, D_2 and N_2 from a Cu(111) surface by Andersson *et al.*[8,9] Typically though the quantum effects were observed for low energy beams, presumably to assure that the deBroglie wavelength is not too small as compared with the lattice length of the surface.[6]

In more recent years, it was realized that quantum diffraction effects may be observed even at high beam energies[10,11] and very large masses.[12–14] A critical property which determines the quantum nature of the scattering event is the extent of collimation of the incident beam. A well collimated beam will have a large coherence wavelength in the direction perpendicular to the motion, so that diffraction may still be observed. This is why diffraction was observed for very fast atoms impinging on a surface at grazing conditions.[10] It was also found in the scattering of very heavy molecules through gratings. Moix and Pollak[15] have recently used model wavepacket propagation methods to demonstrate how the collimation of a beam of incident Ar atoms may affect the measured angular distribution. When the collimation was strong, such that the perpendicular coherence wavelength was longer than the lattice length, one found that the angular distribution was dominated by diffraction peaks. When the angular resolution of the beam was poor, the angular distribution reverted to its classical limit.

In this present paper, we will adapt the semiclassical perturbation (SCP) theory of Hubbard and Miller[1,16] to study how collimation affects the measured angular distribution. In Sec. II, the SCP formalism will be adapted for the final momentum and angular distributions. We show that the SCP theory reduces to the classical perturbation theory we have been using in recent years to analyze angular distributions of heavy atom surface scattering.[17–21] We then account for the initial beam conditions by introducing an appropriate Gaussian averaging over initial conditions. The classical distribution is obtained in the limit of a large angular width of the beam as compared to the angular distance between successive diffraction peaks. The formalism is then applied in Sec. III, using a model potential whose parameters have been previously fitted[18,21] for the observed scattering of Ar from a LiF surface.[22] We demonstrate that the SCP based theory may be used to estimate the effect of collimation of the incident beam on the measured angular distribution. Depending on the extent of angular collimation one can move smoothly from a fully quantum diffraction regime, to the fully incoherent classical regime for the angular distribution. We also find that the incoherence of the beam in the direction of propagation does not destroy the quantum diffraction pattern. We end with a discussion in Sec. IV.

a)Electronic mail: s.miret@iff.csic.es.
b)Electronic mail: eli.pollak@weizmann.ac.il.

II. SEMICLASSICAL PERTURBATION THEORY OF ATOM SURFACE SCATTERING

A. Classical perturbation theory

We will model the dynamics in terms of two degrees of freedom, a vertical coordinate z (with conjugate momentum p_z) describing the distance of the atom (whose mass is M) from the surface, and a horizontal coordinate x (with conjugate momentum p_x) for motion parallel to the surface. The theory presented is readily generalized to include an additional (y) coordinate for motion parallel to the surface, but usually, one measures the in-plane angular distribution so that the limitation to a description with only two degrees of freedom is reasonable and illuminates the results. The usage of a two dimensional model is justified whenever the corrugation may be approximated as an independent sum of corrugations in the two orthogonal horizontal directions. We also note that this is the usual assumption made in many experimental[4] and theoretical papers (for a review see, for example, Ref. 21). The Hamiltonian for the scattering of an atom of mass M from a corrugated surface is then written as[17–19]

$$H = \frac{p_x^2 + p_z^2}{2M} + \bar{V}(z) + \bar{V}'(z)h(x), \tag{2.1}$$

where the interaction potential is split into two terms. $\bar{V}(z)$ is the zeroth order term (for analytic purposes it is taken as a Morse potential) and the perturbation term is given by the product of the first derivative of the vertical potential times the periodic corrugation function $h(x)$, with period (lattice length) l assumed for the surface.

The SCP is based on a classical perturbation theory, in which the small parameter is the height h of the corrugation potential $h(x)$. The unperturbed motion in the vertical direction is governed by the vertical Hamiltonian

$$H_z = \frac{p_z^2}{2M} + \bar{V}(z) \tag{2.2}$$

while to zeroth order, the parallel momentum is conserved. Using a time scale in which the particle reaches the turning point of the vertical potential $\bar{V}(z)$ at time $t = 0$ one has from the solution of the classical equation of motion for the horizontal momentum that the first order change due to the collision at the horizontal point of impact x_0 is given by

$$\delta p_x(x_0) = -\int_{-\infty}^{\infty} dt\, \bar{V}'(z_t) h'\left[x_0 + \frac{p_{x_i}}{M} t\right], \tag{2.3}$$

where z_t is the vertical motion as obtained from the zeroth order Hamiltonian (2.2) and p_{x_i} is the incident (positive) momentum of the particle in the horizontal direction. The change in the vertical momentum is readily obtained from energy conservation. Denoting the initial vertical momentum as p_{z_i} (assumed negative) and retaining only linear terms in δp_x, one readily finds that the vertical momentum change is

$$\delta p_z(x_0) = \frac{\delta p_x(x_0)\, p_{x_i}}{p_{z_i}}. \tag{2.4}$$

The probability for observing the particle with final momenta p_{x_f} and p_{z_f} is then obtained by averaging over the impact points,

$$P(p_{x_f}, p_{z_f}) = \frac{1}{l}\int_0^l dx_0 \delta(p_{x_f} - p_{x_i} - \delta p_x(x_0)) \times \delta(p_{z_f} + p_{z_i} - \delta p_z(\delta p_z(x_0))), \tag{2.5}$$

where $\delta(x)$ denotes the Dirac "delta" function. The (negative) angle of incidence θ_i and the final scattering angle θ_f relative to the normal to the surface are by definition

$$\theta_j = \tan^{-1}\left(\frac{p_{x_j}}{p_{z_j}}\right), \quad j = i, f. \tag{2.6}$$

The final classical angular distribution is then given in terms of the final momentum distribution as,

$$\begin{aligned} P(\theta_f) &= \int_{-\infty}^{\infty} dp_{x_f} \int_0^{\infty} dp_{z_f} \delta\left(\theta_f - \tan^{-1}\left(\frac{p_{x_f}}{p_{z_f}}\right)\right) P(p_{x_f}, p_{z_f}) \\ &= \frac{1}{l\cos^2\theta_f}\int_0^l dx_0 \delta\left(\tan\theta_f + \tan\theta_i\left(1 + \frac{\delta p_x(x_0)}{p_{x_i}\cos^2\theta_i}\right)\right) \\ &\quad \times H\left(1 - \frac{\delta p_x(x_0)\tan^2\theta_i}{p_{x_i}}\right), \end{aligned} \tag{2.7}$$

where $H(x)$ is the Heaviside function; we used the identity

$$\delta\left(\theta - \tan^{-1}(\alpha)\right) = \cos^{-2}\theta\, \delta(\alpha - \tan\theta) \tag{2.8}$$

and to remain consistent with the first order perturbation theory we have retained only terms which are up to linear in the horizontal momentum change $\delta p_x(x_0)$.

B. Semiclassical perturbation theory

Following Hubbard and Miller,[1,16,23] the S-matrix element or amplitude for scattering to a final diffraction channel characterized by the quantum number n from the specular channel 0 is given within the SCP theory approximation by

$$S_{n0} = \frac{1}{l}\int_0^l dx_0 e^{-i\Delta k_x x_0} e^{2i\eta(x_0)}, \tag{2.9}$$

where the phase shift η is given by

$$2\eta(x_0) = -\frac{1}{\hbar}\int_{-\infty}^{+\infty} dt\, V(x_t, z_t), \tag{2.10}$$

where x_t and z_t denote the zeroth order trajectories, as in the classical perturbation theory. The diffraction order number n is defined through the change of the horizontal component of the wavevector $\Delta k_x = k_{x_f} - k_{x_i}$ and guided by Bragg's law as,

$$n = \frac{l\Delta k_x}{2\pi} = \frac{l\delta p_x}{2\pi\hbar} \tag{2.11}$$

but here the horizontal momentum change is no longer a function of the impact parameter x_0 as in the classical case (Eq. (2.3)). Equation (2.9) can be written in a more standard form as

$$S_{n0} = (2\pi)^{-1}\int_0^{2\pi} dq_x e^{-inq_x} e^{2i\eta(q_x)} \tag{2.12}$$

in terms of the angle variable

$$q_x = 2\pi x_0/l, \tag{2.13}$$

which is conjugate to the diffraction order number n. The diffraction probability is given by

$$P_{n0} = |S_{n0}|^2. \tag{2.14}$$

Hubbard and Miller have shown that the SCP estimate of the transition probability is indeed a very good approximation to the exact quantum probability.[1]

In quantum mechanics, the diffraction order number is necessarily an integer so that the final distribution of momenta is

$$P(p_{x_f}, p_{z_f}) = \sum_{n=-\infty}^{\infty} \delta\left(p_{x_f} - p_{x_i} - \frac{2\pi\hbar n}{l}\right) \times \delta(p_{z_f} + p_{z_i} - \delta p_z(\delta p_x))|S_{n0}|^2. \tag{2.15}$$

The change in the vertical momentum is obtained as in the classical case through the conservation of energy (see Eq. (2.4)). The SCP expression for the angular distribution is obtained as in the first equality in Eq. (2.7).

C. The classical limit of the SCP expression

It is of interest to show that the semiclassical expression for the momentum distribution reduces in the limit that $\hbar \to 0$ to the corresponding classical expression. If in Eq. (2.15) the sum over n going from $-\infty$ to $+\infty$ is replaced by an integral over the variable $\hbar n$ then the final momentum distribution is

$$P(p_{x_f}, p_{z_f}) = \frac{l}{\hbar(2\pi)^3}\int_0^{2\pi} dq_x \int_0^{2\pi} dq_x' \delta(p_{z_f} + p_{z_i} - \delta p_z(\delta p_x)) \cdot \exp\left(-i\frac{l\delta p_x}{2\pi\hbar}(q_x - q_x') + 2i[\eta(q_x) - \eta(q_x')]\right). \tag{2.16}$$

Using the sum and difference variables

$$Q = \frac{q_x + q_x'}{2}, \quad \Delta Q = q_x - q_x' \tag{2.17}$$

and linearizing with respect to the difference variable,

$$\eta(q_x) - \eta(q_x') \simeq \eta'(Q)\Delta Q \tag{2.18}$$

we readily find that in the limit that $\hbar \to 0$, the momentum distribution becomes (with $\Delta Q' = \Delta Q/\hbar$)

$$\begin{aligned} P(p_{x_f}, p_{z_f}) &\simeq \frac{l}{(2\pi)^3}\int_0^{2\pi} dQ \int_{-Q/\hbar}^{Q/\hbar} d\Delta Q' \delta(p_{z_f} + p_{z_i} - \delta p_z(\delta p_x)) \\ &\quad \times \exp\left(-i\hbar n \Delta Q' + 2i\hbar\eta'(Q)\Delta Q'\right) \\ &= \frac{1}{l}\int_0^{l} dx_0 \delta(p_{z_f} + p_{z_i} - \delta p_z(\delta p_x)) \\ &\quad \times \delta\left(\delta p_x - \frac{4\pi}{l}\hbar\eta'\left(\frac{2\pi x_0}{l}\right)\right). \end{aligned} \tag{2.19}$$

Using the definition for the phase shift as in Eq. (2.10) one readily finds that this is indeed the classical perturbation theory expression given in Eq. (2.5).

D. The SCP theory for a sine corrugation function

If we now assume a sine corrugation function such that

$$h(x) = h\sin(2\pi x/l) \tag{2.20}$$

then

$$2\eta(q_x) = 2\eta_0 - \frac{h}{\hbar}\int_{-\infty}^{+\infty} dt\, \bar{V}'(z_t)\sin(q_x + \omega_x t), \tag{2.21}$$

where $2\eta_0 = -(1/\hbar)\int_{-\infty}^{+\infty} dt\, \bar{V}(z_t)$ is the constant phase shift due to the unperturbed potential $\bar{V}(z)$ and the frequency along the horizontal direction due to the rectilinear motion is $\omega_x = 2\pi p_{x_i}/(Ml)$. By noting that $\bar{V}'(z_t)$ is an even function in time and inserting Eq. (2.21) into Eq. (2.9) one finds that[1]

$$S_{n0} = \exp(2i\eta_0)\, J_n\left(\frac{A_x}{\hbar}\right), \tag{2.22}$$

where $J_n(y)$ is the nth order Bessel function,

$$A_x = h\int_{-\infty}^{+\infty} dt\, \bar{V}'(z_t)\cos\omega_x t \tag{2.23}$$

and following from Eq. (2.14) the diffraction probability is

$$P_{n0} = J_n^2\left(\frac{A_x}{\hbar}\right). \tag{2.24}$$

The action variable A_x is related to the rainbow shift angle function K which arises in the classical perturbation theory[17–19]

$$K(p_{x_i}, p_{z_i}) = \frac{2\pi}{l p_{z_i}} A_x. \tag{2.25}$$

E. Averaging over initial velocities

Typically the incident beam has a Gaussian distribution of velocities centered about some average values. We may assume that this distribution takes the form

$$P\left(p_\parallel, p_\perp; \bar{p}_\parallel\right) = \frac{1}{\pi\sigma_\parallel\sigma_\perp}\exp\left(-\frac{\left(p_\parallel - \bar{p}_\parallel\right)^2}{\sigma_\parallel^2} - \frac{p_\perp^2}{\sigma_\perp^2}\right), \tag{2.26}$$

where $p_\parallel$ is the (negative) incident momentum in the direction of the average propagation of the beam while $p_\perp$ is the incident momentum perpendicular to the average direction of propagation. The average incident (negative) scattering angle $\bar{\theta}_i$ is by definition the angle between the average (negative) parallel momentum $\bar{p}_\parallel$ and the z axis. We then have that the parallel and perpendicular momenta may be expressed in terms of the vertical and horizontal incident momenta as,

$$p_\parallel = p_{z_i}\cos(\bar{\theta}_i) + p_{x_i}\sin(\bar{\theta}_i) = -p_i\cos(\theta_i - \bar{\theta}_i), \tag{2.27}$$

$$p_\perp = -p_{z_i}\sin(\bar{\theta}_i) + p_{x_i}\cos(\bar{\theta}_i) = p_i\sin(\theta_i - \bar{\theta}_i), \tag{2.28}$$

with

$$p_i^2 = p_{x_i}^2 + p_{z_i}^2 = \sqrt{2ME_i}. \tag{2.29}$$

Inserting these expressions into the incident momentum distribution (Eq. (2.26)) implies that it may be written as

$$P(p_\parallel, p_\perp; \bar{p}_\parallel, \bar{\theta}_i) = \frac{1}{\pi\sigma_\parallel\sigma_\perp} \exp\left(-\frac{(p_i\cos(\theta_i-\bar{\theta}_i)+\bar{p}_\parallel)^2}{\sigma_\parallel^2} - \frac{p_i^2\sin^2(\theta_i-\bar{\theta}_i)}{\sigma_\perp^2}\right). \quad (2.30)$$

In the limit that we have "good" collimation in the perpendicular direction we can approximate the distribution to be

$$P(p_\parallel, p_\perp; \bar{p}_\parallel, \bar{\theta}_i) \simeq \frac{1}{\pi\sigma_\parallel\sigma_\perp} \exp\left(-\frac{(p_i+\bar{p}_\parallel)^2}{\sigma_\parallel^2} - \frac{p_i^2(\theta_i-\bar{\theta}_i)^2}{\sigma_\perp^2}\right). \quad (2.31)$$

Using the notation

$$B_n(\theta_i) = \frac{2\pi\hbar n}{l p_i\cos\theta_i}, \quad (2.32)$$

and replacing $B_n(\theta_i)$ with its value at the maximum, $B_n(\bar{\theta}_i)$ and similarly for $|S_{n0}|^2$ we find that the final angular distribution is

$$P(\theta; \bar{p}_\parallel, \bar{\theta}_i) \simeq \sum_{n=-\infty}^{\infty} \int_0^\infty dp_i\, p_i \frac{|S_{n0}(p_i, \bar{\theta}_i)|^2}{\pi\sigma_\parallel\sigma_\perp} \cdot \exp\left(-\frac{(p_i+\bar{p}_\parallel)^2}{\sigma_\parallel^2} - \frac{p_i^2(\tan^{-1}[B_n(\bar{\theta}_i)]-\theta-\bar{\theta}_i)^2}{\sigma_\perp^2}\right) \quad (2.33)$$

and the remaining integral over the initial momentum has to be carried out numerically.

This result is already instructive. Note that the uncertainty in the parallel momentum only serves to average out the magnitude of the separate diffraction probabilities, but it does not affect the diffraction pattern itself. Each separate diffraction peak is smeared only through the uncertainty in the perpendicular momentum, as expressed by the angular width $\sigma_\perp/(\sqrt{2}p_i)$. This demonstrates that sufficient collimation will reveal the underlying diffraction structure of the angular momentum distribution. It also provides a quick estimate for the collimation needed to expose the diffraction pattern. The angular distance between successive diffraction peaks is

$$\Delta\theta_n = \tan^{-1}[B_{n+1}(\bar{\theta}_i)] - \tan^{-1}[B_n(\bar{\theta}_i)]. \quad (2.34)$$

Thus, the condition for the observation of the nth diffraction peak is

$$\frac{\sigma_\perp}{p_i} \ll \Delta\theta_n. \quad (2.35)$$

We note that the angle difference between diffraction peaks is not linear in the diffraction number. As the diffraction number increases, the angle difference decreases and a better angular resolution is needed to resolve the peak. As is well-known, the angle difference decreases with increasing momentum of the projectile and with increasing mass, as may be also discerned from Eqs. (2.32) and (2.34).

If we further replace p_i with its average value $-\bar{p}_\parallel$ in the argument of the S-matrix element and the term $\tan^{-1}[B_n(\bar{\theta}_i)]$ we readily find that the angular distribution reduces to a sum over error functions

$$P(\theta; \bar{p}_\parallel, \bar{\theta}_i) \simeq \sum_{n=-\infty}^{\infty} \frac{\sigma_\parallel\sigma_\perp|S_{n0}(\bar{p}_\parallel, \bar{\theta}_i)|^2}{2\pi C_n^2} \cdot \left(\exp\left(-\frac{\bar{p}_\parallel^2}{\sigma_\parallel^2}\right) - \frac{\bar{p}_\parallel\sqrt{\pi}\sigma_\perp}{\sigma_\parallel C_n} \times \exp\left(-\frac{\bar{p}_\parallel^2}{\sigma_\parallel^2}\left[\frac{C_n^2-\sigma_\perp^2}{C_n^2}\right]\right)\mathrm{erfc}\left(\frac{\bar{\mathrm{p}}_\parallel\sigma_\perp}{\sigma_\parallel \mathrm{C_n}}\right)\right) \quad (2.36)$$

and we used the notation

$$C_n^2 = \left[\sigma_\perp^2 + \sigma_\parallel^2(\tan^{-1}[B_n(\bar{\theta}_i)] - \theta - \bar{\theta}_i)^2\right]. \quad (2.37)$$

Equation (2.36) is a central result of this paper. Inserting the SCP approximation for the diffraction probability gives a closed expression for the angular distribution after averaging over the Gaussian profile of the incident beam.

To complete the discussion, it is also worthwhile to write down an expression for the classical angular distribution, when averaged over the profile of the incident beam. For the sine corrugation function (Eq. (2.20)) one finds that

$$\delta p_x(x_0) = -p_{z_i} K(p_{x_i}, p_{z_i}) \cos\left(\frac{2\pi x_0}{l}\right),$$

where the rainbow angle shift function $K(p_{x_i}, p_{z_i})$ has been identified in Eq. (2.25). The classical angular distribution becomes,

$$P(\theta_f) = \frac{1}{\pi\sqrt{K^2(p_{x_i}, p_{z_i})\cos^2(\theta_i+\theta_f) - \sin^2(\theta_i+\theta_f)}} \times H(K^2(p_{x_i}, p_{z_i}) - \tan^2(\theta_i+\theta_f)). \quad (2.38)$$

Averaging over the profile of the incident beam is then readily approximated as

$$\langle P(\theta_f)\rangle \simeq \frac{\bar{p}_\parallel}{\pi\sqrt{\pi}\sigma_\perp} \int_{-\pi/2}^{\pi/2} du \times \frac{1}{\sqrt{1+K^2(p_{x_i}, p_{z_i}) - K^2(p_{x_i}, p_{z_i})\sin^2 u}} \cdot \exp\left(-\frac{\bar{p}_\parallel^2}{\sigma_\perp^2}\left[\sin^{-1}\left(\frac{K(p_{x_i}, p_{z_i})}{\sqrt{1+K^2(p_{x_i}, p_{z_i})}}\sin u\right) - \bar{\theta}_i - \theta_f\right]^2\right). \quad (2.39)$$

The averaging over the angular width of the incident beam smooths the classical divergence at the rainbow angles. In the Appendix, we show that this expression is also obtained from the SCP angular distribution (Eq. (2.33)) in the limit that the angular width of the incoming beam is large as compared to the angular distance between successive diffraction peaks.

III. APPLICATION TO THE SCATTERING OF Ar ON A LiF SURFACE

Kondo *et al.*[22] have measured an angular distribution for the scattering of Ar on the LiF(100) surface. In their experiment, the incidence energy was varied between 300 and 700 meV. The angle between the incident beam and the detector was kept fixed at 90° and the final intensity was measured as a function of the angle of incidence which was varied about 45°. The angular distribution measured in this way is qualitatively similar to the angular distribution measured when the incident angle is fixed at 45° relative to the vertical axis and the final angle is measured. To simplify then we will discuss here only the final angular distribution measured at the fixed angle of incidence of 45°.

In Refs. 18–21 we used a Morse potential and a sinusoidal corrugation to fit the experimentally measured results. Here, we will use the same model, with a single sine corrugation term with corrugation height $h = 0.2$ a.u. The lattice length of the surface is $l = 4$ Å, the Morse potential well depth was chosen as $V_0 = 88$ meV and the stiffness parameter α was chosen such that $\alpha l = 3$. The various necessary analytic expressions for this model may be found in Refs. 18–21, here for the sake of completeness we just bring the relevant results. The rainbow shift angle is given by the expression

$$K(p_{x_i}, p_{z_i}) = \frac{4\pi^2 h}{l} \frac{\bar{\Omega}\cosh\left(\Phi\bar{\Omega}\right)}{\sinh\left(\pi\bar{\Omega}\right)}, \tag{3.1}$$

where the dimensionless parameter

$$\bar{\Omega} = \frac{2\pi}{\alpha l}\left|\tan\theta_i\right| \tag{3.2}$$

and the energy dependent angle Φ varies from $\pi/2$ at high incidence energies to π at low energies and is defined as,

$$\cos\Phi = -\sqrt{\frac{V_0}{V_0 + E_i\cos^2\theta_i}}. \tag{3.3}$$

In the experiment the uncertainty in the incidence energy ($\Delta E_i/E_i$) was ∼20% at all energies, implying a momentum uncertainty for the parallel incident momentum of 10%. The experimental paper does not report the angular resolution for the Ar beam, here we use (as also in Ref. 15) a 2° angular width as our base line. We thus have that at all energies studied experimentally we choose the Gaussian widths of the incident beam as

$$\frac{\sigma_\parallel}{\sqrt{2}p_i} = 0.1x_\parallel \tag{3.4}$$

and

$$\frac{\sigma_\perp}{\sqrt{2}p_i} = \frac{\pi}{90}x_\perp, \tag{3.5}$$

where it is understood that the experimental conditions are assumed to correspond to the scaling parameters $x_\parallel$ and $x_\perp$ equaling unity.

In Figure 1 we plot the dependence of the angle difference function as defined in Eq. (2.34) as a function of the quantum number n of the nth diffraction peak at two incident energies. At the lower energy (E = 315 meV), the angle difference function is of the order of 1.5° over the whole region

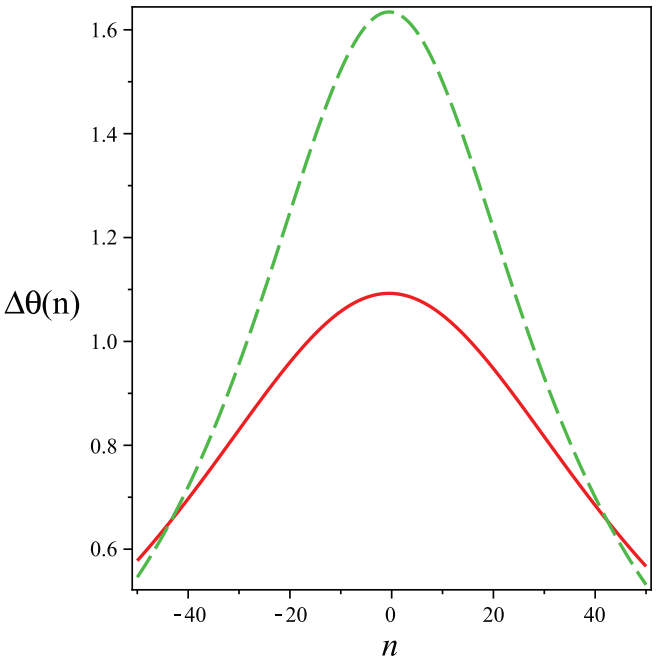

FIG. 1. The angle difference function $\Delta\theta(n)$ (in degrees) needed to resolve individual diffraction peaks is plotted versus the diffraction number n for a model of Ar scattered on a LiF(100) surface at two energies of incidence. The green (dashed) line is at an energy of 315 meV, the red (solid) line is at $E = 705$ meV.

in which one finds measurable scattering amplitude. At the higher energy (E = 705 meV) the angular difference in the experimentally relevant region is ∼1°. Clearly a higher angular resolution is needed for the higher energy, as expected from theory and from the observation that as the projectile's energy increases, one may expect it to be closer to the classical limit.

The angular distributions predicted by our model are shown in Figure 2 for the low energy case (315 meV) and in Figure 3 for the high energy case (705 meV). The uncertainty in the parallel momentum is kept fixed in all computations at 10% . In each of the plots, we show four results. The SCP angular distributions as obtained from Eq. (2.36) are plotted for three values of the perpendicular variance parameter $x_\perp = 1$, 0.25, 0.1 corresponding to angular widths of 2°, 0.5° and 0.1°, respectively. We also show the classical distribution averaged with an angular width of 2° as obtained from Eq. (2.39).

We first note that the SCP angular distribution is almost identical to the classical one when the angular width is 2°. This is to be expected, since as one can see from Figure 1, the angular difference between successive peaks is at most 1.6° at this energy. It is also evident that increasing the resolution by an order of magnitude is sufficient for resolving the complete diffraction pattern. At the higher energy, the angular difference between successive peaks is smaller. Although all diffraction peaks are resolved with a width of 0.2°, one notes that the base line is not zero as it is in the lower energy. One would need to decrease the angular width of the incident beam a bit more.

This analysis also explains why typically, one should expect that the diffraction peaks will be less noticeable around the classical rainbow angles. These angles are at the edge of

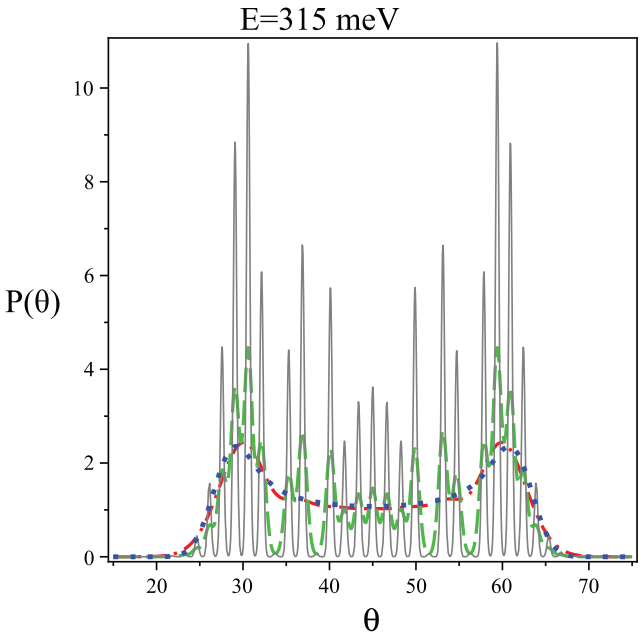

FIG. 2. The SCP angular distribution for the scattering of Ar on LiF(100) at E = 315 meV is plotted for different angular widths of the incident beam. The gray (solid), green (dashed), and red (dashed-dotted) lines correspond to angular widths of 0.2°, 0.5°, and 2°, respectively. The blue (dotted) line is the classical distribution obtained with an angular width of 2°. Note the well resolved diffraction peaks for a beam width of 0.2°, while for a beam width of 2° the SCP and the classical distributions are almost identical.

the observable distribution, where the diffraction number is higher, so that a higher angular resolution of the incident beam is needed to resolve the separate diffraction peaks appearing under the envelope.

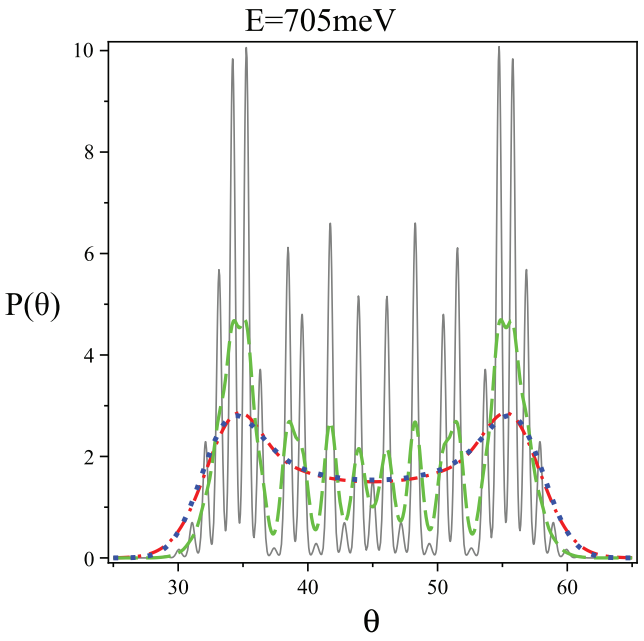

FIG. 3. The SCP angular distribution for the scattering of Ar on LiF(100) at E = 705 meV is plotted for different angular widths of the incident beam. The notation is as in Figure 2. Note that due to the higher energy, the resolution in this figure is somewhat poorer than the resolution with the same beam characteristics as shown in Figure 2 at the energy of 305 meV.

IV. DISCUSSION

In this paper we used the semiclassical perturbation theory of Hubbard and Miller[1] to show how the angular width of an incident atomic beam may be used to resolve the quantum mechanical diffraction pattern of an atom scattered from a surface. The SCP approximation was shown to reduce in the limit of $\hbar \to 0$ to the classical perturbation theory expression for the angular distribution used by us extensively in recent years to analyze the experimental data of heavy atom surface scattering experiments.[5–9] Representing the angular spread of the incoming beam of atoms in terms of a Gaussian distribution, we demonstrated how good collimation of the incident beam may resolve the quantum diffraction peaks even for heavy atom scattering, or high energies. The critical parameter which determines whether one may observe diffraction is the angular width of the incident beam as compared to the angular distance between successive diffraction peaks. This distance, depends inversely on the speed of the projectile and decreases as the square root of the incident particle mass is increased. Both of these aspects are well demonstrated by the experimental results of Boato *et al.*[4] Although they use an effusive beam, the strong collimation of the beam to an angular width of less than 0.1° enabled them to observe diffraction in the scattering of Ne from LiF(001). Finally, we showed how the quantum diffraction pattern decoheres and reduces to the classical angular distribution when the angular spread of the incident beam is sufficiently large.

The theory was then applied to a model for the scattering of Ar on the LiF(100) surface. Assuming a 2° angular spread of the incident beam, we showed that this would prevent observation of quantum diffraction, even if the surface is rigid. However, reducing the angular width by a factor of 10 to 0.2° is sufficient for observing the full diffraction pattern. Of course, the results presented ignore the effects of phonons on the scattering. At room temperature one may assume that the phonon interaction is sufficiently strong so as to destroy the quantum coherence and even with a 0.2° resolution one would not observe diffraction. However, in this paper we limited ourselves only to consideration of the angular spread, without taking into account additional effects. We do note, that the SCP approach is well adapted also to treat phonons, as may be seen from Ref. 23. An analysis of the effect of phonons on the angular distribution as described within the SCP formalism will be discussed separately.[24]

ACKNOWLEDGMENTS

We acknowledge the support of the Israel Science Foundation (ISF), the Weizmann-UK Joint Research Program and the Albert Einstein Minerva Center for Theoretical Physics at the Weizmann Institute for their support of this research. S.M.A. also acknowledges the Ministerio de Economia y Competitividad (Spain) in the framework of the project with reference FIS2010-18132. We also acknowledge the support from the European Cooperation in Scientific and Technical Research COST Action MP1006.

APPENDIX: DERIVING THE CLASSICAL LIMIT WHEN THE ANGULAR SPREAD OF THE INCIDENT BEAM IS LARGE

In this appendix, we demonstrate analytically, how the quantum angular distribution reduces to the classical, in the limit that the angular width of the incident beam is large compared to the distance between successive diffraction peaks. From Eq. (2.33) we have that the Gaussian averaged quantum angular distribution is well approximated as

$$P(\theta;\bar{p}_{\parallel},\bar{\theta}_i) \simeq \sum_{n=-\infty}^{\infty} \frac{1}{\sqrt{\pi}\sigma} |S_{n0}(p_i,\bar{\theta}_i)|^2 \times \exp\left(-\frac{(\tan^{-1}[B_n(\bar{\theta}_i)] - \theta - \bar{\theta}_i)^2}{\sigma^2}\right), \quad \text{(A1)}$$

where we denoted the dimensionless angular width of the incident beam as σ. In the spirit of the perturbation theory we assume that the angular range of the scattered distribution does not deviate too far from the specular angle, or equivalently that the rainbow angle shift $K \ll 1$ (in the Ar-LiF model considered above, $K \simeq 0.2$–0.3). We may then approximate

$$\tan^{-1}[B_n(\bar{\theta}_i)] \simeq B_n(\bar{\theta}_i). \quad \text{(A2)}$$

The fact that the angular width of the incoming beam is larger than the distance between successive peaks implies that

$$\sigma \gg B_{n+1}(\bar{\theta}_i) - B_n(\bar{\theta}_i) = B_1(\bar{\theta}_i). \quad \text{(A3)}$$

Using the integral representation of the Bessel functions (see Eqs. (2.9) and (2.22)), replacing the summation over the diffraction quantum number n with an integration over the variable $u = B_1\left(\bar{\theta}_i\right) n/\sigma$ (which is permitted due to the central assumption of a large angular width as given in Eq. (A3)) allows us to rewrite Eq. (A1) as

$$P(\theta;\bar{p}_{\parallel},\bar{\theta}_i) \simeq \frac{1}{4\pi^2 B_1(\bar{\theta}_i)} \int_0^{2\pi} dq_x \int_0^{2\pi} dq'_x \times \exp\left(i\frac{(\theta+\bar{\theta}_i)(q-q')}{B_1(\bar{\theta}_i)} + \frac{iA_x}{\hbar}(\sin q - \sin q') - \frac{\sigma^2(q-q')^2}{4B_1^2(\bar{\theta}_i)}\right). \quad \text{(A4)}$$

Reverting to sum and difference variables as in Eq. (2.17) then gives

$$P\left(\theta;\bar{p}_{\parallel},\bar{\theta}_i\right) \simeq \frac{1}{4\pi^2 B_1\left(\bar{\theta}_i\right)} \int_0^{2\pi} dQ \int_{-Q}^{Q} d\Delta Q \times \exp\left(i\frac{(\theta+\bar{\theta}_i)\Delta Q}{B_1(\bar{\theta}_i)} + \frac{2iA_x}{\hbar}\cos Q \sin\left(\frac{\Delta Q}{2}\right) - \frac{\sigma^2\Delta Q^2}{4B_1^2\left(\bar{\theta}_i\right)}\right). \quad \text{(A5)}$$

Scaling the difference variable as $\Delta r = \sigma\Delta Q$, noting that σ is large so that the integration limits $\pm\sigma Q$ may be replaced with $\pm\infty$ and that $\sin(\Delta r/(2\sigma)) \sim \Delta r/(2\sigma)$ allows us to perform the Gaussian integral over the variable Δr,

$$P\left(\theta;\bar{p}_{\parallel},\bar{\theta}_i\right) \simeq \frac{1}{\sqrt{\pi}\sigma 2\pi} \int_0^{2\pi} dQ \times \exp\left(-\frac{1}{\sigma^2}[\theta + \bar{\theta}_i + K\cos Q]^2\right), \quad \text{(A6)}$$

where we made use of the fact that $B_1\left(\bar{\theta}_i\right) A_x/\hbar = K$ (see Eqs. (2.25) and (2.32)). Changing variables such that

$$\sin(K\cos Q) = \frac{K}{\sqrt{1+K^2}}\sin u \quad \text{(A7)}$$

and noting that to order K^2 one may assume that $\cos Q \simeq \sin u$ then gives the classical result as in Eq. (2.39).

[1] L. M. Hubbard and W. H. Miller, J. Chem. Phys. **78**, 1801 (1983).
[2] R. R. Hancox, Phys. Rev. **42**, 864 (1932).
[3] B. R. Williams, J. Chem. Phys. **55**, 1315 (1971).
[4] G. Boato, P. Cantini, and L. Mattera, Surf. Sci. **55**, 141 (1976).
[5] K. H. Rieder and W. Stocker, Phys. Rev. Lett. **52**, 352 (1984).
[6] E. K. Schweizer and C. T. Rettner, Phys. Rev. Lett. **62**, 3085 (1989).
[7] E. K. Schweizer, C. T. Rettner, and S. Holloway, Surf. Sci. **249**, 335 (1991).
[8] T. Andersson, F. Althoff, P. Linde, M. Hassel, M. Persson, and S. Andersson, J. Chem. Phys. **113**, 9262 (2000).
[9] T. Andersson, F. Althoff, P. Linde, S. Andersson, and K. Burke, Phys. Rev. B **65**, 045409 (2002).
[10] A. Schueller, S. Wethekam, and H. Winter, Phys. Rev. Lett. **98**, 016103 (2007).
[11] P. Rousseau, H. Khemliche, A. G. Borisov, and P. Roncin, Phys. Rev. Lett. **98**, 016104 (2007).
[12] M. Arndt, O. Nairz, J. Voss-Andreae, C. Keller, G. van der Zouw, and A. Zeilinger, Nature (London) **401**, 680 (1999).
[13] O. Nairz, M. Arndt, and A. Zeilinger, Am. J. Phys. **71**, 319 (2003).
[14] M. Gring, S. Gerlich, S. Eibenberger, S. Nimmrichter, T. Berrada, M. Arndt, H. Ulbricht, K. Hornberger, M. Mueri, M. Mayor, M. Bockmann, and N. L. Doltsinis, Phys. Rev. A **81**, 031604(R) (2010).
[15] J. M. Moix and E. Pollak, J. Chem. Phys. **134**, 011103 (2011).
[16] W. H. Miller and F. T. Smith, Phys. Rev. A **17**, 17 (1978).
[17] E. Pollak, S. Sengupta, and S. Miret-Artés, J. Chem. Phys. **129**, 054107 (2008); E. Pollak and S. Miret-Artés, *ibid.* **130**, 194710 (2009).
[18] E. Pollak, J. M. Moix, and S. Miret-Artés, Phys. Rev. B **80**, 165420 (2009); Phys. Rev. Lett. **104**, 116103 (2010).
[19] E. Pollak and S. Miret-Artés, Chem. Phys. **375**, 337 (2010).
[20] E. Pollak and J. Tatchen, Phys. Rev. B **80**, 115404 (2009).
[21] S. Miret-Artés and E. Pollak, Surf. Sci. Rep. **67**, 161 (2012).
[22] T. Kondo, H. S. Kato, T. Yamada, S. Yamamoto, and M. Kawai, Eur. Phys. J. D **38**, 129 (2006).
[23] L. M. Hubbard and W. H. Miller, J. Chem. Phys. **80**, 5827 (1984).
[24] S. Daon, E. Pollak, and S. Miret-Artés, "Semiclassical perturbation theory for surface temperature effects in atom surface scattering" (unpublished).

34 Appendix 2: Full Text of Published Paper: "Communication: Semi-classical perturbation theory for the quantum diffractive scattering of atoms on thermal surfaces"

Full text of:

Shauli Daon, Eli Pollak, and S. Miret-Artés. J. Chem. Phys. 137, 201103 (2012)

Communication: Semiclassical perturbation theory for the quantum diffractive scattering of atoms on thermal surfaces

Shauli Daon,[1] Eli Pollak,[1,a)] and S. Miret-Artés[2]
[1]*Chemical Physics Department, Weizmann Institute of Science, 76100 Rehovot, Israel*
[2]*Instituto de Física Fundamental, Consejo Superior de Investigaciones Científicas, Serrano 123, 28006 Madrid, Spain*

(Received 19 September 2012; accepted 6 November 2012; published online 30 November 2012)

Inspired by the semiclassical perturbation theory of Hubbard and Miller [J. Chem. Phys. **80**, 5827 (1984)], we derive explicit expressions for the angular distribution of particles scattered from thermal surfaces. At very low surface temperature, the observed experimental background scattering is proportional to the spectral density of the phonons. The angular distribution is a sum of diffraction peaks and a broad background reflecting the spectral density. The theory is applied to measured angular distributions of Ne, Ar, and Kr scattered from a Cu(111) surface. © *2012 American Institute of Physics*. [http://dx.doi.org/10.1063/1.4768227]

The first observations of quantum diffraction of He scattered from a LiF surface were reported 80 years ago.[1] Since then, many authors repeated such experiments with increasing sophistication.[2] It is now well understood that diffraction peaks found in surface scattering of atoms as heavy as Kr are due to the periodic corrugation of the surface.

Surface phonons tend to smear out the angular distribution and it then becomes difficult to distinguish between features arising from the corrugation or the interaction of the particle with the phonons.[3] It is thus of special interest to have a reliable estimate of the phonon spectral density. The spectral density also provides information on the diffusional properties of the same atom on the surface. It also controls energy transfer to the surface as well as sticking probabilities. The spectral density is a fundamental building block in the theory of the dynamics of atoms in the presence of solid surfaces.

At very low surface temperatures, the angular distribution of a scattered particle will be dominated by two contributions. One is elastic scattering, which leads to sharp Bragg peaks in the angular distribution.[2] The second is the broad background, which results from imparting a single quantum of energy to one of the surface phonon modes of the surface.[4] A central theme of this letter is to show how this broad background may be inverted to determine the phonon spectral density and predict the angular distribution as a function of surface temperature. The theory developed here provides a good description of the quantum dominated low energy and low surface temperature measurement of the scattering of Ne, Ar, and Kr on a Cu(111) surface.[4,5]

The quantum theory of scattering from surfaces has been developed extensively by Manson using a distorted wave theory.[6] Here, we provide a different route, based on the semiclassical perturbation (SCP) theory of Hubbard and Miller.[7] This enables us to provide an analytic theory, which includes realistic force fields. The SCP theory provides a direct route between the spectral density and the observed measured low surface temperature angular distribution. For the sake of brevity, we will make a few inessential simplifying assumptions. We limit the dynamics to two degrees of freedom for the scattered particle (with mass M), the vertical z and horizontal x directions. The particle phonon interaction will be limited to the vertical motion since it is the major route for the dissipation of energy from the particle to the surface.[3]

The starting point is a Hamiltonian (operators are denoted with a caret) with linear coupling to the phonon bath,[3] whose (mass weighted) phase space variables are $x_j, p_j; j = 1, \ldots, N$ and whose frequencies are ω_j:

$$\hat{H} = \frac{\hat{p}_x^2 + \hat{p}_z^2}{2M} + \bar{V}(\hat{z}) + \bar{V}'(\hat{z})h(\hat{x}) + \sum_{j=1}^{N}\left[\frac{\hat{p}_j^2}{2m_j} + \frac{m_j\omega_j^2}{2}\left(\hat{x}_j - \frac{\sqrt{M}c_j}{\omega_j^2}\bar{V}'(\hat{z})\right)^2\right]. \quad (1)$$

$\bar{V}(z)$ is the vertical interaction potential, $h(x)$ is the corrugation function with period l taken to be: $h(x) = h\sin(2\pi x/l)$ and h is the corrugation height. The prime in Eq. (1) denotes the derivative with respect to the argument. The c_j's are the coupling coefficients of the vertical motion to the bath modes. The continuum limit is obtained by defining the spectral density

$$J_z(\omega) = \frac{\pi}{2}\sum_{j=1}^{N}\frac{c_j^2}{\omega_j}\delta(\omega - \omega_j), \quad (2)$$

which is a central object of this Communication. In contrast to the surface phonon density of states,[6] the spectral density depends on the specific coupling of the scattered particle to the surface through the coupling coefficients c_j.

The SCP theory is based on the observation that typically the corrugation and the coupling to the phonon bath is weak. The zero-th order motion is that of a conserved horizontal momentum, independent oscillator motion, and the vertical motion is governed by the potential $\bar{V}(z)$. When choosing the Morse potential form, with well depth V_0 and stiffness

a)Electronic mail: eli.pollak@weizmann.ac.il.

parameter α, the vertical motion is known analytically, thus allowing a fully analytical theory of the scattering. Due to the periodicity of the surface, one may show from the SCP theory that (as expected) the difference between the final p_{x_f} and initial p_{x_i} horizontal momentum is quantized according to Bragg's law $p_{x_f} = p_{x_i} + \frac{2\pi\hbar n}{l}$ with n taking integer values, whose range is limited by energy conservation. The S matrix element for scattering from the elastic ($n = 0$) channel and initial harmonic bath oscillator state defined by the vector $\mathbf{n} = (n_1, \ldots, n_N)$, which gives the occupation number in each mode, to the nth Bragg peak and $\mathbf{n}_f$ final bath state is given by the expression[7]

$$S_{n,\mathbf{n}_f;0,\mathbf{n}_i} = \frac{1}{2\pi}\int_0^{2\pi} dq_x \frac{1}{(2\pi)^N} \times \int_0^{2\pi} d\mathbf{q} e^{-inq_x} e^{-i\Delta\mathbf{n}\cdot\mathbf{q}} e^{2i\eta(q_x,\mathbf{q})}. \quad (3)$$

Here, $q_x = 2\pi x/l$ and $\mathbf{q}$ denotes the vector of harmonic bath angle variables defined by the relationship $x_j = \sqrt{\frac{2\hbar(n_j+\frac{1}{2})}{\omega_j}}\cos(q_j + \omega_j t)$. The phase shift $2\eta(q_x, \mathbf{q})$ is determined by the unperturbed classical dynamics and has the form

$$2\eta(q_x, \mathbf{q}) = 2\eta_0 - hA(\omega_x)\sin q_x - F(\omega_j; c_j) + \sum_{j=1}^{N} \bar{A}_j(n_j)\cos q_{j_z}, \quad (4)$$

where η_0 is a phase shift due to the unperturbed potential $\bar{V}(z)$; the coefficient

$$A(\omega) = \frac{1}{\hbar}\int_{-\infty}^{+\infty} dt \bar{V}'(z_t)\cos\omega t, \quad (5)$$

where z_t denotes the unperturbed motion in the vertical direction; the frequency $\omega_x = 2\pi p_{x_i}/(Ml)$; $F(\omega_j; c_j)$ is a constant phase due to the bath and the phase amplitude for the jth oscillator is

$$\bar{A}_j(n_j) = \sqrt{M}c_j\sqrt{\frac{2\hbar(n_j+\frac{1}{2})}{\omega_j}}A(\omega_j). \quad (6)$$

One may now readily carry out the integrations in Eq. (3) to find that the S-matrix element squared is a product of Bessel functions[7]

$$\left|S_{n,\mathbf{n}_f;0,\mathbf{n}_i}\right|^2 = J_n^2(hA(\omega_x))\prod_{j=1}^{N} J_{n_{j_f}-n_{j_i}}^2\left(\bar{A}_j(n_{j_{if}})\right), \quad (7)$$

with $\omega_x = 2\pi p_{x_i}/(Ml)$. In principle, the S matrix must be symmetrical with respect to inversion of the initial and final bath states. In Eq. (7), we have imposed this symmetry by replacing the argument of $\bar{A}_j(n_j)$ with its symmetrized version $\bar{A}_j(n_{j_{if}} = \frac{n_{j_i}+n_{j_f}}{2})$. This symmetrization also guarantees unitarity when expanding to order $\bar{A}_j(n_{j_{if}})^2$. Energy conservation implies

$$p_{z_f}^2 = |p_{z_i}|^2\left[\frac{\cos(|\theta_i| + 2\theta(n))}{\cos|\theta_i|\cos^2\theta(n)} - \frac{2M\hbar\Delta\mathbf{n}\cdot\omega}{|p_{z_i}|^2}\right] \equiv |p_{z_i}|^2\zeta^2, \quad (8)$$

where the vector $\omega = (\omega_1, \ldots, \omega_N)$; $\Delta\mathbf{n} = \mathbf{n}_f - \mathbf{n}_i$; $\tan\theta(n) = \frac{2\pi\hbar n}{l|p_{z_i}|}$, and $\tan\theta_i = p_{x_i}/p_{z_i}$. For an initial choice of the bath oscillator states, the final momentum and angular distributions are then by definition:

$$P(p_{x_f}, p_{z_f}; \mathbf{n}_i) = \sum_n\sum_{\mathbf{n}_f}\left|S_{n,\mathbf{n}_f;0,\mathbf{n}_i}\right|^2\delta(p_{z_f} - |p_{z_i}|\zeta) \times \delta\left(p_{x_f} - p_{x_i} - \frac{2\pi\hbar n}{l}\right), \quad (9)$$

$$P(\theta; \mathbf{n}_i) = \int_{-\infty}^{\infty} dp_{x_f}\int_0^{\infty} dp_{z_f}\delta\left(\theta - \tan^{-1}\frac{p_{x_f}}{p_{z_f}}\right)P(p_{x_f}, p_{z_f}; \mathbf{n}_i) = \sum_n\sum_{\mathbf{n}_f}|S_{n,\mathbf{n}_f;0,\mathbf{n}_i}|^2\frac{2E_i\sin^2(|\theta_i| + \theta(n))}{\hbar|\sin^2\theta\tan\theta|\cos^2\theta(n)}\delta(\Delta\mathbf{n}\cdot\omega - \bar{\Omega}). \quad (10)$$

Here, $E_i = (p_{x_i}^2 + p_{z_i}^2)/(2M)$ and the "phonon frequency" $\bar{\Omega}$ is defined as

$$\bar{\Omega}(\theta, \theta_i, n) = \frac{E_i}{\hbar}\left[1 - \frac{\sin^2(|\theta_i| + \theta(n))}{\cos^2\theta(n)\sin^2\theta}\right]. \quad (11)$$

The surface is in thermal equilibrium prior to the collision. The final angular distribution is obtained by thermal averaging over the initial phonon states. We first consider zero-phonon transitions ($n_{j_f} - n_{j_i} = 0$). Within the SCP theory, the phase amplitudes $\bar{A}_j(n_{j_{if}})$ are small, due to the weak coupling to the phonon bath, so that we approximate the Bessel function $J_0^2(x) \simeq \exp(-x^2/2)$. Within the same order, we approximate the thermal average $\langle\exp(-\gamma_j(n_j + 1/2))\rangle \simeq \exp(-\gamma_j\langle n_j + 1/2\rangle)$ with $\langle n_j + \frac{1}{2}\rangle = \frac{1}{2}\coth(\frac{\hbar\beta\omega_j}{2})$. One then readily finds that the zero phonon contribution to the angular distribution is (the arguments of $\bar{\Omega}$ are henceforth suppressed)

$$\langle P(\theta; \Delta n{=}0)\rangle \simeq \sum_n J_n^2(hA(\omega_x))\frac{2E_i\sin^2(|\theta_i| + \theta(n))}{\hbar|\sin^2\theta\tan\theta|\cos^2\theta(n)} \times \delta(\bar{\Omega})\exp(-2W), \quad (12)$$

and we identify the Debye-Waller factor[8] as

$$2W \equiv \sum_{j=1}^{N}\frac{M\hbar c_j^2 A^2(\omega_j)}{2\omega_j}\coth\left(\frac{\hbar\beta\omega_j}{2}\right) = \frac{M}{2\pi\hbar}\int_{-\infty}^{+\infty} dt''\int_{-\infty}^{+\infty} dt'\bar{V}'(z_{t'})\bar{V}'(z_{t''}) \times \int_0^{\infty} d\omega J_z(\omega)\coth\left(\frac{\hbar\beta\omega}{2}\right)\cos(\omega(t' - t'')). \quad (13)$$

In the last line, we used the definition of the spectral density (Eq. (2)). The zero phonon contribution is thus a series of delta function peaks whose intensity is temperature dependent, via the Debye-Waller factor. The expression (13) has been derived for neutron scattering through surfaces[9] and for surface scattering.[8] What is new here is the derivation of the same result, based on the SCP theory of Hubbard and Miller.[7]

This derivation is valid also for very low temperatures, justifying its usage by Andersson *et al.*[10]

The one phonon contribution follows similar lines. Any oscillator is allowed to add or lose one phonon, so that $n_{j_f} - n_{j_i} = \pm 1$. Keeping terms only up to order $\bar{A}_j(n_{j_if})^2$, we approximate $J_1^2(x)/J_0^2(x) \simeq x^2/4$ to find that

$$\langle P(\theta;\Delta n=1)\rangle + \langle P(\theta;\Delta n=-1)\rangle \simeq \sum_n J_n^2(hA(\omega_x))\exp(-2W)J_z(|\bar{\Omega}|)A(\bar{\Omega})^2 \cdot \frac{ME_i\cos\theta\sin^2(|\theta_i|+\theta(n))}{\pi|\sin^3\theta|\cos^2\theta(n)} \times \left[\coth\left(\frac{\hbar\beta|\bar{\Omega}|}{2}\right) + H(\bar{\Omega}) - H(-\bar{\Omega})\right], \quad (14)$$

where $H(x)$ is the unit step function. This result, central to this Communication, shows explicitly that in the continuum bath limit, the contribution from one phonon transitions to the angular distribution, is a smooth background contribution, proportional to the spectral density. This smooth background has contributions from all Bragg peaks since the effective phonon frequency $\bar{\Omega}$ depends on the Bragg diffraction number n. When the temperature is sufficiently low, the angular distribution is composed of "delta" function peaks at the Bragg angles (Eq. (12)) and a broad background (Eq. (14)) that reflects the spectral density of the surface phonons. When $T = 0$ K, the phonon frequency $\bar{\Omega}$ must be positive as the oscillators can only gain a phonon. This causes a decrease in the vertical energy so that the dominant background scattering for $n = 0$ will appear only for angles greater than specular. This is indeed observed in the measured low temperature angular distributions.[4]

For the two phonon contribution, one has to consider five possibilities: a single mode absorbing two phonons; two different modes, each absorbing a single phonon; two different modes, one absorbing and one emitting a phonon; two different modes, each emitting a phonon; one mode, emitting two phonons. The thermal averaging follows the same reasoning as before. We approximate $J_2^2(x)/J_0^2(x) \simeq x^4/64$ and ignore contributions of the form $\sum_j g_j c_j^4$ since they vanish in the continuum limit. One then finds that the two phonon contribution to the angular distribution is

$$\langle P(\theta;2)\rangle = \sum_n J_n^2(hA(\omega_x))\exp(-2W) \times \frac{\hbar M^2 E_i \sin^2(|\theta_i|+\theta(n))}{4\pi^2|\sin^2\theta\tan\theta|\cos^2\theta(n)}[S_2+S_0+S_{-2}], \quad (15)$$

$$S_2 = H(\bar{\Omega})\int_0^{\bar{\Omega}} d\omega J_z(\omega)J_z(\bar{\Omega}-\omega)A^2(\omega)A^2(\bar{\Omega}-\omega) \cdot \left[\coth\left(\frac{\hbar\beta\omega}{2}\right)+1\right]\left[\coth\left(\frac{\hbar\beta(\bar{\Omega}-\omega)}{2}\right)+1\right], \quad (16)$$

TABLE I. Parameters used for Ne, Ar, and Kr scattered on a Cu(111) surface.

	$\alpha \cdot l$	V_0 [meV]	$\bar{\gamma}$ [dimensionless]	h [a.u.]
Kr	4.2	134.0	0.1205	2.82×10^{-3}
Ar	3.3	70.0	0.05782	1.98×10^{-3}
Ne	3.0	31.6	0.01234	1.10×10^{-3}

$$S_0 = \int_0^{\infty} d\omega J_z(\omega)J_z(\bar{\Omega}+\omega)A^2(\omega)A^2(\bar{\Omega}+\omega)H(\bar{\Omega}+\omega) \cdot \left[\coth\left(\frac{\hbar\beta\omega}{2}\right)-1\right]\left[\coth\left(\frac{\hbar\beta(\bar{\Omega}+\omega)}{2}\right)+1\right], \quad (17)$$

$$S_{-2} = H(-\bar{\Omega})\int_0^{|\bar{\Omega}|} d\omega J_z(\omega)J_z(|\bar{\Omega}|-\omega)A^2(\omega)A^2(|\bar{\Omega}|-\omega) \cdot \left[\coth\left(\frac{\hbar\beta\omega}{2}\right)-1\right]\left[\coth\left(\frac{\hbar\beta(|\bar{\Omega}|-\omega)}{2}\right)-1\right]. \quad (18)$$

In the following, we use the SCP theory to analyze the measured low temperature angular distribution of Ne, Ar, and Kr scattered from a Cu(111) surface.[4,5] The vertical potential is taken to be a Morse potential. The well depths are taken from recent *ab initio* computations.[11] The lattice length is 3.61 Å.[12] The "corrugation height" is determined from the measured ratio of the $n = 0$ to $n = -1$ Bragg peaks, which determines the magnitude of the phase amplitude $hA(\omega_x)$ appearing in the argument of the respective Bessel functions. The spectral density is chosen to be Ohmic (for a theoretical justification see Ref. 13) with an exponential cutoff $J(\omega) = \gamma\omega\exp(-\omega/\omega_c)$. The cutoff frequency is considered here to be a property of the surface and is the same for all the atoms. The friction coefficient γ is fit separately for each atom. The theory thus involves only two parameters for each atom (γ, α) and the cutoff frequency ω_c, common to all cases. The parameters are given in Table I ($\bar{\gamma} = M^2\omega_0^3\gamma$ where $\omega_0^2 = 2V_0\alpha^2/M$). The results for the temperature dependence of the Debye-Waller factor are shown in Fig. 1. These fits are substantially improved as compared to those given previously in Refs. 5 and 10. The Morse potential provides an adequate description and there is no need to use more elaborate functional forms.[5]

The Debye-Waller factors leave very little freedom in the fitting procedure, except for the cutoff frequency $\hbar\omega_c$ chosen to be 6 meV. The results for Ne, Ar, and Kr are shown in Fig. 2 (the plots were scaled by 0.02412 and 0.1150 for Kr, 0.01441 and 0.06670 for Ar, 0.01410 and 0.01896 for Ne, for the low and high temperatures, respectively, so as to fit the maxima of the reported experimental unnormalized distributions). In all cases, the elastic peaks were Gaussian broadened ($\Delta\theta = 0.4°$), to agree with the experimental broadening, as also detailed in Ref. 5. For Ne scattering at 10 K, the two phonon contribution is negligible. This provides an objective criterion

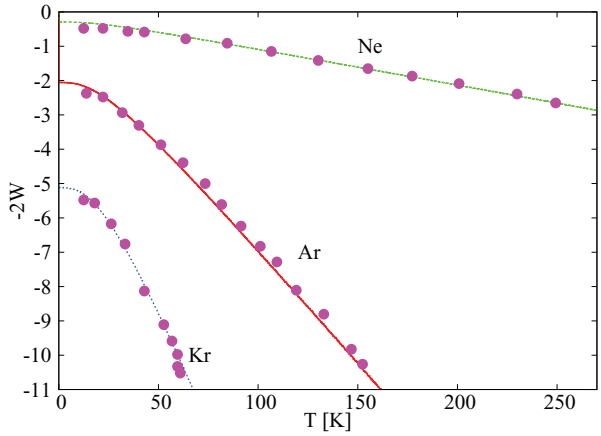

FIG. 1. The SCP fit to the measured temperature dependence of the Debye-Waller factor for Ne, Ar, and Kr scattered from Cu(111). The solid circles represent the experimental results of Ref. 4 while solid lines are the fits obtained with Eq. (13) and the parameters given in Table I.

for determining that at this temperature, only single phonon scattering takes place. The fit to experiment indicates that the chosen Ohmic spectral density provides a good description for the coupling of the Ne atom to the surface phonons. The minuscule Bragg peak at $n = -1$, which cannot be seen on the scale of the figure, implies that the corrugation is very weak. It is remarkable that at the elevated temperature of 300 K, the complete angular distribution is well described by adding only the two phonon contribution. This is a reflection of the weak friction coefficient, which effectively disallows higher order phonon transitions. Even at this elevated surface temperature, the angular distribution is dominated by the elastic quantum diffraction peak. The results for Ar are similar in quality, though here the reduced friction coefficient is larger so that at the higher temperature three or more phonons may be excited. Finally, for Kr even at a surface temperature of 15 K, multiphonon transitions cannot be neglected and the theoretical distribution remains somewhat lower than the measured one. To correctly describe the high temperature Kr results one may derive a classical bath "infinite phonon" limit of the present theory.[14]

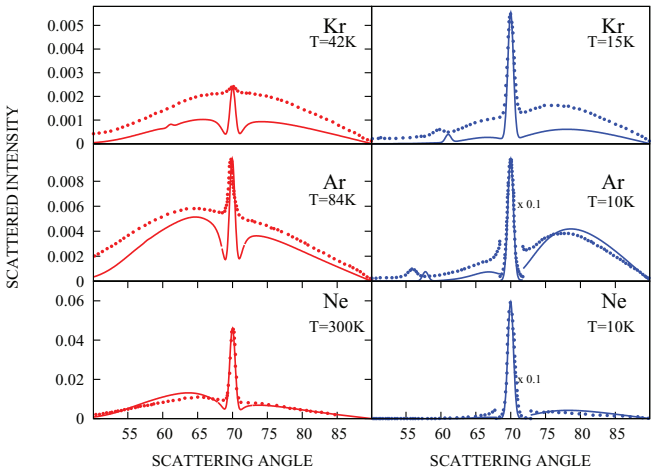

FIG. 2. Comparison of the SCP theoretically generated (solid lines) angular distributions using Eqs. (12)–(18) and the experimental measurements (dotted lines)[5] for low (right panel) and high (left panel) surface temperatures. The low temperature experimental and theoretical specular peaks for Ne and Ar are multiplied by 0.1 to fit them into the scale of the plots.

In summary, we demonstrated by application of the semiclassical perturbation theory to experimentally measured data that the low temperature scattering of atoms from surfaces provides direct information on the spectral density of the phonons. The same theory can now be used to describe many other surface phenomena, such as quantum energy transfer to the surface, quantum sticking probabilities, diffusion, selective adsorption resonances, and more. It may be generalized to include the full three dimensions of the scattered particle as well as coupling to horizontal phonons.

This work has been graciously supported by grants from the Israel Science Foundation and the German-Israel Foundation for Basic Research, FIS2011-29596-C01-02 (Spain) and COST action MP1006.

[1] I. Estermann and O. Stern, Z. Phys. **61**, 95 (1930).
[2] G. Benedek and J. P. Toennies, Surf. Sci. **299/300**, 587 (1994).
[3] S. Miret-Artés and E. Pollak, Surf. Sci. Rep. **67**, 161 (2012).
[4] F. Althoff, T. Andersson, and S. Andersson, Phys. Rev. Lett. **79**, 4429 (1997).
[5] T. Andersson, F. Althoff, P. Linde, S. Andersson, and K. Burke, Phys. Rev. B **65**, 045409 (2002).
[6] J. R. Manson, Phys. Rev. B **43**, 6924 (1991).
[7] L. M. Hubbard and W. H. Miller, J. Chem. Phys. **80**, 5827 (1984).
[8] Equations 4.35 and 4.36 of A. C. Levi, and H. Suhl, Surf. Sci. **88**, 221 (1979); K. Burke and W. Kohn, Phys. Rev. B **43**, 2477 (1991).
[9] V. F. Sears and S. A. Shelley, Acta Crystallogr. **A47**, 441 (1996), see Eq. (2), published online.
[10] See the comment and response in A. Siber and B. Gumhalter, Phys. Rev. Lett. **81**, 1742 (1998); F. Althoff, T. Andersson, and S. Andersson, *ibid.* **81**, 1743 (1998).
[11] P. L. Silvestrelli, A. Ambrosetti, S. Grubisic, and F. Ancilotto, Phys. Rev. B **85**, 165405 (2012).
[12] M. Wilms, P. Broekman, C. Stuhlmann, and K. Wandelt, Surf. Sci. **416**, 121 (1998).
[13] Y. Georgievskii, M. A. Kozhushner, and E. Pollak, J. Chem. Phys. **102**, 6908 (1995).
[14] S. Daon, E. Pollak, and S. Miret-Artés, "A semiclassical theory for scattering from thermal surfaces" (unpublished).

35 Appendix 3: Full Text of Published Paper: "Semiclassical multi-phonon theory for atom-surface scattering: Application to the Cu(111) system"

Full text of:

Shauli Daon and Eli Pollak. J. Chem. Phys. 142, 174102 (2015)

Semiclassical multi-phonon theory for atom-surface scattering: Application to the Cu(111) system

Shauli Daon and Eli Pollak
Chemical Physics Department, Weizmann Institute of Science, 76100 Rehovoth, Israel

(Received 6 March 2015; accepted 17 April 2015; published online 1 May 2015)

The semiclassical perturbation theory of Hubbard and Miller [J. Chem. Phys. **80**, 5827 (1984)] is further developed to include the full multi-phonon transitions in atom-surface scattering. A practically applicable expression is developed for the angular scattering distribution by utilising a discretized bath of oscillators, instead of the continuum limit. At sufficiently low surface temperature good agreement is found between the present multi-phonon theory and the previous one-, and two-phonon theory derived in the continuum limit in our previous study [Daon, Pollak, and Miret-Artés, J. Chem. Phys. **137**, 201103 (2012)]. The theory is applied to the measured angular distributions of Ne, Ar, and Kr scattered from a Cu(111) surface. We find that the present multi-phonon theory substantially improves the agreement between experiment and theory, especially at the higher surface temperatures. This provides evidence for the importance of multi-phonon transitions in determining the angular distribution as the surface temperature is increased. © *2015 AIP Publishing LLC*. [http://dx.doi.org/10.1063/1.4919345]

I. INTRODUCTION

The first observations of quantum diffraction of He scattered from a LiF surface were reported 80 years ago.[1,2] Since then, many authors repeated such experiments with increasing sophistication.[3] It is well understood that diffraction peaks found in surface scattering of atoms as heavy as Kr are due to the periodic corrugation of the surface.

The quantum theory of scattering from surfaces has been developed extensively. Manson and coworkers used a Distorted Wave Born Approximation (DWBA) approach.[4–6] A semiclassical theory of atom-surface scattering was proposed by Billing.[7,8] The surface was treated as a set of coupled quantum oscillators perturbed by the time-dependent force imposed by the colliding atom/molecule. Miret-Artés and others used a quantum trajectory-based formalism to describe quantum mechanical phenomena such as selective adsorption[9,10] and quantum close-coupling calculations to describe the He surface interaction potential for scattering on Sb(111) and ZnO surfaces.[11–13] Jackson used a time-dependent mean-field approach[14] and wavepacket propagation methods[15] in a restricted two-dimensional model to simulate the underlying quantum dynamics. Gumhalter and co-workers developed an evolution operator theory and applied it to atom-surface scattering.[16–18] Gross used reduced-dimensional quantum mechanics simulations[19] along with a potential obtained using density functional theory to study the scattering of hydrogen molecules from a Pd(100) surface.[20] Nieto *et al.*,[21] using a combination of quantum scattering theory and experiment, showed that the scattering of H_2 from a metal surface occurs on a single Born-Oppenheimer potential energy surface. Three dimensional semiclassical studies of atom surface scattering were carried out by Drolshagen and Heller, employing a thawed Gaussian wavepacket method giving good agreement with numerically exact quantum mechanical results.[22]

The classical theory of atom surface scattering has also been developed.[23] The double lobe structure found in many measurements of the angular distribution of the scattered particle was attributed to classical rainbows. The study of model hard wall corrugated potentials has shown that for weak corrugation, one should expect that at the inflection points of the corrugation, the derivative of the angular deflection function vanishes, leading to a divergence of the scattering probability. Smearing of this divergence due to thermal fluctuations then leads to the double lobe structure. The earliest models considered a hard wall corrugated potential for which one can solve the scattering analytically.[24–30] Adding a potential well in front of the hard wall accounted for the energy dependence of the angular distance between the rainbow peaks. As the energy is increased, the refraction caused by the potential well decreases, and the rainbow angles come closer to each other. This class of models was then improved to include thermal effects, by treating the surface as a particle with an effective mass and thermally distributed velocity, and is known as the washboard model.[26]

In recent years, the classical theory has been further developed to include more realistic "soft" potentials and a harmonic continuum description of surface phonons.[31–35] Noting that both the corrugation height and the friction felt by the incoming particle are typically small, one can solve for the classical dynamics using a classical perturbation theory. This accounts well for many of the qualitative features of the angular distributions, including the dependence on incident energy, incident angle, surface temperature, and more. If one models the interaction potential in terms of a Morse potential and sinusoidal corrugations along the horizontal surface directions, one can derive an analytic theory for the scattering. This approach was then used to invert the measured angular distributions in terms of interaction potentials. Very recently, the perturbation theory has been expanded to include the second order corrections due to the surface corrugation.[36]

In this paper, we follow a semiclassical route, pioneered by Miller and coworkers. Using SemiClassical Perturbation Theory (SCPT),[37] Hubbard and Miller derived[38,39] simple expressions, in terms of integer Bessel functions for the elastic scattering of an atom from a frozen surface. They, then, also considered thermal effects[39] albeit in a limited manner, considering an Einstein phonon spectrum.

Notwithstanding these developments, there remain many experimental features, associated with the quantum scattering of heavy atoms on surfaces which have yet to receive a satisfactory explanation. Andersson and co-workers[40,41] studied in some detail the scattering of Ne, Ar, and Kr on a Cu(111) surface. Using very cold surfaces and low energy beams, they were able to observe diffraction peaks in the angular distribution even for an atom as heavy as Kr. They also observed a relatively smooth "background" angular scattering. A theory which correctly accounts for both the diffraction peaks and the smooth background as well as their temperature dependence is the central objective of this paper. In a previous Communication,[42] we noted that the broad background may be inverted to determine the phonon spectral density. However, our previous analysis was restricted to only single and two phonon transitions and so did not provide a complete description of the thermal effects.

The theory we use is an extension of the SCPT of Hubbard and Miller.[39] Our starting point is a Hamiltonian description of the scattering in which the particle is coupled linearly to a bath of harmonic oscillators, whose properties are described by a continuum spectral density. Systematic application of SCPT enables us to derive a practical theory which includes realistic force fields as well as thermal effects of the surface.

The SCPT approach is based on the observation that often, especially when scattering from metal surfaces, the corrugation of the surface is weak so that the corrugation height may be considered as a small parameter justifying a perturbative solution of the equations of motion. Similarly, the coupling to the phonons is weak so that this coupling too may be considered within perturbation theory.

In contrast, though, to previous work, we introduce here a form factor which enables the computation of the angular distribution with an arbitrary number of phonon transitions. The resulting multi-phonon theory, which uses a discretization of the spectral density, is then applied to a study of the scattering of Ne, Ar, and Kr on a Cu(100) surface, as measured by Andersson and coworkers.[40,41]

The semiclassical theory is developed in Sec. II. It is applied in Sec. III to the experimental results of Andersson and coworkers[40,41] for the scattering of Ne, Ar, and Kr from the Cu(100) surface. We end with a discussion of the limitations and further possible extensions of the semiclassical theory.

II. SEMICLASSICAL PERTURBATION THEORY

A. The framework

Since the typical experimental measurements are carried out in the plane of the incident and outgoing beams, we will restrict ourselves here and model the dynamics in terms of two degrees of freedom. One is the vertical distance z (with conjugate momentum p_z) describing the distance of the atom (whose mass is M) from the surface, the other is the horizontal coordinate x (with conjugate momentum p_x) parallel to the surface. Recent classical studies have shown[43] that the two planar degrees of freedom (x and y) are not necessarily separable so that inclusion of the second planar degree of freedom can change the classical scattering dynamics. It should be thus understood that the present treatment is valid provided that the coupling between the two degrees of freedom may be neglected. Furthermore, we will assume that the coupling to the vertical phonons is much more important than the coupling to the horizontal surface phonons. This assumption has also been verified in recent on the fly molecular dynamics computations.[43]

The model Hamiltonian we use is based on the assumption that the interaction of the particle with the surface is only dependent on the instantaneous distance of the particle from the fluctuating surface which is $z + h(x) + \frac{1}{\sqrt{M}}\sum_{j=1}^{N} c_j x_j$. The fluctuational part is assumed small so that to leading order in the coupling, the potential of interaction is a sum of three terms $\bar{V}(z + h(x) + \frac{1}{\sqrt{M}}\sum_{j=1}^{N} c_j x_j) \simeq \bar{V}(z) + \bar{V}'(\hat{z})h(\hat{x}) + \bar{V}'(\hat{z})\frac{1}{\sqrt{M}}\sum_{j=1}^{N} c_j x_j$. The resulting "standard" model Hamiltonian[23,42] describing the scattering dynamics is

$$\hat{H} = \frac{\hat{p}_x^2 + \hat{p}_z^2}{2M} + \bar{V}(\hat{z}) + \bar{V}'(\hat{z})h(\hat{x}) + \sum_{j=1}^{N}\left[\frac{\hat{p}_j^2}{2} + \frac{\omega_j^2}{2}\left(\hat{x}_j - \frac{c_j\bar{V}'(\hat{z})}{\sqrt{M}\omega_j^2}\right)^2\right], \tag{2.1}$$

where $\bar{V}(\hat{z})$ is the potential of interaction in the vertical direction; $\bar{V}'(\hat{z})$ denotes the derivative of the potential $\bar{V}(\hat{z})$ with respect to z; $h(\hat{x})$ is the horizontal corrugation function which in this paper will take the simple form

$$h(\hat{x}) = h\sin\left(\frac{2\pi\hat{x}}{l}\right), \tag{2.2}$$

where h is the corrugation height parameter, considered to be small compared to the lattice length l of the surface in the horizontal direction, $\hat{p}_j$ and $\hat{x}_j$ are the respective mass weighted momentum and coordinate operators for the j-th bath oscillator, and c_j is the dimensionless coupling constant which couples the j-th bath oscillator to the vertical motion.

The continuum limit is introduced through the spectral density defined as

$$J_z(\omega) = \frac{\pi}{2}\sum_{j=1}^{N}\frac{c_j^2}{\omega_j}\delta(\omega - \omega_j). \tag{2.3}$$

The associated friction function is

$$\gamma(t) = \sum_{j=1}^{N}\frac{c_j^2}{\omega_j^2}\cos(\omega_j t). \tag{2.4}$$

In this paper, we concentrate on the angular distribution of the scattered particle initiated far away from the surface at the time $-t_0$ with initial (negative) momentum p_{z_i} and (positive) horizontal momentum p_{x_i}. We are then interested in the

distribution of the final momenta p_{z_f} and p_{x_f} of the particle at the time $+t_0$, which is taken to be sufficiently large to assure that the scattering event is over. The initial state of the system is also characterized by the initial quantum number n_{j_i} of the j-th bath oscillator and the final quantum state n_{j_f} of the j-th oscillator after the collision is over.

The periodicity of the surface in the horizontal direction implies that the final momentum must obey the Bragg condition, that is,

$$p_{x_f} = p_{x_i} + \frac{2\pi\hbar n}{l}, \tag{2.5}$$

with n an integer and referred to as the Bragg number. Energy conservation then implies that the vertical momentum of the particle, after the collision is over, $p_{z_{t_0}}$, is related to all other observables through the energy conservation relationship

$$\frac{p_{z_{t_0}}^2 + \left(p_{x_i} + \frac{2\pi\hbar n}{l}\right)^2}{2M} + \sum_{j=1}^{N}\left(n_{j_f} + \frac{1}{2}\right)\hbar\omega_j = \frac{p_{z_i}^2 + p_{x_i}^2}{2M} + \sum_{j=1}^{N}\left(n_{j_i} + \frac{1}{2}\right)\hbar\omega_j. \tag{2.6}$$

The exact quantum mechanical final particle momentum distribution, summed over all possible final bath states, is then by definition

$$P(p_{x_f}, p_{z_f}; \boldsymbol{n}_i) = \sum_{n,\boldsymbol{n}_f} \delta(p_{x_f} - p_{x_i} - \frac{2\pi\hbar n}{l}) \times \delta(p_{z_f} - p_{z_{t_0}}) P_{n,\boldsymbol{n}_f;\,0,\boldsymbol{n}_i}, \tag{2.7}$$

where the vector notation $\mathbf{n} = (n_1, \ldots, n_N)$ is used to describe all the bath mode quantum numbers. $P_{n,\boldsymbol{n}_f;\,0,\boldsymbol{n}_i}$ is the quantum probability for going from the initial state of the bath ($\boldsymbol{n}_i$) and the initial momenta of the particle (p_{x_i}, p_{z_i} with Bragg number $n_i = 0$ by definition) to the respective final momenta and oscillator quantum states. For future use, we note that the change in the occupation numbers of the oscillators is defined as

$$\Delta\mathbf{n} = \mathbf{n}_f - \mathbf{n}_i. \tag{2.8}$$

The heart of the theory is the diffraction probability

$$P_{n,\boldsymbol{n}_f;\,0,\boldsymbol{n}_i} = |S_{n,\boldsymbol{n}_f;\,0,\boldsymbol{n}_i}|^2, \tag{2.9}$$

where $S_{n,\boldsymbol{n}_f;\,0,\boldsymbol{n}_i}$ is the corresponding S-matrix element.

Typically, the surface is in thermal equilibrium with temperature T, so that the initial condition for the bath is described by the thermal bath density operator

$$\hat{P}_B = \frac{\exp\left(-\beta\hat{H}_B\right)}{Z_B}, \tag{2.10}$$

where $Z_B = Tr_B \exp\left(-\beta\hat{H}_B\right)$ is the bath partition function and the bath Hamiltonian is defined as

$$\hat{H}_B = \sum_{j=1}^{N}\left[\frac{\hat{p}_j^2}{2} + \frac{\omega_j^2}{2}\hat{x}_j^2\right] \tag{2.11}$$

and $\beta = 1/(k_B T)$. The thermally averaged final momentum distribution is then

$$\left\langle P(p_{x_f}, p_{z_f})\right\rangle_\beta = \sum_{\boldsymbol{n}_i=0}^{\infty}\sum_{n,\boldsymbol{n}_f} \delta(p_{x_f} - p_{x_i} - \frac{2\pi\hbar n}{l})\delta(p_{z_f} - p_{z_{t_0}}) \cdot P_{n,\boldsymbol{n}_f;\,0,\boldsymbol{n}_i} \frac{\exp\left(-\beta\hbar\left(\left(\mathbf{n}_i + \frac{1}{2}\mathbf{I}\right)\cdot\boldsymbol{\omega}\right)\right)}{Z_B}. \tag{2.12}$$

The (negative) angle of incidence θ_i and the final scattering angle θ_f relative to the normal to the surface are by definition

$$\theta_j = \tan^{-1}\left(\frac{p_{x_j}}{p_{z_j}}\right), \quad j = i, f. \tag{2.13}$$

The thermally averaged final angular distribution of the scattered particle is then given in terms of the final momentum distribution as

$$\left\langle P(\theta_f)\right\rangle_\beta = \int_{-\infty}^{\infty} dp_{x_f} \int_0^{\infty} dp_{z_f} \delta\left(\theta_f - \tan^{-1}\left(\frac{p_{x_f}}{p_{z_f}}\right)\right) \times \left\langle P(p_{x_f}, p_{z_f})\right\rangle_\beta. \tag{2.14}$$

B. Semiclassical theory

Forty-five years ago, Miller[44,45] formulated an initial value representation for the S-matrix element. To introduce his expression, we first define the classical action angle variables for the system and the bath. The system angle variable q_x is defined in terms of the horizontal coordinate of the particle and the lattice length of the surface as

$$q_x = \frac{2\pi x}{l}. \tag{2.15}$$

The corresponding horizontal action variable is defined as

$$I_x = \frac{l p_x}{2\pi}. \tag{2.16}$$

The bath action (I_j) and angle (q_j) variables for the j-th bath oscillator are defined by the canonical transformation

$$x_j = \sqrt{\frac{2I_j}{\omega_j}}\cos(q_j), \tag{2.17}$$

$$p_j = -\sqrt{2\omega_j I_j}\sin(q_j). \tag{2.18}$$

The initial conditions for the classical actions are

$$I_{j_i} = \hbar\left(n_{j_i} + \frac{1}{2}\right), \quad j = 1, \ldots, N. \tag{2.19}$$

To get rid of infinities at long times after the collision, Miller also introduced the pseudo angle variables

$$\bar{q}_{j_t} = q_{j_t} - \frac{M z_t \omega_j}{p_{z_t}}, \quad j = 1, \ldots, N \tag{2.20}$$

such that at long times after the classical collision is over, when the particle is moving freely, one has that for the j-th oscillator $\frac{d\bar{q}_{j_t}}{dt} = 0$. Similarly one introduces a pseudo angle variable for the horizontal motion

$$\bar{q}_{x_t} = q_{x_t} - \frac{M z_t \omega_{x_t}}{p_{z_t}}, \tag{2.21}$$

where the horizontal frequency is defined as

$$\omega_{x_t} = \frac{2\pi p_{x_t}}{Ml}. \tag{2.22}$$

Miller derived the following initial value representation for the classical S-matrix element:[45]

$$S_{n_{x_f},\mathbf{n}_f;0,\mathbf{n}_i} = \lim_{t_0\to\infty} \int_0^{2\pi} \frac{dq_{x_i}}{2\pi} \int_0^{2\pi} \prod_{j=1}^{N} \frac{dq_{j_i}}{2\pi} |\mathbf{D}|^{1/2} \cdot \exp\left(\frac{i}{\hbar}\left[\varphi_{t_0} + \bar{q}_{x_{t_0}}(I_{x_{t_0}} - \hbar n_{x_f}) + \sum_{j=1}^{N} \bar{q}_{j_{t_0}}\left(I_{j_{t_0}} - \hbar\left(n_{j_f} + \frac{1}{2}\right)\right)\right]\right), \tag{2.23}$$

where $I_{x_{t_0}}$, $\bar{q}_{x_{t_0}}$ and $I_{j_{t_0}}, \bar{q}_{j_{t_0}}$, $j = 1,\ldots,N$ are the values of the respective action and pseudo angle variables, after the collision is over. The action is

$$\varphi_{t_0} = -\int_{-t_0}^{t_0} dt\ [q_{x_t}\dot{I}_{x_t} + z_t\dot{p}_{z_t} + \sum_{j=1}^{N} q_{j_t}\dot{I}_{j_t}]. \tag{2.24}$$

The matrix $\mathbf{D}$ is the Jacobian of the transformation from the $N+1$ final pseudo action variables to the $N+1$ initial variables.

Miller and Smith[37] and Hubbard and Miller[38,39] then used first order classical perturbation theory, in which the small parameters are the corrugation height h and the coupling parameters $c_j, j = 1,\ldots,N$ for the bath variables, setting the Jacobian prefactor to unity, to derive a relatively simple expression for the transition probability in terms of integer Bessel functions,

$$\left|S_{n,\mathbf{n}_f;0,\mathbf{n}_i}\right|^2 = J_n^2(hA(\omega_x)) \prod_{j=1}^{N} J^2_{n_{j_f}-n_{j_i}}\left(\bar{A}_j\left(n_{j_{if}}\right)\right), \tag{2.25}$$

with

$$n_{j_{if}} = \frac{n_{j_i} + n_{j_f}}{2}. \tag{2.26}$$

The arguments of the Bessel functions for the bath variables are

$$\bar{A}_j(n) = c_j\sqrt{\frac{2\hbar\left(n+\frac{1}{2}\right)}{M\omega_j}}A(\omega_j), \tag{2.27}$$

with

$$A(\omega) = \frac{1}{\hbar}\int_{-\infty}^{+\infty} dt\bar{V}'(z_{t,0})\cos\omega t. \tag{2.28}$$

Here, $z_{t,0}$ is the zero-th order solution for the classical vertical motion governed by

$$M\ddot{z}_{t,0} + \bar{V}'(z_{t,0}) = 0, \tag{2.29}$$

with the initial condition that the vertical momentum is p_{z_i} and the initial coordinate z_i is sufficiently far out such that the potential $\bar{V}(z_i)$ vanishes.

C. Thermal averaging

All that remains to be done is to perform the summation over final bath states and averaging over initial bath states to obtain the final momentum distribution and the related angular distribution. For this purpose, using the notation

$$\tan\theta(n) = \frac{2\pi\hbar n}{l\left|p_{z_i}\right|}, \tag{2.30}$$

we note that energy conservation (Eq. (2.6)) implies that the final vertical momentum is a function of the initial vertical momentum, the Bragg quantum number, and the initial and final horizontal and bath actions,

$$p^2_{z_{t_0}} = \left|p_{z_i}\right|^2\left[\frac{\cos(|\theta_i| + 2\theta(n))}{\cos|\theta_i|\cos^2\theta(n)} - \frac{2M\hbar\Delta\mathbf{n}\cdot\omega}{\left|p_{z_i}\right|^2}\right] \equiv \left|p_{z_i}\right|^2\zeta(n,\Delta\mathbf{n}\cdot\omega)^2 \tag{2.31}$$

and energy conservation imposes the condition that

$$\zeta(n,\Delta\mathbf{n}\cdot\omega) \geq 0. \tag{2.32}$$

Inserting unity as $1 = \int_{-\infty}^{\infty} d\bar{\Omega}\delta\left(\bar{\Omega} - \Delta\mathbf{n}\cdot\omega\right)$ and then using the Fourier representation of the Dirac delta function imply that the thermally averaged final momentum distribution may be rewritten as (with $H(x)$ denoting the unit step function)

$$\left\langle P(p_{x_f},p_{z_f})\right\rangle_\beta = \sum_n \int_{-\infty}^{\infty} d\bar{\Omega}\delta(p_{x_f} - p_{x_i} - \frac{2\pi\hbar n}{l}) \times \delta(p_{z_f} - \left|p_{z_i}\right|\zeta(n,\bar{\Omega}))H(\zeta(n,\bar{\Omega})) \times \tilde{F}(\bar{\Omega},\beta,n). \tag{2.33}$$

All the dynamical information is hidden within the "form factor" $F(\tau,\beta,n)$ defined as

$$F(\tau,\beta,n) = \frac{1}{Z_B}\sum_{\mathbf{n}_i=0}^{\infty}\sum_{\mathbf{n}_f=0}^{\infty} P_{n,\mathbf{n}_f;0,\mathbf{n}_i}\exp\left[-i\tau\Delta\mathbf{n}\cdot\omega - \beta\hbar\left(\left(\mathbf{n}_i + \frac{1}{2}\mathbf{I}\right)\cdot\omega\right)\right], \tag{2.34}$$

with

$$\tilde{F}(\bar{\Omega},\beta,n) = \frac{1}{2\pi}\int_{-\infty}^{\infty} d\tau\exp(i\tau\bar{\Omega})F(\tau,\beta,n). \tag{2.35}$$

The associated angular distribution is

$$\left\langle P(\theta_f)\right\rangle_\beta = \sum_n \int_{-\infty}^{\infty} d\bar{\Omega}\delta\left(\theta_f - \tan^{-1}\left(\frac{p_{x_i} + \frac{2\pi\hbar n}{l}}{\left|p_{z_i}\right|\zeta(n,\bar{\Omega})}\right)\right) \times H(\zeta(n,\bar{\Omega}))\tilde{F}(\bar{\Omega},\beta,n). \tag{2.36}$$

This may be rewritten in the more convenient form

$$\left\langle P(\theta_f)\right\rangle_\beta = \sum_n \frac{2E_i\sin^2(|\theta_i| + \theta(n))}{\hbar\cos^2\theta(n)\sin^2\theta_f\tan\theta_f} \cdot \int_{-\infty}^{\infty} d\bar{\Omega}\delta\left(\bar{\Omega} - \frac{E_i}{\hbar}\left[1 - \frac{\sin^2(|\theta_i| + \theta(n))}{\sin^2\theta_f\cos^2\theta(n)}\right]\right) \times H(\zeta(n,\bar{\Omega}))\tilde{F}(\bar{\Omega},\beta,n), \tag{2.37}$$

with

$$E_i = \frac{p^2_{x_i} + p^2_{z_i}}{2M}. \tag{2.38}$$

Equations (2.32) and (2.37) are exact. However, within the semiclassical perturbation theory, the transition probability

factorizes so that one may rewrite the form factor in terms of a product of separate form factors for each oscillator,

$$F(\tau,\beta,n) = J_n^2(hA(\omega_x))\prod_{j=1}^{N} f_j(\tau,\beta), \tag{2.39}$$

with

$$f_j(\tau,\beta) = \left[1-\exp\left(-\hbar\beta\omega_j\right)\right]\sum_{n_f=0}^{\infty}\sum_{n_i=0}^{\infty}\exp\left[-n_i\hbar\beta\omega_j - i\tau\omega_j\left(n_f-n_i\right)\right]J^2_{n_f-n_i}\left(\bar{A}_j\left(n_{j_{if}}\right)\right). \tag{2.40}$$

Equations (2.39) and (2.40) are central to the numerical computations which will be presented below. However, first, we consider their simplification resulting from the fact that the coupling to the bath modes is weak.

Keeping in mind that the argument of the Bessel functions $\bar{A}_j\left(n_{j_{if}}\right)$ is linear in the coupling coefficients c_j and thus small, one may expand to first order in c_j^2. This implies that only no phonon or single phonon transitions ($\Delta n = 0, \pm 1$) contribute to the j-th form factor,

$$f_j(\tau,\beta,\Delta n=0) \simeq 1-\frac{c_j^2A^2(\omega_j)}{2M\omega_j}\hbar\coth\left(\frac{\hbar\beta\omega_j}{2}\right), \tag{2.41}$$

$$f_j(\tau,\beta,\Delta n=1) \simeq \exp\left(-i\tau\omega_j\right)\times\frac{\hbar c_j^2A^2(\omega_j)}{2M\omega_j\left[1-\exp\left(-\hbar\beta\omega_j\right)\right]}, \tag{2.42}$$

$$f_j(\tau,\beta,\Delta n=-1) \simeq \exp\left(i\tau\omega_j\right)\times\frac{\hbar c_j^2A^2(\omega_j)\exp\left(-\hbar\beta\omega_j\right)}{2M\omega_j\left[1-\exp\left(-\hbar\beta\omega_j\right)\right]}. \tag{2.43}$$

Allowing then only up to a change of one phonon during the collision process implies that

$$F(\tau,\beta,n) \simeq J_n^2(hA(\omega_x))\prod_{j=1}^{N} f_j(\tau,\beta,\Delta n=0)\times\left[1+\sum_{j=1}^{N}\frac{f_j(\tau,\beta,\Delta n=1)+f_j(\tau,\beta,\Delta n=-1)}{f_j(\tau,\beta,\Delta n=0)}\right]. \tag{2.44}$$

Using the definition of the spectral density (Eq. (2.3)) and the exponentiation $1-x\simeq\exp(-x)$, one readily finds that

$$\prod_{j=1}^{N} f_j(\tau,\beta,\Delta n=0) = \exp(-2W), \tag{2.45}$$

and the Debye Waller factor is

$$W = \frac{1}{2\pi\hbar M}\int_{-\infty}^{+\infty}dt_1\int_{-\infty}^{+\infty}dt_2\bar{V}'(z_{t_1,0})\bar{V}'(z_{t_2,0})\times\int_0^{\infty}d\omega J_z(\omega)\cos\left[\omega\left(t_1-t_2\right)\right]\coth\left(\frac{\hbar\beta\omega}{2}\right). \tag{2.46}$$

The same expression has been derived previously for neutron scattering through surfaces in Ref. 46 and for surface scattering in Ref. 47.

The single phonon contributions may also be written in the continuum limit. Defining

$$F_1(\tau,\beta) \equiv \sum_{j=1}^{N}\frac{f_j(\tau,\beta,\Delta n=1)+f_j(\tau,\beta,\Delta n=-1)}{f_j(\tau,\beta,\Delta n=0)}, \tag{2.47}$$

one may readily carry out the Fourier transform over τ in Eq. (2.33) and using the definition of the spectral density to find that

$$\begin{aligned}\tilde{F}_1(\bar{\Omega},\beta) &\equiv \frac{1}{2\pi}\int_{-\infty}^{\infty}d\tau\exp\left(i\tau\bar{\Omega}\right)F_1(\tau,\beta)\\ &= \frac{J_z\left(|\bar{\Omega}|\right)\left[H\left(\bar{\Omega}\right)+H\left(-\bar{\Omega}\right)\exp\left(-\hbar\beta\left|\bar{\Omega}\right|\right)\right]}{\pi\hbar M\left[1-\exp\left(-\hbar\beta\left|\bar{\Omega}\right|\right)\right]}\\ &\cdot\int_{-\infty}^{+\infty}dt_1\int_{-\infty}^{+\infty}dt_2\bar{V}'(z_{t_1,0})\bar{V}'(z_{t_2,0})\cos\left[\bar{\Omega}\left(t_1-t_2\right)\right].\end{aligned} \tag{2.48}$$

One then finds that the resulting final angular distribution is

$$\begin{aligned}\left\langle P(\theta_f)\right\rangle_\beta &= \exp(-2W)\sum_n\frac{\sin\left(|\theta_i|+\theta(n)\right)}{\sin\theta_f\cos\theta(n)}J_n^2(hA(\omega_x))\cdot\delta\left[\theta_f-\sin^{-1}\left(\frac{\sin\left(|\theta_i|+\theta(n)\right)}{\cos\left(\theta(n)\right)}\right)\right]H\left(\zeta(n,0)\right)\\ &+\exp(-2W)\sum_n\frac{2J_n^2(hA(\omega_x))}{\tan\theta_f}\cdot\int_{-\infty}^{\infty}d\bar{\Omega}\left(\frac{E_i}{\hbar}-\bar{\Omega}\right)\delta\left(\frac{E_i}{\hbar}-\bar{\Omega}-\frac{E_i}{\hbar}\frac{\sin^2\left(|\theta_i|+\theta(n)\right)}{\sin^2\theta_f\cos^2\theta(n)}\right)H\left(\zeta\left(n,\bar{\Omega}\right)\right)\tilde{F}_1\left(\bar{\Omega},\beta,n\right).\end{aligned} \tag{2.49}$$

The zero phonon contribution is thus a series of delta function peaks at the Bragg angles whose intensity is temperature dependent, via the Debye-Waller factor. The single phonon transitions contribute a smooth background to the angular distribution, since the function $\tilde{F}_1\left(\bar{\Omega},\beta,n\right)$ is a smooth function of the phonon frequency $\bar{\Omega}$. One may continue this process to also include the two phonon contribution, the explicit expression may be found in Eqs. (15)-(18) of Ref. 42.

III. IMPLEMENTATION TO SCATTERING OF Ne, Ar, AND Kr ON Cu(111)

A. Theoretical considerations

A central purpose of this paper is to compute the thermal angular distribution within the semiclassical perturbation theory framework but without restricting the theory to only a few phonon transitions. To achieve this, we discretize the problem, that is, instead of using continuum limit expressions, we assume a continuum limit spectral density and then approximate it with a finite sum over harmonic oscillators. Then for each oscillator, we compute its form factor as given in Eq. (2.40).

The discretization is carried out following the methodology of Refs. 48 and 49 (for different discretizations, see Refs. 50 and 51). The spectral density is modeled as Ohmic with an exponential cutoff, that is,

$$J_z(\omega) = \gamma\omega \exp\left(-\frac{\omega}{\omega_c}\right), \tag{3.1}$$

γ is the friction coefficient and ω_c is referred to as the cutoff frequency, although, in fact, it is the frequency at which the spectral density reaches its maximum value.

To evaluate the angular distribution, the bath oscillator frequencies ω_j and coupling coefficients c_j are needed. Following the suggestion of Ref. 48 for $N_B + 1$ bath oscillators, the discretized frequencies for the first N_B oscillators are determined as

$$\omega_j = -\omega_c ln\left(1 - \frac{j}{N_B + 1}\right), \quad j = 1, \ldots, N_B \tag{3.2}$$

and the associated coupling coefficients as

$$c_j = \sqrt{\frac{2\omega_j^2 \gamma \omega_c}{\pi(N_B + 1)}}, \quad j = 1, \ldots, N_B. \tag{3.3}$$

The Fourier transform of the form factor is computed by introducing a Gaussian smoothing,

$$\left\langle \tilde{F}\left(\bar{\Omega}, \beta, n\right)\right\rangle = \frac{1}{2\pi\sqrt{2\pi T_{sm}^2}} \int_{-\infty}^{\infty} d\tau \times \exp\left(-\frac{\tau^2}{2T_{sm}^2} + i\tau\bar{\Omega}\right) F(\tau, \beta, n). \tag{3.4}$$

The smoothing period T_{sm} is chosen to be

$$T_{sm} = \frac{2\pi}{\Delta\omega}, \tag{3.5}$$

where $\Delta\omega$ is taken to be a typical spacing between adjacent frequencies of the discretized oscillators.

B. The Morse potential model

To apply the theory, we choose the vertical interaction potential to be the Morse potential

$$\bar{V}(z) = V_0[(\exp(-\alpha z) - 1)^2 - 1], \tag{3.6}$$

which is characterized by the well depth V_0 and the stiffness parameter α. The advantage of the Morse form is that the arguments of the Bessel functions may be evaluated analytically.

TABLE I. Parameters used for Ne, Ar, and Kr atoms scattered on a Cu(111) surface.

Atom	αl	V_0 (meV)	$\bar{\gamma}$	h (a.u.)
Kr	4.2	134.0	0.120 5	2.82×10^{-3}
Ar	3.3	70.0	0.057 82	1.98×10^{-3}
Ne	3.0	31.6	0.012 34	1.10×10^{-3}

One readily finds (Ref. 32) that (see Eq. (2.28))

$$A(\omega) = -\frac{2\pi M\omega}{\alpha\hbar} \frac{\cosh(\Phi\frac{\omega}{\Omega})}{\sinh(\pi\frac{\omega}{\Omega})}, \tag{3.7}$$

with

$$\Omega^2 = \frac{2\alpha^2 E_z}{M} \tag{3.8}$$

and

$$\cos(\Phi) = -\sqrt{\frac{V_0}{E_z + V_0}}. \tag{3.9}$$

C. Application to scattering of Ne, Ar, and Kr from Cu(111)

The SCPT theory is now applied to analyze and interpret the measured low temperature angular distribution of Ne, Ar, and Kr atoms scattered from a Cu(111) surface.[40,41] The parameters used (Table I) are the same as in Ref. 42. The well depths of the Morse potentials for all three cases were taken from recent *ab-initio* computations.[52] The lattice length is 3.61 Å.[53] The corrugation height was determined from the measured ratio of the $n = 0$ to $n = -1$ Bragg peaks since this ratio determines the magnitude of the phase amplitude $hA(\omega_x)$ appearing in the argument of the respective Bessel functions.

The spectral density is chosen to be Ohmic (for a theoretical justification, see Ref. 54) with an exponential cutoff $J(\omega) = \gamma\omega \exp(-\omega/\omega_c)$. The cutoff frequency, $\hbar\omega_c = 6$ meV, is the same for all atoms since it is a property of the surface. It was chosen by fitting the Debye-Waller factor to the experimental data. The reduced friction coefficient ($\bar{\gamma} = M^2\omega_0^3\gamma$, where $\omega_0^2 = 2V_0\alpha^2/M$) is fit separately for each atom. The theory thus involves three parameters for each atom (γ, V_0, α) and the cutoff frequency ω_c, common to all cases. In all cases that will be presented using this model, the elastic peaks were Gaussian broadened ($\Delta\theta = 0.4°$), to agree with the experimental broadening in the incident beam, as also detailed in Ref. 41.

A first check on the theory is to determine how well the continuum limit expression for the Debye-Waller factor (Eq. (2.46)) (obtained by expansion of the Bessel functions to lowest order and exponentiation) agrees with its discretized form which is a sum of the logarithm of the form factors as given in Eq. (2.45). The results are presented in Fig. 1. The good comparison between the continuum limit expression and the experimentally measured Debye-Waller factors has already been presented in Fig. 1 of Ref. 42 but is also added here (solid dots).

A second check of the present theory is to compare the results for the discretized theory (dashed lines) with the

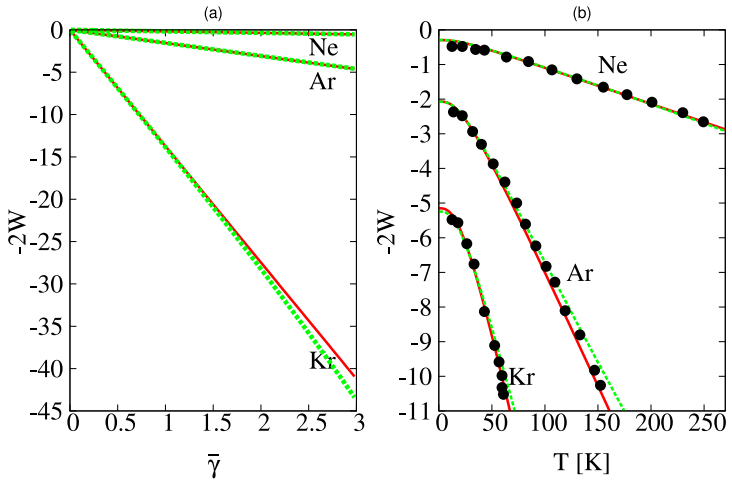

FIG. 1. Comparison of the continuum limit expression for the Debye-Waller factor (Eq. (2.46)) and its estimate as the discretized sum of the logarithm of the form factors (Eq. (2.45)). The results are presented (continuum limit — dashed, green line and discretized expression — solid, red line) for the scattering of Ne, Ar, and Kr as a function of the reduced friction coefficient in panel (a) and as a function of the surface temperature in panel (b). The solid dots are the experimental data of Ref. 41. The number of oscillators used was 40.

continuum limit expressions (solid lines) for up to two phonon contributions, as given in Eqs. (14)-(18) of Ref. 42. This is shown in Fig. 2. One notes that apart from the oscillations due to the finite discretization, there is good agreement between the various computations.

In Ref. 42, only up to two phonon contributions were included, using the continuum form. The comparison with the experimental results showed good agreement at very low temperature, but as the temperature was increased, especially for Ar and Kr scattering, there were deviations which we attributed to higher order phonon scattering contributions. That this is so is evident from Fig. 3 where we plot the angular distributions obtained using one-, two-, and multi-phonon contributions. As the temperature is increased, the all phonon contribution becomes larger relative to the continuum one and two phonon results.

Finally, in Fig. 4, we compare the discretized theory, including all multi-phonon contributions with the experimental results of Ref. 41. We find good agreement between experiment and theory for the scattering of Ne and Ar (the small oscillations in the theoretical results are due to the finite number of oscillators used, increasing the number reduces the oscillations). From Fig. 3, it is clear that for Ne, more than two phonon transitions are not important, even at room temperature. This is not the case for the scattering of Ar, where only inclusion of the multi-phonon transitions at T = 84 K gives quantitative agreement with experiment. Finally, for Kr scattering, the results, especially at the higher temperature (T = 42 K) where the multi-phonon contributions are significant, are in better agreement with experiment than the previous results based on only up to two phonon transitions. We do note that already the low temperature theoretical results, presented in Ref. 42, were a bit low, so the lack of quantitative agreement is not surprising.

IV. DISCUSSION

In this paper, we derived a new semiclassical multi-phonon theory for atom surface scattering. Using a discretized

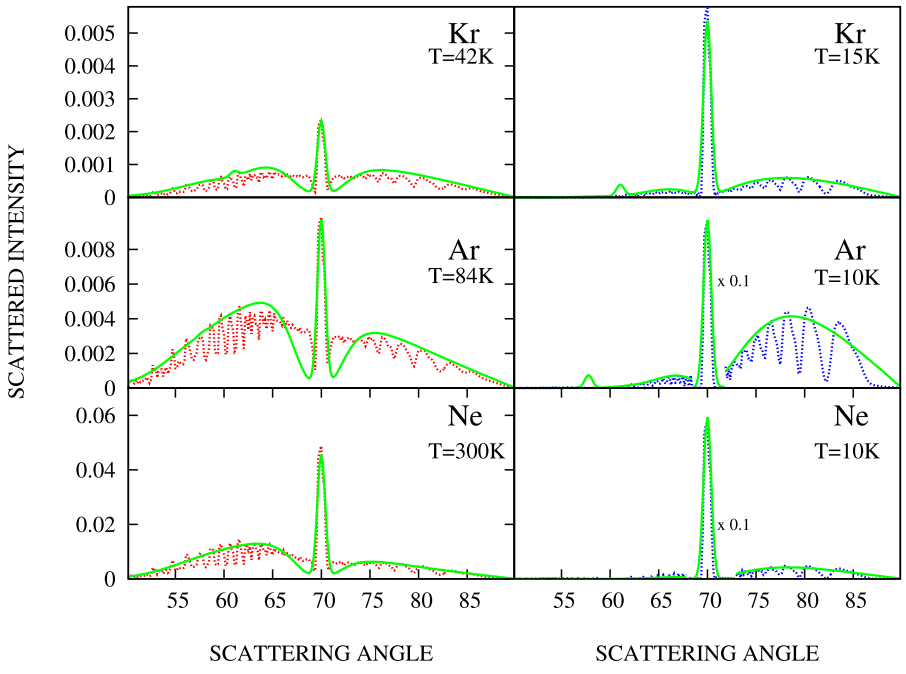

FIG. 2. Comparison between the discretized theory (dotted red and blue lines) and the continuum (solid green lines) angular distributions when only one and two phonon contributions are allowed. Apart from the oscillatory character of the discretized results, there is good agreement between the two computations. The number of oscillators used for the discretization was 20.

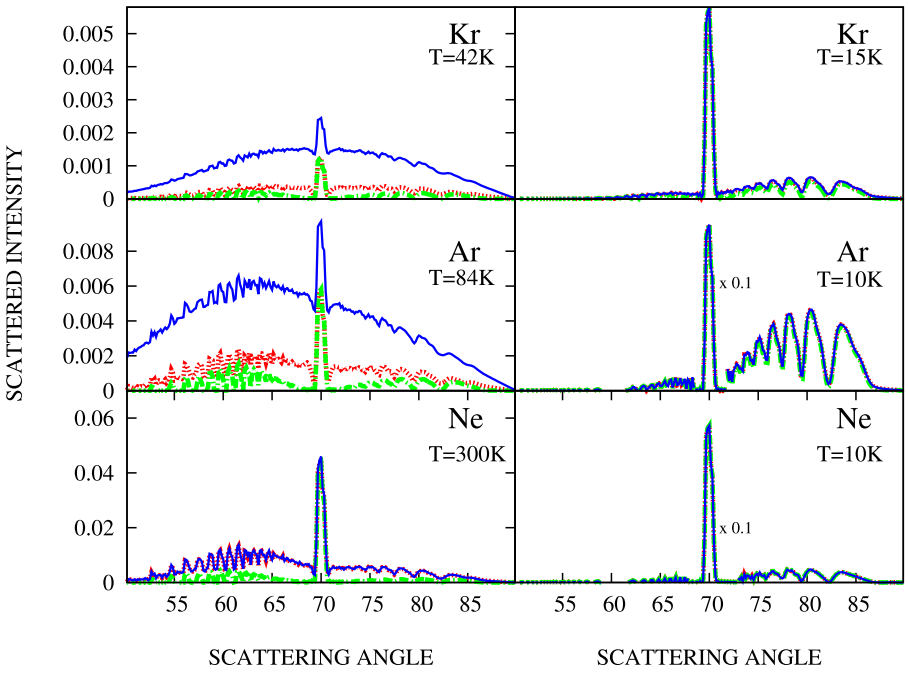

FIG. 3. The contributions of multi-phonon transitions as the surface temperature is increased. The one (dashed-dotted green lines), one+two (dotted red lines) and all phonon (solid blue lines) contributions are shown for the angular distributions of Ne, Ar, and Kr, scattered on the Cu(100) surface. Note the increased contribution from multi-phonon transitions as the temperature is increased. The number of oscillators used in the discretized computation is 20.

representation of the spectral density, an expression was derived for the angular distribution for an atom scattered from a thermal surface. The discretized results were shown to be in good agreement with the continuum results, both for the Debye-Waller factor as well as for low temperature scattering when only up to two phonon transitions are important. The multi-phonon theory accounts well for the measured features of the angular distribution, which are the superposition of elastic "delta" function peaks on a smooth and broad background whose intensity increases as the surface temperature is increased.

The multi-phonon theory confirms our previous conjecture given in Ref. 42 that the broad background measured in the angular distribution at increased surface temperature comes from multi-phonon transitions. Comparison of the present theory with the experimentally measured results was favorable; we note that we used the same parameters as in our previous Communication.[42]

The theory presented here can be developed in further directions. One is a study of the energy transferred from the scattered atom to and from the bath, as a function of angle of incidence, incident energy, and surface temperature. A second direction is extension to include second order surface corrugation effects.[55] It should also be possible to extend the present formulation of a multi-phonon theory based on the definition of a form factor to the continuum limit. Finally, the theory should be readily applicable to many experimental results on atom surface scattering.

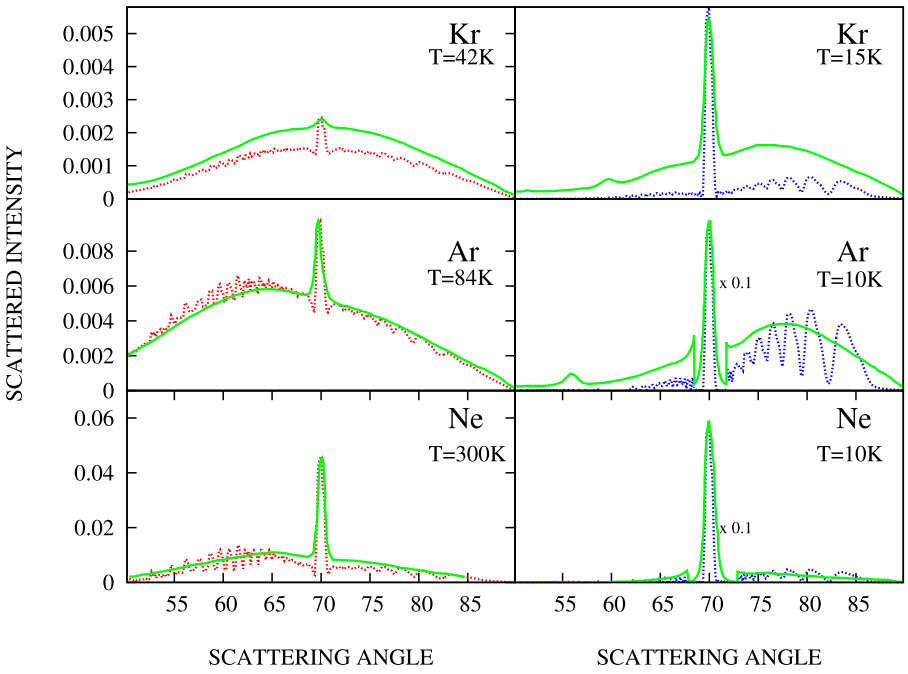

FIG. 4. Comparison of the theoretically generated (dashed red and blue lines) angular distributions using the multi-phonon discretized theory with the experimental measurements (solid green lines) of Ref. 41 for the scattering of Ne, Ar, and Kr on the Cu(100) surface. The experimental and theoretical distributions were scaled to agree with each other at the specular peak. The discretized theory is based on 20 oscillators.

ACKNOWLEDGMENTS

We thank Professor S. Miret-Artés for stimulating discussion. This work was supported by grants from the Israel Science Foundation, the German Israel Foundation for Basic Research and the Minerva Foundation (Munich).

[1]F. Knauer and O. Stern, Z. Phys. **53**, 779 (1929).
[2]I. Estermann and O. Stern, Z. Phys. **61**, 95 (1930).
[3]G. Benedek and J. P. Toennies, Surf. Sci. **299-300**, 587 (1994).
[4]N. Cabrera, V. Celli, F. O. Goodman, and R. Manson, Surf. Sci. **19**, 67 (1970).
[5]N. Cabrera, V. Celli, and R. Manson, Phys. Rev. Lett. **22**, 346 (1969).
[6]J. R. Manson, Phys. Rev. B **43**, 6924 (1991).
[7]G. D. Billing, Chem. Phys. **70**, 223 (1982).
[8]G. D. Billing, Chem. Phys. **74**, 143 (1983).
[9]R. Guantesa, A. S. Sanzb, J. Margalef-Roiga, and S. Miret-Artés, Surf. Sci. Rep. **53**, 199 (2004).
[10]A. S. Sanz and S. Miret-Artés, Phys. Rep. **451**, 37 (2007).
[11]R. Martinez-Casado, S. Miret-Artés, B. Meyer, F. Traeger, and C. Woll, J. Phys.: Condens. Matter **22**, 304011 (2010).
[12]M. Mayrhofer-Reinhartshuber, P. Kraus, A. Tamtogl, S. Miret-Artés, and W. E. Ernst, Phys. Rev. B **88**, 205425 (2013).
[13]P. Kraus, M. Mayrhofer-Reinhartshuber, C. Gosweiner, F. Apolloner, S. Miret-Artés, and W. E. Ernst, Surf. Sci. **630**, 208-215 (2014).
[14]B. Jackson, J. Chem. Phys. **90**, 140 (1989); **92**, 1458 (1990).
[15]B. Jackson and H. Metiu, J. Chem. Phys. **86**, 1026 (1987).
[16]B. Gumhalter, Phys. Rep. **351**, 1 (2001).
[17]K. Burke, B. Gumhalter, and D. C. Langreth, Phys. Rev. B **47**, 12852 (1993).
[18]B. Gumhalter, K. Burke, and D. C. Langreth, Surf. Rev. Lett. **1**, 133 (1994).
[19]A. Gross, in *Handbook of Material Modeling*, edited by S. Yip (Springer, 2005), p. 1713.
[20]A. Gross and M. Scheffler, Chem. Phys. Lett. **263**, 567 (1996).
[21]P. Nieto, E. Pijper, D. Barredo, G. Laurent, R. A. Olsen, E.-J. Baerends, G.-J. Kroes, and D. Faras, Science **312**, 86 (2006).
[22]G. Drolshagen and E. J. Heller, J. Chem. Phys. **79**, 2072 (1983).
[23]S. Miret-Artés and E. Pollak, Surf. Sci. Rep. **67**, 161 (2012).
[24]R. M. Logan and R. E. Stickney, J. Chem. Phys. **44**, 195 (1966).
[25]R. M. Logan and J. C. Keck, J. Chem. Phys. **49**, 860 (1968).
[26]J. C. Tully, J. Chem. Phys. **92**, 680 (1990).
[27]W. A. Steele, Surf. Sci. **38**, 1 (1973).
[28]U. Garibaldi, A. C. Levi, R. Spadacini, and G. E. Tommei, Surf. Sci. **48**, 649 (1975).
[29]E. F. Greene and E. A. Mason, Surf. Sci. **75**, 549 (1978).
[30]J. R. Klein and M. W. Cole, Surf. Sci. **79**, 269 (1979).
[31]E. Pollak, S. Sengupta, and S. Miret-Artés, J. Chem. Phys. **129**, 054107 (2008).
[32]E. Pollak, J. M. Moix, and S. Miret-Artés, Phys. Rev. B **80**, 165420 (2009); Erratum **81**, 039902 (2010).
[33]E. Pollak and J. Tatchen, Phys. Rev. B **80**, 115404 (2009); Erratum **81**, 049903 (2010).
[34]E. Pollak and S. Miret-Artés, J. Chem. Phys. **130**, 194710 (2009); Erratum **132**, 049901 (2010).
[35]E. Pollak and S. Miret-Artés, Chem. Phys. **375**, 337 (2010).
[36]Y. Zhou, E. Pollak, and S. Miret-Artés, J. Chem. Phys. **140**, 024709 (2014).
[37]W. H. Miller and F. T. Smith, Phys. Rev. A **17**, 939 (1978).
[38]L. M. Hubbard and W. H. Miller, J. Chem. Phys. **78**, 1801 (1983).
[39]L. M. Hubbard and W. H. Miller, J. Chem. Phys. **80**, 5827 (1984).
[40]F. Althoff, T. Andersson, and S. Andersson, Phys. Rev. Lett. **79**, 4429 (1997).
[41]T. Andersson, F. Althoff, P. Linde, S. Andersson, and K. Burke, Phys. Rev. B **65**, 045409 (2002).
[42]S. Daon, E. Pollak, and S. Miret-Artés, J. Chem. Phys. **137**, 201103 (2012).
[43]A. Azuri and E. Pollak, J. Chem. Phys. **139**, 044707 (2013).
[44]W. H. Miller, J. Chem. Phys. **53**, 1949 (1970).
[45]W. H. Miller, J. Chem. Phys. **53**, 3578 (1970).
[46]Equation (2) of V. F. Sears and S. A. Shelley, Acta Crystallogr., Sect. A: Found. Crystallogr. **A47**, 441 (1991).
[47]Equations (4.35) and (4.36) of A. C. Levi and H. Suhl, Surf. Sci. **88**, 221 (1979); K. Burke and W. Kohn, Phys. Rev. B **43**, 2477 (1991).
[48]H. Wang, M. Thoss, and W. H. Miller, J. Chem. Phys. **112**, 47 (2000).
[49]M. Thoss, H. Wang, and W. H. Miller, J. Chem. Phys. **114**, 9220 (2001).
[50]C.-M. Goletz, W. Koch, and F. Grossmann, Chem. Phys. **375**, 227 (2010).
[51]N. Wu, L. Duan, X. Li, and Y. Zhao, J. Chem. Phys. **138**, 084111 (2013).
[52]P. L. Silvestrelli, A. Ambrosetti, S. Grubisic, and F. Ancilotto, Phys. Rev. B **85**, 165405 (2012).
[53]M. Wilms, P. Broekman, C. Stuhlmann, and K. Wandelt, Surf. Sci. **416**, 121 (1998).
[54]Y. Georgievskii, M. A. Kozhushner, and E. Pollak, J. Chem. Phys. **102**, 6908 (1995).
[55]E. Pollak and S. Miret-Artes, "Second-order semiclassical perturbation theory for diffractive scattering from a surface," J. Phys. Chem. C (published online).

Part III

Abstract -Hebrew

תזה זו מכילה בעיקר ניתוח תוצאות ניסויים בנושא פיזור אטומים ממשטחים. אנו משתמשים ומפתחים שיטות תאורטיות חדשות כדי לחקור ניסויים כאלה. אנו לוקחים בחשבון אפקטים קוונטיים כמו גם אפקטים קלאסיים. אפקטים אלה כוללים דיפרקציה, אפקטי מירכוז (קולימציה) של האלומה, ועוד. אנו מספקים הסברים חדשים ומועילים לניסויים בנושא, עם הסברים איכותיים כמו גם כמותיים. התיאוריה שלנו היא הראשונה שיכולה לתאר באופן מלא את אפקטי הפיזור הנובעים מדיפרקציה של הפיזור הזוויתי שנצפה בניסויי פיזור של אטומי נאון, ארגון וקריפטון ממשטחי אלומיניום. אנו גם מסבירים את התנהגות הפקטור של דבי-וואלר אשר נמדד בניסויים. הכלי המרכזי שמשמש אותנו לאורך המחקר הוא התיאוריה הסמי-קלאסית של האבארד ומילר אשר פותחה לפני 45 שנים. היא פותחה במקור כדי להסביר את אפקטי הסופר-פוזיציה הקוונטית שנמצאו בהרבה ניסויי פיזור. הם מצאו דרך פשוטה להסביר את האפקטים האלה באמצעות שימוש במסלולים קלאסיים בלבד, תוך שימוש בהסתברויות קוונטיות.

בעבודה זו אנו משפרים ומרחיבים את התיאוריה שלהם על ידי הכנסת אפקטים מיוחדים שמעניינים אותנו ואחרים אשר מבצעים ומנתחים ניסויים כאלה. אנו חוקרים אפקטי מרכוז אלומה (קולימציה) - מה קורה כאשר משנים את רוחב האלומה האטומית הנכנסת. כמו כן אנו חוקרים את האפקטים של אמבט הפונונים, אשר משפיעים על המסלולים של החלקיקים, משום שדבר זה מאפשר להבין את ההשפעה של טמפרטורת המשטח. אנו לוקחים בחשבון את התרומות של מעברים של 0 , 1 ו-2 פונונים מן החלקיק אל המשטח ומן המשטח אל החלקיק, ומציגים אותם בנפרד, תוך ניתוח מדוייק של ההשפעה של כל תרומה. אנו עושים זאת גם על ידי שימוש במודל רציף מקורב ואנליטי, וגם בעזרת מודל דיסקרטי מדוייק, שבעזרתו אפשר להגיע להשפעה של אינסוף פונונים.

התיאוריה שפיתחנו מספקת הסבר טוב לניסויים של פיזור נאון, ארגון וקריפטון ממשטח אלומיניום בטמפרטורה נמוכה, ניסויים שבהם האפקטים הקוונטיים ניכרים לעין. ניתן להשתמש בתאוריה גם לנתח ניסויים אחרים של פיזור חלקיקים ממשטחים. התאוריה ניתנת להרחבה לפיזור מולקולות ממשטחים, לפיזור תלת-מימדי של אטומים ממשטחים, וניתן להשתמש בה כדי לחקור תצפיות אחרות, כגון התפלגויות איבוד אנרגיה מהמשטח, הסתברויות הדבקה למשטח, ועוד.